No. 045
May 1970

SHIP VIBRATIONS

Lecture Notes

Horst Nowacki

THE DEPARTMENT OF NAVAL ARCHITECTURE AND MARINE ENGINEERING

THE UNIVERSITY OF MICHIGAN
COLLEGE OF ENGINEERING

No. 045
May 1970

SHIP VIBRATIONS

Lecture Notes
by
Horst Nowacki

Third Printing: March 1973

Department of Naval Architecture
and Marine Engineering
College of Engineering
The University of Michigan
Ann Arbor, Michigan 48104

FOREWORD

This set of lecture notes was written during my visit at the Federal University of Rio de Janeiro, Engineering Post-Graduate School (COPPE), in 1968. The students who were taking my course there had had a graduate level course in dynamics and were primarily interested in applications of elastic vibration theory to problems occurring aboard ships. For this reason my treatment of any elementary aspects of dynamics was kept rather sketchy.

If these notes are used as a first introduction to elastic vibrations, as for example in our undergraduate course NA 446, "Ship Vibrations," they must be supplemented by some other introductory material. This should include a comprehensive treatment of the dynamics of single and two degree of freedom systems as well as a thorough introduction to Euler beam dynamics. Fortunately these topics are covered in many good textbooks.

In graduate level work on ship vibrations the notes may primarily serve as a general survey suggesting areas for deeper study of the many specialized topics covered in the extensive literature on this subject. The references contain many worthwhile articles the graduate student should become familiar with.

I acknowledge again with gratitude the help received from Professor Alberto Luiz Coimbra and his staff at COPPE when preparing these notes.

Horst Nowacki

SHIP VIBRATIONS

Contents:

SHIP VIBRATIONS

RECOMMENDED LITERATURE

A. Books:

1. W. T. Thomson: Vibration Theory and Applications, Prentice-Hall, May 1965.
2. L. Meirovitch: Analytical Methods in Vibrations, Macmillan, New York, 1967.
3. Comstock, editor: Principles of Naval Architecture, Society of Naval Architects and Marine Engineers, chapter X, by F. M. Lewis, New York, 1968.
4. F. H. Todd: Ship Hull Vibration, Edward Arnold Ltd., London, 1961.
5. Yoshiki, M., Kumai, T., Kanazawa, T.: "Recent Studies on Ship Vibration in Japan," Society of Naval Architects of Japan, 60th Anniversary Series, vol. 10, Tokyo, 1965.

B. Papers and Reports:

6. Mc Goldrick, R. T.: "Ship Vibration," David Taylor Model Basin Report 1451, Dec. 1960.
7. Leibowitz, R. C. and Kennard, E. H.: "Theory of Freely Vibrating Nonuniform Beams, Including Methods of Solution and Application to Ships," David Taylor Model Basin Report 1317, May 1961.
8. Csupor, D.: "Methods for Calculating the Free Vibrations of a Ship's Hull," David Taylor Model Basin Translation 288, May 1959. Original paper: Transactions Schiffbautechnische Gesellschaft 1956.
9. Lewis, F. M.: "The Inertia of the Water Surrounding a Vibrating Ship," Transactions SNAME, 1929.
10. Todd, F. H. and Marwood, W. F.: "Ship Vibration," Transactions North East Coast Institution, 1948.
11. Wendel, K.: "Hydrodynamic Masses and Hydrodynamic Moments of Inertia," David Taylor Model Basin Translation 260, July 1956. Original paper: Transactions

Schiffbautechnische Gesellschaft, 1950.

12. Lewis, F. M.: "Propeller Vibration Forces," Transactions SNAME, 1963.
13. Tsakonas, S., Breslin, J. P., Jen, N.: "Pressure Field Around a Marine Propeller Operating in a Wake," Journal of Ship Research, April 1963.
14. Kruppa, C.: "Beitrag zum Problem der Hydrodynamischen Trägheitsgrössen bei elastischen Schiffsschwingungen," Schiffstechnik, January 1962.
15. Proceedings of the First Conference on Ship Vibration, Stevens Institute of Technology, Hoboken, New Jersey, January 1965.
16. Kuo, C.: "Review on Ship Vibration Problems—Chairman's Contribution," Submitted to Third International Ship Structures Congress, Oslo, 1967.
17. Ogilvie, T. F.: "Theory of Ship Vibrations I," lecture notes, Department of Naval Architecture and Marine Engineering, The University of Michigan, Winter Term 1968.
18. F. M. Lewis and A. J. Tachmindji: "Propeller Forces Exciting Hull Vibration," Transactions of The Society of Naval Architects and Marine Engineers, 1954.
19. S. Schuster and E. A. Walinski: "Beitrag zur Analyse des Propellerkraftfeldes," Schiffstechnik, 1957.
20. J. P. Breslin: "The Pressure Field Near a Ship Propeller," JSR, 1958.
21. J. P. Breslin and S. Tsakonas: "Marine Propeller Pressure Field Due to Loading and Thickness Effects," Transactions of The Society of Naval Architects and Marine Engineers, 1959.
22. A. J. Tachmindji and R. T. McGoldrick: "Note on Propeller-Excited Hull Vibrations," JSR, 1959.
23. K. H. Pohl: "The Fluctuating Pressure Field in the Vicinity of a Ship's Propeller and the Periodic Forces Produced by It on Neighboring Plates," Schiffstechnik, 1959.

24. J. P. Breslin: "Review and Extension of Theory for Near Field Propeller-Induced Vibratory Effects," Fourth Symposium on Naval Hydrodynamics, 1962.
25. J. P. Breslin, S. Tsakonas, and W. R. Jacobs: "The Vibratory Force and Moment Produced by a Marine Propeller on a Long Rigid Strip," JSR, 1962.
26. N. A. Brown: "Theory and Experiment for Propeller Forces in Nonuniform Flow," First Conference on Ship Vibration, Hoboken, 1965.
27. J. P. Breslin and K. S. Eng: "A Method for Computing Propeller-Induced Vibratory Forces of Ships," First Conference on Ship Vibration, Hoboken, 1965.
28. S. Tsakonas: "Propeller Vibratory Thrust and Torque in Unsteady Three-Dimensional Flows," First Conference on Ship Vibration, Hoboken, 1965.
29. S. Tsakonas, J. Breslin, and M. Miller: "Correlation and Application of an Unsteady Flow Theory for Propeller Forces," Transactions of The Society of Naval Architects and Marine Engineers, 1967.
30. J. Hadler and H. Cheng: "Analysis of Experimental Wake Data in Way of Propeller Plane of Single- and Twin-Screw Ship Models," Transactions of The Society of Naval Architects and Marine Engineers, 1965.
31. J. E. Kerwin and R. Leopold: "A Design Theory for Subcavitating Propellers," Transactions of The Society of Naval Architects and Marine Engineers, 1964.
32. E. J. Adams: "The Steady-State Response of a Ship Hull to a Simple Harmonic Driving Force," Report 1317, Washington, D.C.: David Taylor Model Basin, 1961.
33. H. Schwanecke: "Gedanken zur Frage der hydrodynamisch erregten Schwingungen des Propellers und der Wellenleitung," Transactions, Schiffbautechnische Gesellschaft, 1963.

34. R. T. McGoldrick and V. L. Russo: "Hull Vibration Investigation on SS GOPHER MARINER," Transactions of The Society of Naval Architects and Marine Engineers, 1955.
35. D. C. Robinson: "Vibration Characteristics of NS SAVANNAH," First Conference on Ship Vibration, Hoboken, 1965.
36. E. Huse: "The Magnitude and Distribution of Propeller-Induced Surface Forces on a Single-Screw Ship Model," Norwegian Ship Model Experiment Tank, Publication No.100, Trondheim, December 1968.
37. R.C. Leibowitz and R. L. Harder: "Mechanized Computation of Ship Parameters," David Taylor Model Basin Report 1841, June 1965.
38. R. C. Leibowitz: "Comparison of Theory and Experiment for Slamming of a Dutch Destroyer," David Taylor Model Basin Report 1511, June 1962.
39. G. W. Dutton and R. C. Leibowitz: "A Procedure for Determining the Virtual Mass J-Factors for the Flexural Modes of a Vibrating Beam," David Taylor Model Basin Report 1623, August 1962.
40. R. C. Leibowitz: "A Method for Predicting Slamming Forces on and Response of a Ship Hull," David Taylor Model Basin Report 1691, September 1963.
41. R. C. Leibowitz and J. E. Greenspon: "A Method for Predicting the Plate-Hull Girder Response of a Ship Incident to Slam," David Taylor Model Basin Report 1706, October 1964.
42. T. Kumai: "On the Estimation of Natural Frequencies of Vertical Vibration of Ships," Zosen Kiokai, June 1967.
43. J. Ormondroyd et al.: "Dynamics of a Ship's Structure," Final Report on Project M670-4, University of Michigan, Ann Arbor, June 1951.
44. O. Grim: "Elastic Support of the Propeller Shaft in the Stern Tube," Transactions, Schiffbautechnische Gesellschaft, 1960.
45. A. R. Minson: "Some Notes on Vibration Problems," Lloyd's Register of Shipping, Publication No.36.

46. T. A. Lamplough: "Some Aspects of Propeller Excited Vibration," Lloyd's Register of Shipping, Publication No.29.
47. E. H. Cuthill and F. H. Henderson: "Description and Usage of GBRC1-General Bending Response Code 1," David Taylor Model Basin Report 1925, October 1964.
48. W. Hinterthan: "A Procedure for Calculating Propeller-Excited Vibratory Forces from Wake Surveys," Naval Ship Research and Development Center, Report 2519, January 1969.
49. F. M. Lewis, "Propeller Vibration Forces in Single-Screw Ships," Transactions of the Society of Naval Architects and Marine Engineers, 1969.

1. INTRODUCTION.

1.1 Definitions.

Vibrations are oscillatory motions of a dynamic system.

A dynamic system is a combination of matter possessing mass whose parts are capable of relative motion.

For the resulting motion of a free system to be of oscillatory character, there must also exist some restoring force mechanism since the effect of inertia forces alone could only produce a monotonous motion.

In elastic vibrations, the restoring force is provided by the elasticity of the material according to Hooke's law.

Ship hull vibrations are the elastic vibrations of the ship structure and of its parts.

The basic force categories involved in elastic vibrations can best be illustrated by the example of the simple linear mass-spring-system (system of one degree of freedom), Fig. 1.

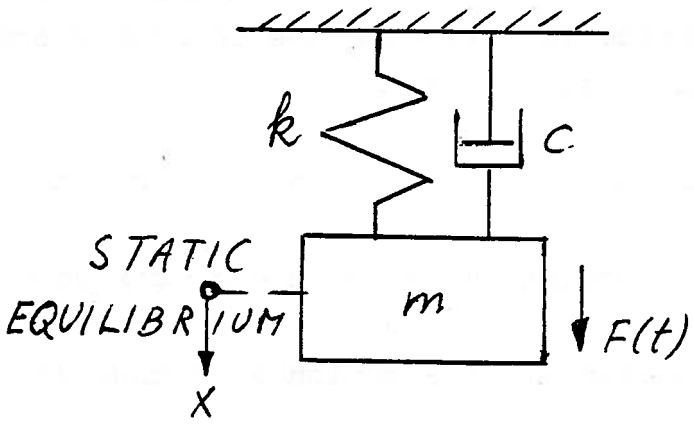

Fig. 1: Mass-spring-damper system

The basic forces involved are:

a) Passive elements, due to system properties:

Inertia force: $m\ddot{x}$

Damping force: $c\dot{x}$

Spring force: kx

b) Active element, acting on system from outside:
Excitation force $F(t)$.
The excitation is either periodic or non-periodic. The most important example of periodic excitation is harmonic excitation $F(t) = F_o \cos \omega t$. Any other periodic excitation can be converted into a series of harmonic excitation terms by Fourier analysis. The steady-state response of a linear system to any periodic excitation is therefore obtainable by superposition from its response to harmonic excitation.
By contrast, one can study the step response (response to a step function) or the impulse function response of a linear system to get a characteristic description of its transient response behavior.

1.2 Complex Representation of Harmonic Motions and Forces.

In dealing with harmonic motions (or forces) it is of great convenience to introduce the following complex notation:

Let us agree that

the real notation $x = X \cdot \cos \omega t$

and the complex notation $\vec{x} = X \cdot \cos \omega t + iX \sin \omega t = X \cdot e^{i\omega t}$ (1)

are equivalent. The motion x is thus defined as the real part of $\vec{x}$.

$$x = \mathrm{Re}[\vec{x}] \tag{2}$$

The advantage of the complex notation lies in the ease with which one can differentiate, superimpose, or otherwise manipulate motion expressions. Differentiating (1) for example:

Real Notation:	Complex Notation:	
$\dot{x} = \frac{dx}{dt} = -\omega X \cdot \sin \omega t$	$\frac{d\vec{x}}{dt} = i\omega X \cdot e^{i\omega t} = i\omega\vec{x}$	(3)
$= \omega X \cdot \cos(\omega t + \pi/2)$		
$\ddot{x} = \frac{d^2x}{dt^2} = -\omega^2 X \cdot \cos \omega t$	$\frac{d^2\vec{x}}{dt^2} = -\omega^2 X e^{i\omega t} = -\omega^2\vec{x}$	

Note that in complex notation the time-dependent term $e^{i\omega t}$ is the same throughout whereas in real notation the cosine arguments differ in their phases so that tedious trigonometric operations would be necessary to superimpose such functions.

The factor in front of the exponential function is called complex amplitude, and carries amplitude and phase information. For the velocity for example, the complex amplitude is

$$\bar{X} = i\omega X \tag{4}$$

which means the magnitude of the velocity is

$$\left|\bar{X}\right| = \omega X \tag{5}$$

and the phase is the argument of the complex number $\bar{X}$:

$$\alpha = \arctan \frac{\mathrm{Im}(\bar{X})}{\mathrm{Re}(\bar{X})} = \arctan \frac{\omega X}{0} = \frac{\pi}{2} \tag{6}$$

The velocity is thus a quarter of a cycle in advance of the displacement.

A <u>phase vector diagram</u> is often used to illustrate the phase relationships of harmonic motions of the same frequency.

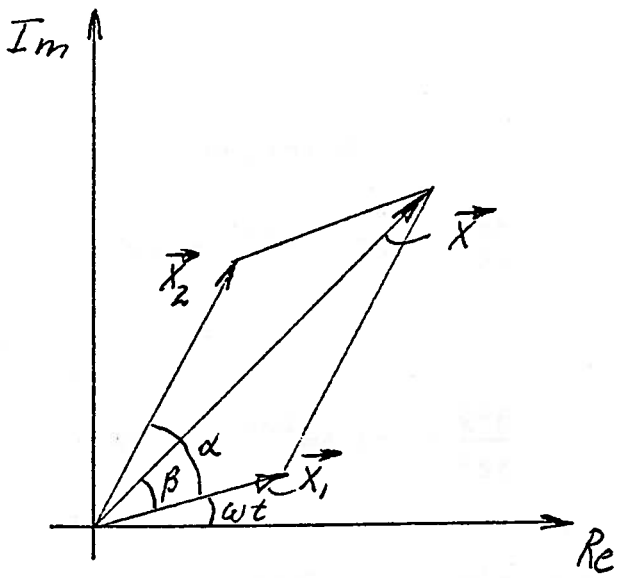

Fig. 2
Phase vector diagram for addition of two vectors.

Fig. 2 shows the vectorial addition of the motions

$$\vec{x}_1 = X_1 \cdot e^{i\omega t}$$
$$\vec{x}_2 = X_2 \cdot e^{i(\omega t + \alpha)} = X_2 e^{i\alpha} \cdot e^{i\omega t} \qquad (7)$$

It can be shown by trigonometry:

$$\vec{x} = X \cdot e^{i(\omega t + \beta)} = X \cdot e^{i\beta} \cdot e^{i\omega t} \qquad (8a)$$

where

$$\left.\begin{aligned} X &= \sqrt{(X_1 + X_2 \cdot \cos\alpha)^2 + (X_2 \cdot \sin\alpha)^2} \\ \beta &= \arctan \frac{X_2 \cdot \sin\alpha}{X_1 + X_2 \cos\alpha} \end{aligned}\right\} \qquad (8b)$$

In summary, it may be stated that in complex notation it is easily possible to separate the representation of a motion or force into one time-dependent factor, and two others expressing amplitude and phase, respectively.

2. SEISMIC VIBRATION MEASURING INSTRUMENTS

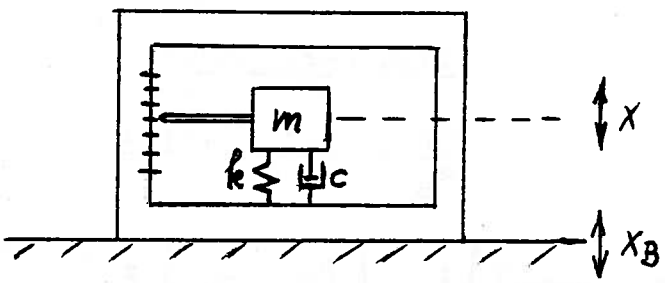

Fig. 3: Seismic Instruments

A seismic instrument consists of a box containing a spring-mass-damper system as shown in Fig. 3.

A. Displacement measurement, vibrometer.

The base motion x_B is to be measured. The motion of the mass m is x, and by means of a pen or electronic equivalent we can record the difference between box motion and mass motion:

$$x_R = x_B - x \tag{9}$$

The system is an example of a base-excited one degree of freedom system. We are interested in the steady-state response to some harmonic excitation

$$x_B = A_B \cdot e^{i\omega t} \tag{10}$$

The differential equation of the system is obtained as follows:

$$\left.\begin{aligned} &m\ddot{x} + c(\dot{x} - \dot{x}_B) + k(x - x_B) = 0 \\ &\text{or, substituting } x_R\text{:} \\ &m\ddot{x}_R + c\dot{x}_R + kx_R = m\ddot{x}_B \end{aligned}\right\} \tag{11}$$

The solution has the form

$$x_R = A_R \cdot e^{-i\alpha} \cdot e^{i\omega t} \tag{12}$$

Substituting:

$$(-m\omega^2 + ic\omega + k)\, A_R \cdot e^{-i\alpha} = -A_B m\omega^2 \tag{13}$$

Real part:

$$\frac{A_R}{A_B} = \frac{-m\omega^2 \cdot \cos\alpha}{k - m^2\omega^2}$$

Imaginary part:

$$\frac{A_R}{A_B} = \frac{-m\omega^2 \cdot \sin\alpha}{c\omega} \tag{14}$$

$$\cos^2\alpha + \sin^2\alpha = 1 = \left(\frac{A_R}{A_B} \cdot \frac{k-m\omega^2}{m\omega^2}\right)^2 + \left(\frac{A_R}{A_B} \cdot \frac{c\omega}{m\omega^2}\right)^2 \tag{15}$$

$$\left(\frac{A_R}{A_B}\right)^2 = \frac{\omega^4 m^2}{(k-m\omega^2)^2 + (c\omega)^2} = \frac{\left(\frac{\omega}{\omega_n}\right)^4}{\left(1 - \left(\frac{\omega}{\omega_n}\right)^2\right)^2 + \left(\frac{c}{m\omega_n} \cdot \frac{\omega}{\omega_n}\right)^2} \tag{16}$$

or with $\eta = \frac{\omega}{\omega_n}$ and $\zeta = \frac{c}{2m\omega_n}$

$$\frac{A_R}{A_B} = \frac{\eta^2}{\sqrt{(1-\eta^2)^2 + (2\zeta\eta)^2}} \tag{17}$$

Correspondingly from equation (14):

$$\alpha = \arctan \frac{c\omega}{k-m\omega^2} = \arctan \frac{2\zeta\eta}{1-\eta^2} \tag{18}$$

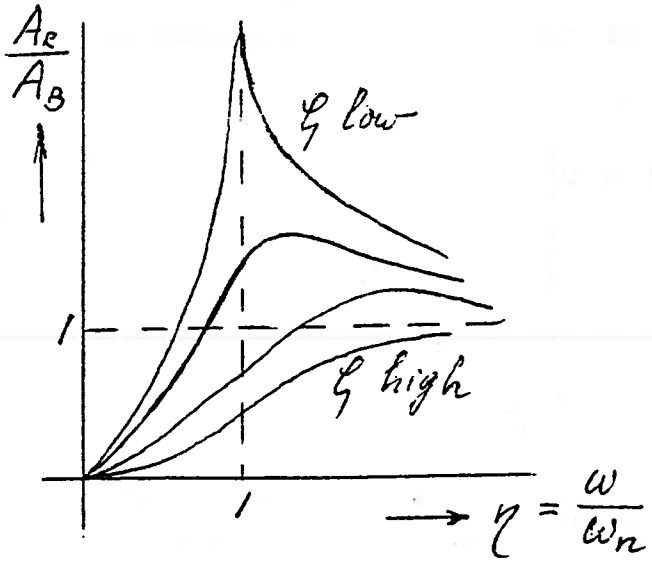

Fig. 4: Amplitude response of vibrometer

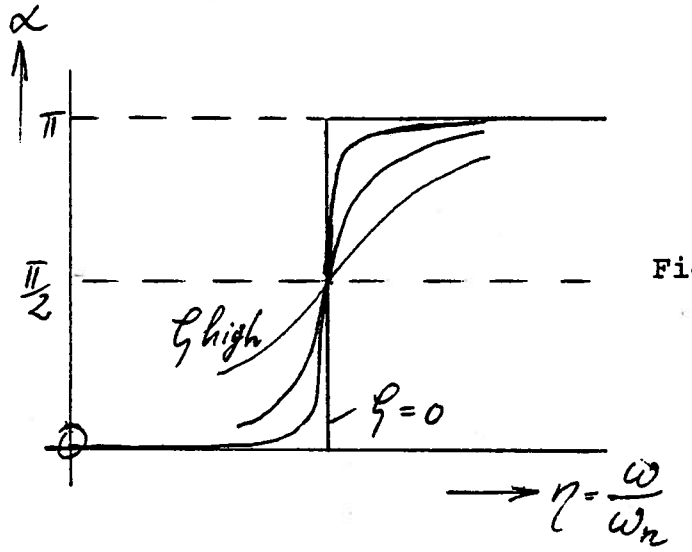

Fig. 5: Phase response of vibrometer and accelerometer

The amplitude response of the instrument is shown in Fig. 4. The magnification factor A_R/A_B is fairly constant in the higher frequency range whereas it varies rapidly at and below frequencies near $\eta = 1$, $\omega = \omega_n$.

In practical application we therefore want to limit the use of the instrument as a vibrometer to the range of higher frequencies where the amplitude distortion (deviation from $A_R/A_B = 1.$) remains within specified limits.

This leads to the conclusion that a vibrometer should be built with the lowest feasible natural frequency so that it remains reliable down to relatively low excitation frequencies. A soft spring and a heavy mass are hence desirable, but size and weight impose practical limits on the design.

As an illustration one may study the problem of selecting vibrometer damping for the widest permissible frequency range if an amplitude error of, say, 10 percent is the specified tolerance.

Finally a word about phase errors. Take for example a signal

$$x_{B_1} = A_{B_1} \cdot e^{i\omega_1 t} \tag{19}$$

which will be recorded as

$$x_{R_1} = A_{B_1} \cdot \frac{A_{R_1}}{A_{B_1}} \quad e^{i(\omega_1 t - \alpha_1(\omega_1))} \tag{20}$$

The time shift of the recording relative to the signal is

$$t_1 = \frac{\alpha_1(\omega_1)}{\omega_1} \tag{21}$$

Analogously for any second signal of frequency ω_2

$$t_2 = \frac{\alpha_2(\omega_2)}{\omega_2} \tag{22}$$

The time shifts are the same only if α is linearly proportional to the frequency ω. This is strictly true only for the instrument of zero damping below $\eta = 1$. Otherwise a certain phase error occurs.

But satisfactory operation will also be possible for intermediate damping near the resonance where the phase curves are approximately straight, and at very high frequencies where $\alpha_1 \approx \alpha_2 = \omega t$ and $\omega_1 \approx \omega_2$ for practical purposes.

In general the phase distortion is only of secondary importance, and will not govern the design of the instrument.

B. Velocity Measurement

The differential equation (11) yields by differentiation

$$m\ddot{\ddot{x}}_R + c\ddot{x}_R + k\dot{x}_R = m\ddot{\ddot{x}}_B \tag{23}$$

or with the velocities $V_R = \dot{x}_R$, and $V_B = \dot{x}_B$

$$m\ddot{V}_R + c\dot{V}_R + kV_R = m\ddot{V}_B \tag{24}$$

This equation is analogous to (11) and the same response considerations hold. But note that the pick-up must now sense velocity rather than displacement.

C. Acceleration Measurement, Accelerometer

For the accelerometer, we rewrite equation (11) as

$$m\ddot{x}_R + c\dot{x}_R + kx_R = a_B m e^{i\omega t} \tag{25}$$

where a_B the acceleration amplitude. Then from the response of the mass-excited single degree of freedom system

$$\frac{\frac{A_R}{a_B m}}{k} = \frac{A_R \cdot \omega_n^2}{a_B} = \frac{1}{\sqrt{(1-\eta^2)^2 + (2\zeta\eta)^2}} \tag{26}$$

This function is fairly constant for low values of η so that the accelerometer ought to be designed for high ω_n and operated with $\omega<\omega_n$. This is the contrary of the vibrometer. The phase response, however, is the same as before.

3. THE VIBRATION ABSORBER

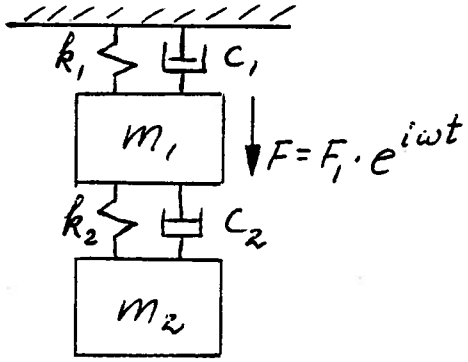

Fig. 6: Vibration Absorber

If a given single-degree of freedom system (m_1, k_1, c_1) vibrates excessively at or near its resonant frequency, $\omega_n = \sqrt{k_1/m_1}$, due to the excitation $F = F_1 \cdot e^{i\omega t}$ it may be advantageous to add a second elastic system (m_2, k_2, c_2) in order to obviate the resonant vibrations by the so-called absorber effect.

To understand the principles of vibration absorbers we have to examine the steady-state response of a two degree of freedom system as shown in Fig. 6.

The differential equations for the motions of the two masses are:

$$m_1\ddot{x}_1 + (c_1+c_2)\dot{x}_1 + (k_1+k_2)x_1 - c_2\dot{x}_2 - k_2x_2 = F_1 \cdot e^{i\omega t} \tag{27}$$

$$m_2\ddot{x}_2 + c_2\dot{x}_2 + k_2x_2 - c_2\dot{x}_1 - k_2x_1 = 0 \tag{28}$$

Let the complex solution:

$$\left.\begin{aligned} \vec{x}_1 &= \bar{x}_1 \cdot e^{i\omega t} \\ \vec{x}_2 &= \bar{x}_2 \cdot e^{i\omega t} \end{aligned}\right\} \tag{29}$$

Substituting:

$$\left.\begin{aligned} &[(k_1+k_2) - m_1\omega^2 + i(c_1+c_2)\omega]\ \bar{x} - (k_2+ic_2\omega)\ \bar{x}_2 = F_1 \\ &-(k_2+ic_2\omega)\ \bar{x}_1 + [k_2-m_2\omega^2+ic_2\omega]\ \bar{x}_2 = 0 \end{aligned}\right\} \tag{30}$$

The steady-state response is obtained from this complex set of equations by means of Kramer's rule:

$$\bar{x}_1 = x_1 \cdot e^{-i\phi_1} = \frac{\begin{vmatrix} F_1 & -(k_2 + ic_2\omega) \\ 0 & k_2 - m_2\omega^2 + ic_2\omega \end{vmatrix}}{D(\omega)} \tag{31a}$$

$$\bar{x}_2 = x_2 \cdot e^{-i\phi_2} = \frac{\begin{vmatrix} k_1 + k_2 - m_1\omega^2 + i(c_1+c_2)\omega & F_1 \\ -(k_2 + ic_2\omega) & 0 \end{vmatrix}}{D(\omega)} \tag{31b}$$

$$\text{where } D(\omega) = \begin{vmatrix} k_1+k_2-m_1\omega^2+i(c_1+c_2)\omega & -(k_2+ic_2\omega) \\ -(k_2+ic_2\omega) & k_2-m_2\omega^2+ic_2\omega \end{vmatrix} \tag{31c}$$

Let us discuss the simplified case of the undamped system: $c_1 = c_2 = 0$. There, obviously, only the real parts are retained, and $\phi_1 = \phi_2 = 0$.

$$\left.\begin{aligned} x_1 &= \frac{F_1 (k_2 - m_2\omega^2)}{D(\omega)} \\ x_2 &= \frac{F_1 k_2}{D(\omega)} \\ D(\omega) &= (k_1 + k_2 - m_1\omega^2)(k_2 - m_2\omega^2) - k_2^2 = \\ &= m_1 \cdot m_2 (\omega_1^2 - \omega^2) \cdot (\omega_2^2 - \omega^2) \end{aligned}\right\} \quad (32)$$

The last result is known from the transient response solution for the natural frequencies of the system, ω_1 and ω_2.

The steady-state response is therefore of the form:

$$\left.\begin{aligned} x_1 &= \frac{F_1 (k_2 - m_2\omega^2)}{m_1 m_2 (\omega_1^2 - \omega^2)(\omega_2^2 - \omega^2)} \\ x_2 &= \frac{F_1 k}{m_1 m_2 (\omega_1^2 - \omega^2)(\omega_2^2 - \omega^2)} \end{aligned}\right\} \quad (33)$$

The two-mass system has of course two resonant conditions at $\omega = \omega_1$, and $\omega = \omega_2$. But the original resonance at $\omega_n = \sqrt{k_1/m_1}$ does not appear any more. In fact, we can select m_2 and k_2 so that x_1 vanishes at the original resonant frequency:

or

$$\left.\begin{aligned} k_2 - m_2\omega_n^2 &= 0 \\ k_2 - m_2 \frac{k_1}{m_1} &= 0 \end{aligned}\right\} \quad (34)$$

Hence, if we ensure suitable tuning of the added mass-spring system:

$$\boxed{\frac{k_1}{m_1} = \frac{k_2}{m_2}} \quad (35)$$

we have cancelled any motion of the mass m_1. This is obviously at the expense of two new resonances not too far from the original one. It can be shown that the frequencies ω_1, ω_2 depend on the ratio of the masses m_2/m_1 as shown in Fig. 7. The frequency response of the system is shown in the magnification factor diagrams, Fig. 8 and Fig. 9.

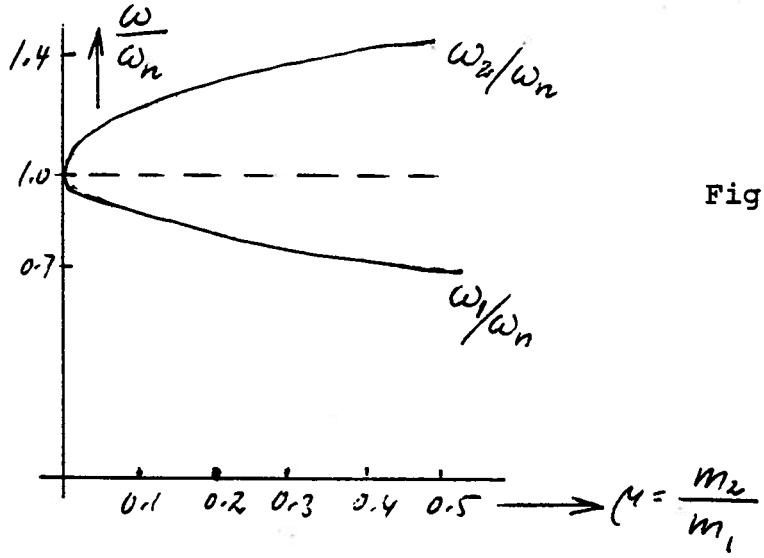

Fig. 7: Natural frequencies ω_1, ω_2 against mass ratio.

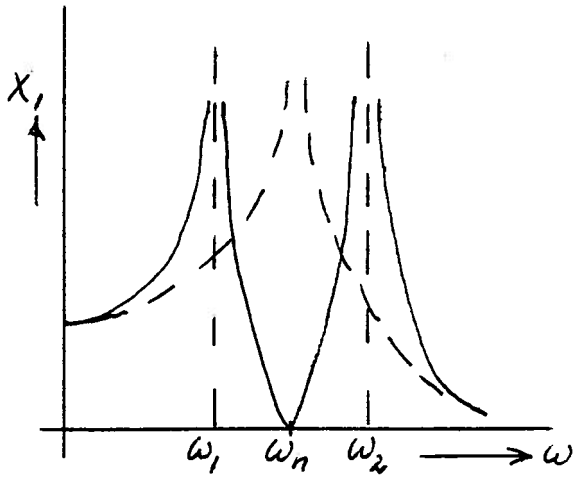

Fig. 8: Response of mass m_1

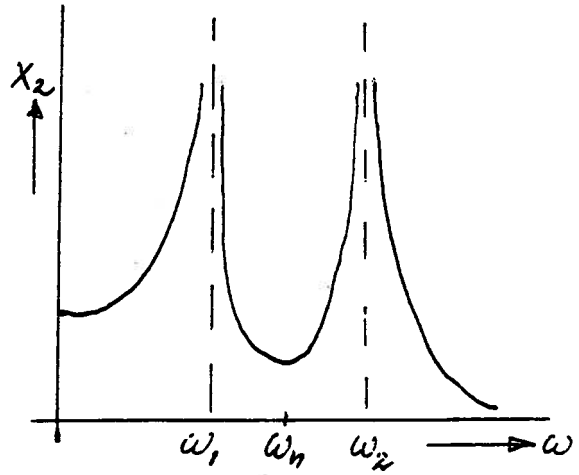

Fig. 9: Response of mass m_2

The absorber is effective only in a relatively small frequency range as shown in Fig. 8, where the dashed line represents the response of the original system (undamped). The economy of size in the design usually prevents m_2/m_1 from reaching any significant values so that the band between ω_1 and ω_2 is fairly narrow in most practical cases. The range where the absorber is superior to the original system is only a fraction of that range.

Moreover, if damping is introduced ($c_1 \neq 0$, $c_2 \neq 0$, the response curves flatten out, and the gains due to the absorber at the resonant frequency are reduced, sometimes very drastically, Fig. 10.

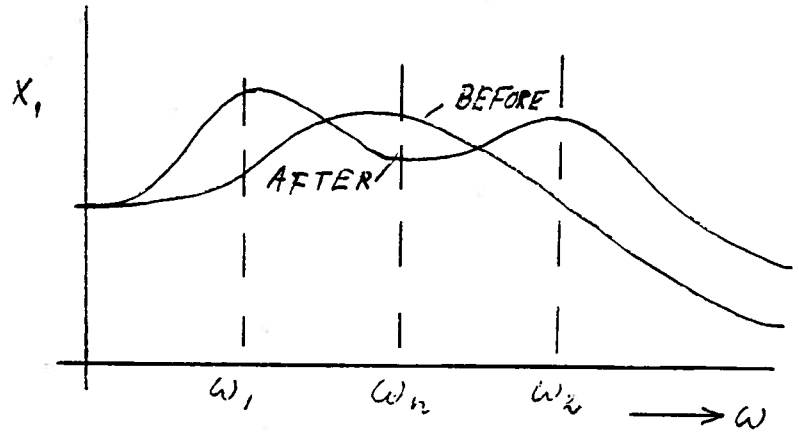

Fig. 10: Influence of damping on neutralizer effect.

Nevertheless, the absorber may find useful application in reducing local shipboard vibrations whenever a narrow, steep resonance needs to be removed.

4. MARINE SHAFTING VIBRATIONS

4.1 The Substitution System.

Shaft vibrations are common in any type of rotating machinery, and marine shafting systems are frequently subject to some torsional and longitudinal vibration. These vibrations may be excited by the engine whose gas torques are not uniform during each revolution, and by the propeller operating in a nonuniform wake field.

The systems under consideration may be direct drive or geared, turbine or diesel driven, single or multiple engine per shaft etc.

Shafting systems have characteristic mass concentrations at certain stations, for example at the cylinders of a diesel engine. It is therefore a natural conclusion to deal with these systems as discrete multi-mass systems, lumping the heavy masses at their stations and treating the stiffness between consecutive stations as torsional or longitudinal springs.

For some elements of the shafting system the quantities mass, moment of inertia, and stiffness can be found in an elementary, although sometimes tedious manner. This may be true for the inertia of a turbine rotor, or the stiffness of straight shafting elements. But the following other elements require some special consideration:

<u>The moment of inertia of piston, connecting rod, crank etc.:</u>

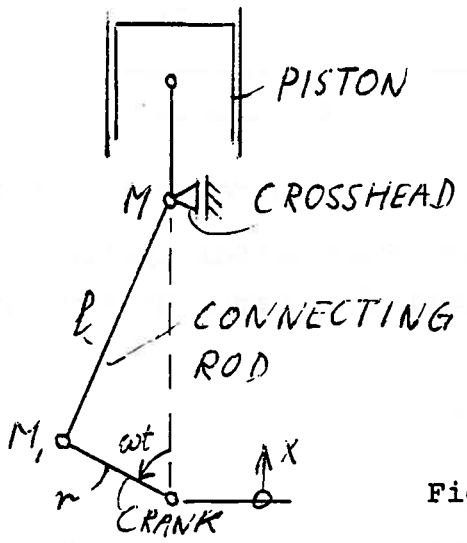

To determine the contribution of the piston and its drive to the rotary inertia at the station of a given cylinder, we want to lump all reciprocating masses at the crosshead (M) and treat the others as follows:

Fig. 11: Geometry of drive.

a) <u>The crank</u>: Determine the mass moment of inertia about the crankshaft axis, I_c, and put the equivalent mass $m_c = I_c/r^2$ at the crankpin.

b) Connecting rod: Find moment of inertia, I_r, about crosshead, and put equivalent mass $m_r = I_r/\ell^2$ at crankpin. The difference between the actual mass of the rod and m_r is placed at the crosshead $(m - m_r)$.

In summary, we find:

At the crosshead: Mass M = piston, piston rod, crosshead, $m - m_r$

At the crankpin : Mass $M_1 = m_c + m_r$

In the next step, we want to find the kinetic energy of two masses and then equate it to that of an equivalent disk.

The crankshaft rotates at the speed ω (rad/sec). The velocity of M_1 is: $V_1 = \omega r$.

To find the velocity of M, we express the location of the crosshead x:

$$x = r \cdot \cos \omega t + \ell \cos \alpha \tag{36}$$

With:

$$\cos \alpha = \sqrt{1 - \sin^2\alpha} = \sqrt{1 - \left(\frac{r}{\ell}\right)^2 \sin^2\omega t}$$

and for $\ell >> r$

$$\cos \alpha \approx 1 - \frac{1}{2}\left(\frac{r}{\ell}\right)^2 \sin^2\omega t \tag{37}$$

$$x \approx r \cdot \cos \omega t + \ell - \frac{r^2}{2\ell} \sin^2\omega t \tag{38}$$

$$\dot{x} \approx -r\omega \sin \omega t - \frac{r^2\omega}{2\ell} \cdot \underbrace{2 \sin \omega t \cdot \cos \omega t}_{\sin 2 \omega t} \tag{39}$$

Kinetic energy at time t:

$$T = \frac{M_1}{2} (\omega r)^2 + \frac{M}{2} (\omega r)^2 \{\sin \omega t + \frac{r}{2\ell} \sin 2\omega t\}^2 \tag{40}$$

Average kinetic energy during cycle

$$\text{Period:}\quad T_P = \frac{2\pi}{\omega}$$

$$\bar{T} = \frac{\omega}{2\pi} \int_0^{T_P} \{M_1 \frac{(\omega r)^2}{2} + M \frac{(\omega r)^2}{2} [\sin \omega t + \frac{r}{2\ell} \sin 2\omega t]^2\} dt = \quad (41a)$$

$$\bar{T} = \frac{1}{2} \left\{ M_1 + \frac{M}{2} \left(1 + \frac{r^2}{4\ell^2} \right) \right\} (\omega r)^2 \quad (41b)$$

The kinetic energy of an equivalent disk is:

$$\frac{I_e \omega^2}{2}$$

hence the moment of inertia

$$I_e = \left[M_1 + \frac{M}{2} \left(1 + \frac{r^2}{4\ell^2} \right) \right] r^2 \quad (42)$$

Propeller inertia:

Determine the mass moment of inertia by integration (or experiment), and add correction for added mass.

Crude approximation: 25 percent increase.

Refined formulas accounting for hydrodynamic effects more accurately are available, for example: C. Kruppa, High-Speed Propeller Design, Lecture Notes, The University of Michigan.

Stiffness of the crankshaft

The torsional stiffness of a crank is defined as

$$k = \frac{M}{\Theta} \quad (43)$$

where M = the torque applied, maybe unit torque,

Θ = the angular displacement produced by M

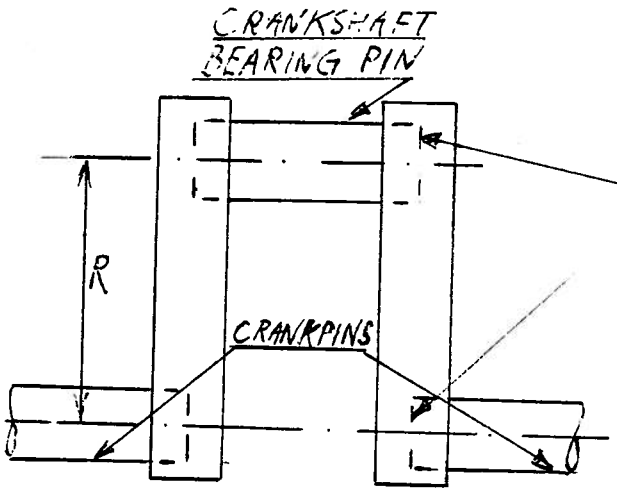

Pins extended halfway into cheeks to account for elasticity of cheek mounting.

Fig. 12: Crank

The geometry of the crank permits two ways of applying a torque resulting in two different deformations of the crankshaft element:

a) If a pure torque M is applied to two neighboring crankpins, the three pins will deflect torsionally and the crank cheeks will experience a bending moment M; they must be treated as cantilever beams. The total angular displacement is then composed of five contributions, and the stiffness is determined like for five springs in series.
This type of crankshaft torsion is called torsion of the first kind. Note that the presence of the bearings which will influence the bending deflections is disregarded in this approach.

b) If discrete circumferential forces are applied to two neighboring crankpins we speak of torsion of the second kind. The pin in the crankshaft axis will still be under torsion and the cheeks are being bent, but the crankpins are free of torsion.

In actuality, both types of torsion are always present in engines. Strictly speaking, one would have to use a mixed stiffness definition. But in practice, one is usually satisfied with the simplified stiffness concept associated with torsion of the first kind.

For more detail see: Biezeno-Grammel, Technische Dynamik, Springer-Verlag.

Engine damping:

Damping in diesel engines is primarily due to the frictional losses in the lubricating films in the cylinder and in the bearings. There may also be some structural damping caused by the hysteresis properties of the material and by bearing slack.

Since these types of damping have been too difficult to separate in experiment or analysis, results of measurements were usually interpreted as cylinder damping coefficients because most of the losses presumably occur in the cylinders. Cylinder damping coefficients C_{CYL} are defined so that the damping torque can be expressed as:

$$M_{CYL} = C_{CYL} \cdot \dot{\theta}_{CYL} \tag{44}$$

$\dot{\theta}_{CYL}$ = angular velocity of crankshaft at cylinder (rad/sec)

For numerical values see Handbook of Torsional Vibrations, British Internal Combustion Engine Research Association, London, editor: Nestorides.

Propeller damping:

The hydrodynamic effects of propeller damping in torsional and longitudinal shaft vibrations are not fully understood. The literature shows considerable disagreement as to the magnitude of the damping torque and longitudinal force. The torsional and longitudinal vibrations are usually coupled, and their

measurement requires special apparatus and careful dynamic analysis. (See Wereldsma, Experiments on Vibrating Propeller Models, TNO Report No. 70M, Netherlands' Research Centre T.N.O. for Shipbuilding and Navigation, March 1965).

The following summarizes some of the conventional methods of estimating propeller damping in torsional vibrations.

The quasisteady method assumes very slow propeller motions (frequency $\omega \to 0$) and uses propeller open water test data to predict torque variations with rotational speed. The damping torque is expressed linearly as

$$T_D = C_P \cdot \dot{\theta}$$

where the propeller damping coefficient (45)

$$C_P \approx \frac{a \cdot Q}{N}$$

Q = steady average torque
N = number of revolutions/min.

The factor a is given as follows:

a = 30 (average) in the BICERA handbook quoted above.
a = 20...50 depending on pitch and blade area ratio for Wageningen B - series, according to Archer, Institute of Mechanical Engineers, 1951.

Den Hartog, Mechanical Vibrations, McGraw-Hill Book Co., New York, recommends multiplying the quasisteady coefficient by 1.5 to account for dynamic effects.

Wereldsma (see reference above) measured damping values that were above quasisteady predictions, but were in good agreement with predictions by Dernedde based on an asymptotic high-frequency theory utilizing two-dimensional foil theory.

Other results from high-frequency asymptotic theories by Lewis and Auslander (Journal of Ship Research 1960) and Schmiechen (Proceedings, 11th ITTC, Tokyo) are, however, considerably lower than the quasisteady predictions.

The reference by Schmiechen gives a good survey of the state of knowledge in torsional and longitudinal propeller damping including coupling effects.

Propeller excitation:

A fair amount of data is available on unsteady propeller forces exciting both shaft and hull vibrations. The subject will be presented in a later section on propeller excitation.

At this time, let us just assume that the given excitation torque can be expressed as a Fourier series:

$$T = \sum_{n=1}^{\infty} t_{on} \cdot e^{-i\alpha_n} \cdot e^{in\omega t} \qquad (46)$$

where t_{on} = amplitude of n'th torque harmonic

α_n = phase angle of n'th torque harmonic

ω = circular frequency corresponding to one revolution = $2\pi \cdot RPM/60$

Engine excitation

Harmonic analysis will also be applied to the gas torques of each cylinder, and exactly the same expression will be used as above.

Note, however, that for four-stroke engines one engine cycle corresponds to two revolutions so that the fundamental frequency becomes:

$$\omega = \frac{2\pi \cdot RPM}{60 \cdot 2} \qquad (47)$$

Amplitude (and phase) data for the gas torque harmonics can best be derived fron cylinder pressure measurements. In earlier design stages one may also use the systematic data compiled in the BICERA handbook for various typical engines.

The phase of the cylinders is usually related to cylinder no. 1 according to the firing sequence and crankshaft configuration. Section 4.5 will give a more specific example.

4.2 Torsional Vibrations, Natural Frequencies

The substitution system whose torsional natural frequencies we want to determine consists of N masses of mass moment of inertia I_n, and (N-1) shaft elements of stiffness k_n. Figure 13 illustrates the situation for a system of four masses. Θ_n are the angular displacements.

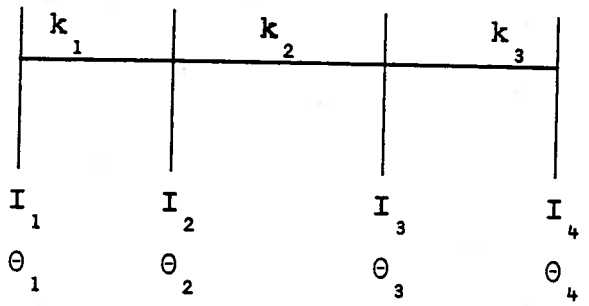

Fig. 13 Torsional system

The differential equations for each of the masses are as follows:

$$\left.\begin{aligned}
I_1\ddot{\Theta}_1 + k_1(\Theta_1-\Theta_2) &= 0\\
I_2\ddot{\Theta}_2 + k_1(\Theta_2-\Theta_1) + k_2(\Theta_2-\Theta_3) &= 0\\
I_3\ddot{\Theta}_3 + k_2(\Theta_3-\Theta_2) + k_3(\Theta_3-\Theta_4) &= 0\\
I_4\ddot{\Theta}_4 + k_3(\Theta_4-\Theta_3) &= 0
\end{aligned}\right\} \qquad (48)$$

Let us assume a solution of the form:

$$\Theta_1 = A_1 \cdot e^{i\omega t},\ \Theta_2 = A_2 \cdot e^{i\omega t},\ \text{etc.} \qquad (49)$$

Substituting:

$$\left.\begin{aligned}(-I_1\omega^2 + k_1)A_1 - k_1A_2 &= 0\\ (-I_2\omega^2 + k_1 + k_2)A_2 - k_1A_1 - k_2A_3 &= 0\end{aligned}\right\} \qquad (50a)$$

$$\left.\begin{aligned}(-I_3\omega^2 + k_2 + k_3)A_3 - k_2A_2 - k_3A_4 &= 0\\ (-I_4\omega^2 + k_3)A_4 - k_3A_3 &= 0\end{aligned}\right\} \qquad (50b)$$

This set of algebraic equations is equivalent to the frequency equation. But instead of determining the natural frequencies ω_{nj} ($j = 1, \ldots, 4$) directly by solving an equation of the order 2N, we apply a convenient recursive scheme, the well-known Holzer method. For this purpose we rewrite the equations.

$$\left.\begin{aligned}A_2 &= A_1 - \frac{I_1\omega^2A_1}{k_1}\\ A_3 &= A_2 - \frac{I_2\omega^2A_2}{k_2} + \frac{k_2A_2 - k_1A_1}{k_2} =\\ &= A_2 - \frac{I_2\omega^2A_2 + I_1\omega^2A_1}{k_2}\\ A_4 &= A_3 - \frac{I_3\omega^2A_3}{k_3} + \frac{k_3A_3 - k_2A_2}{k_3} =\\ &= A_3 - \frac{I_3\omega^2A_3 + I_2\omega^2A_2 + I_1\omega^2A_1}{k_3}\end{aligned}\right\} \qquad (51)$$

Or, in general form

$$A_{n+1} = A_n - \frac{\sum_{i=1}^{n} I_i\omega^2A_i}{k_n} \qquad (52)$$

This recursive equation has a physical interpretation that becomes evident from the formulation:

$$k_n(A_{n+1} - A_n) = -\sum_{i=1}^{n} I_i\omega^2 A_i \qquad (52a)$$

If we free the left-hand end of the system just to the left of mass (n+1) the shaft element k_n will have the sum of the inertia torques up to mass n acting on its left-hand end. This torque is balanced by the elastic restoring torque due to the deformation of this element, $A_{n+1} - A_n$.

By adding up the equations (48) we obtain an overall dynamic equilibrium condition of the system:

$$\sum_{i=1}^{N} I_i\ddot{\theta}_i = 0, \text{ or algebraically: } \sum_{i=1}^{N} (-I_i\omega^2 A_i) = 0 \qquad (53)$$

The sum of the inertia torques must vanish for a free vibration to be possible.

The foregoing deductions lead to the following <u>solution procedure</u> (Holzer scheme):

1. Estimate a natural frequency ω.
2. Assume $A_1 = 1.$ at one end of the system.
3. Determine all other amplitudes recursively according to equation (52).
4. For the final station N check if the equation (53), the closing condition, is satisfied.
5. If the estimate of ω was wrong make a new estimate and iterate until satisfactory agreement with the closing condition is reached.

The computations can be conveniently arranged in tabular form.

①	②	③	④	⑤	⑥	⑦	⑧
STA n	I_n	$I_n\omega^2$	A_n	$I_n\omega^2 A_n$	$\sum_{i=1}^{n} I_i\omega^2 A_i$	k_n	$\frac{\Sigma I_i\omega^2 A_i}{k_n}$
1	I_1	---	1.0	$I_1\omega^2$	----	k_1	----
2	I_2	---	④$_{n-1}$-⑧$_{n-1}$	③$_n$ · ④$_n$	⑥$_{n-1}$+⑤$_n$	k_2	⑥ / ⑦
3	I_3	---	-----			k_3	
4	I_4	---	-----		⑧		
Given					Must be zero for correct frequency.	Given	

HOLZER - TABLE

The solution can be greatly accelerated by using a plot of the closing torque from column ⑥$_N$ against frequency and seeking guidance from the mode shape. Figure 14 illustrates the relation between closing torque, frequency, and mode shape.

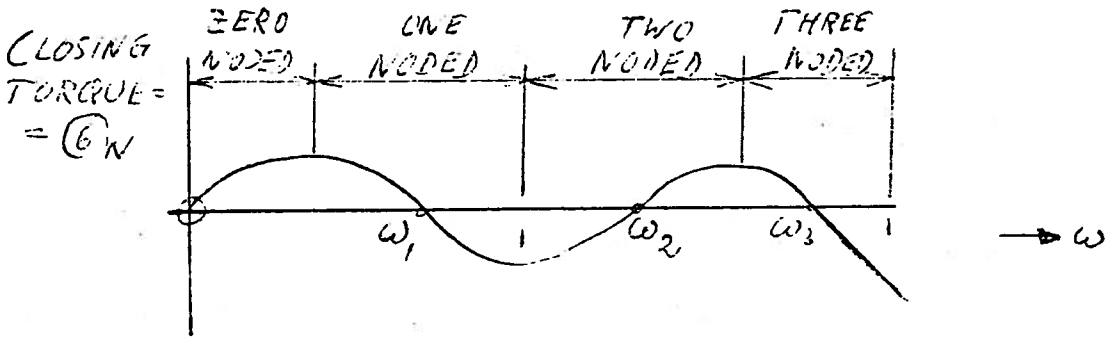

Fig. 14: Frequency behavior of closing torque and node character.

4.3 Longitudinal Vibrations, Natural Frequencies

Longitudinal vibrations are very similar to torsional vibrations of shafting systems. The main difference is that the system is built in at one end at the thrust bearing, Fig. 15.

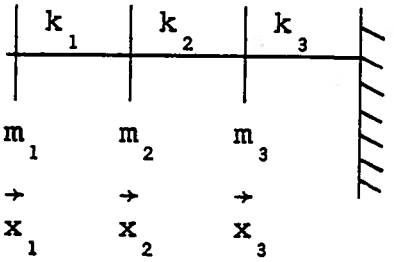

Fig. 15: Longitudinal shaft vibration system

The model of the system ought to include the propeller mass (m_1), shaft stiffness (k_1), and the masses and stiffnesses of the thrust bearing and, its foundation (m_2, m_3, k_2, k_3). The fixed point is to be assumed in the ship under the bearing foundation.

The differential equations are analogous to equation (48) except for a minor difference at the built-in end.

$$\left.\begin{aligned} m_1\ddot{x}_1 + k_1(x_1 - x_2) &= 0 \\ m_2\ddot{x}_2 + k_1(x_2 - x_1) + k_2(x_2 - x_3) &= 0 \\ m_3\ddot{x}_3 + k_2(x_3 - x_2) + k_3x_3 &= 0 \end{aligned}\right\} \qquad (54)$$

The recursive equation is obtained in analogy to equations (50) and (51):

$$A_{n+1} = A_n - \frac{\sum_{i=1}^{n} m_i\omega^2 A_i}{k_n} \qquad (55)$$

The same Holzer table can be used, but the closing condition is different. Instead of a free end, we have a built-in end this time so that the amplitude at the wall must be zero. If we carry the Holzer table to the amplitude predictions at station N + 1, the closing condition is

$$A_{N+1} = \text{col. } ④_{N+1} = 0 \tag{56}$$

We iterate for the correct natural frequencies just as before. See Figure 16.

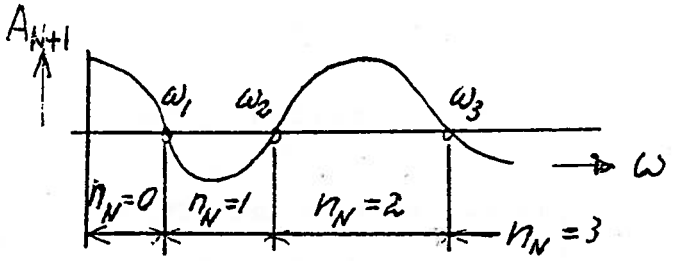

n_N = number of nodes .

Fig. 16: Amplitude - Frequency Relation

4.4 Geared and Branched Torsional Systems

a) Geared System

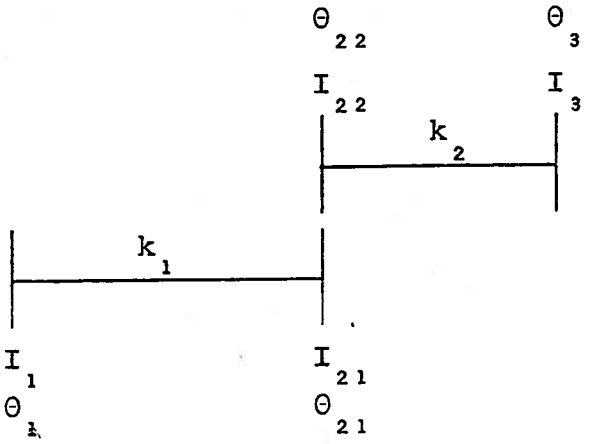

GEAR RATIO:

$$n = \frac{\Theta_{22}}{\Theta_{21}}$$

Fig. 17: Geared System

In dealing with multi-speed systems as described in Fig. 17 we find it convenient to transform the system into one of constant speed using suitable equivalent masses and stiffness coefficients. The energy theorem will be used to derive the equations of motion of the system. The system is conservative, hence:

$$\frac{d}{dt}(T + V) = \dot{T} + \dot{V} = 0 \tag{57}$$

The kinetic energy:

$$2T = I_1\dot{\theta}_1^2 + I_{21}\dot{\theta}_{21}^2 + I_{22}\dot{\theta}_{22}^2 + I_3\dot{\theta}_3^2 =$$

$$= I_1\dot{\theta}_1^2 + (I_{21} + n^2 I_{22}) \cdot \dot{\theta}_{21}^2 + I_3\dot{\theta}_3^2 \tag{58}$$

The potential energy:

$$2V = k_1(\theta_1 - \theta_{21})^2 + k_2(\theta_{22} - \theta_3)^2 =$$

$$= k_1(\theta_1^2 - 2\theta_1\theta_{21} + \theta_{21}^2) + k_2(n^2\theta_{21}^2 - 2n\theta_{21}\theta_3 + \theta_3^2) \tag{59}$$

The derivatives:

$$\left.\begin{aligned} \dot{T} &= I_1\dot{\theta}_1\ddot{\theta}_1 + (I_{21} + n^2 I_{22})\dot{\theta}_{21} \cdot \ddot{\theta}_{21} + I_3\dot{\theta}_3\ddot{\theta}_3 \\ \dot{V} &= k_1(\theta_1\dot{\theta}_1 - \theta_1\dot{\theta}_{21} - \dot{\theta}_1\theta_{21} + \theta_{21}\dot{\theta}_{21}) + \\ &+ k_2(n^2\theta_{21}\dot{\theta}_{21} - n\theta_{21}\dot{\theta}_3 - n\dot{\theta}_{21}\theta_3 + \theta_3\dot{\theta}_3 \end{aligned}\right\} \tag{60}$$

Equating coefficients in equation (60) for terms in $\dot{\theta}_1$, $\dot{\theta}_2$, $\dot{\theta}_3$:

$$\left.\begin{aligned} I_1\ddot{\Theta}_1 + k_1(\Theta_1 - \Theta_{21}) &= 0 \\ I_{2e}\ddot{\Theta}_2 + k_1(\Theta_{21} - \Theta_1) + k_{2e}(\Theta_{21} - \tfrac{\Theta_3}{n}) &= 0 \\ I_3\ddot{\Theta}_3 + k_2(\Theta_3 - n\Theta_{21}) &= 0 \end{aligned}\right\} \qquad (61)$$

where

$$\begin{aligned} I_{2e} &= I_{21} + n^2 I_{22} \\ k_{2e} &= n^2 k_2 \end{aligned} \qquad (62)$$

Introducing $\overline{\Theta}_3 = \Theta_3/n$ and $I_{3e} = n^2 I_3$ the last equation becomes

$$I_{3e} \cdot \ddot{\overline{\Theta}}_3 + k_{2e}(\overline{\Theta}_3 - \Theta_{21}) = 0 \qquad (63)$$

We have now converted the original system into the single-line system shown in Fig. 18. This can be treated in the usual way. The generalization for more than one gear is obvious.

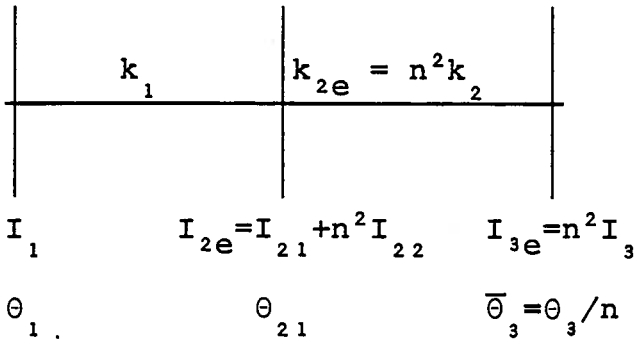

Fig. 18: Single-line replacement of geared system.

b) Branched System

Branched systems are frequent in ship shafting installations either as twin-screw or as twin-engine systems. The figure at the bottom of page 37 shows an example for which we will derive

the equations of motions by means of the energy method as before. The gear ratios are n_1, and n_2. The equivalent moments of inertia I_{2e}, I_{3e}, I_{4e} and the stiffnesses k_{23e}, and k_{24e} are also found on page 37.

For the kinetic energy of the system:

$$2T = I_1\dot{\theta}_1^2 + I_{20}\dot{\theta}_{20}^2 + I_{21}n_1^2\dot{\theta}_{20}^2 + I_{3e}\dot{\bar{\theta}}_3^2 + I_{22}n_2^2\dot{\theta}_{20}^2 + I_{4e}\dot{\bar{\theta}}_4^2 \tag{64}$$

Potential energy:

$$2V = k_1(\theta_1 - \theta_{20})^2 + k_{23}(\bar{\theta}_3 - \theta_{21})^2 + k_{24} \cdot (\bar{\theta}_4 - \theta_{22})^2 \tag{65}$$

The derivatives:

$$\left.\begin{aligned}\dot{T} = {} & I_1\dot{\theta}_1\ddot{\theta}_1 + I_{20}\dot{\theta}_{20}\ddot{\theta}_{20} + I_{21}n_1^2\dot{\theta}_{20} \cdot \ddot{\theta}_{20} + I_{3e}\dot{\bar{\theta}}_3\ddot{\bar{\theta}}_3 + \\ & + I_{22}n_2^2\dot{\theta}_{22}\ddot{\theta}_{22} + I_{4e}\dot{\bar{\theta}}_4\ddot{\bar{\theta}}_4 = \\ & = I_1\dot{\theta}_1\ddot{\theta}_1 + I_{2e}\dot{\theta}_{20}\ddot{\theta}_{20} + I_{3e}\dot{\bar{\theta}}_3 \cdot \ddot{\bar{\theta}}_3 + I_{4e}\dot{\bar{\theta}}_4 \cdot \ddot{\bar{\theta}}_4\end{aligned}\right\} \tag{66}$$

$$\left.\begin{aligned}\dot{V} = {} & k_1 \cdot (\theta_1\dot{\theta}_1 - \theta_1\dot{\theta}_{20} - \dot{\theta}_1 \cdot \theta_{20} + \theta_{20} \cdot \dot{\theta}_{20}) + \\ & + k_{23e}(\bar{\theta}_3\dot{\bar{\theta}}_3 - \bar{\theta}_3 \cdot \dot{\theta}_{20} - \dot{\bar{\theta}}_3\theta_{20} + \theta_{20}\dot{\theta}_{20}) + \\ & + k_{24e}(\bar{\theta}_4\dot{\bar{\theta}}_4 - \bar{\theta}_4 \cdot \dot{\theta}_{20} - \dot{\bar{\theta}}_4\theta_{20} + \theta_{20} \cdot \dot{\theta}_{20})\end{aligned}\right\} \tag{67}$$

Equating coefficients:

$$
\left.
\begin{aligned}
I_1\ddot{\Theta}_1 + k_1(\Theta_1 - \Theta_{20}) &= 0 \\
I_{2e}\ddot{\Theta}_{20} + k_1(\Theta_{20}-\Theta_1) + k_{23e}(\Theta_{20}-\overline{\Theta}_3) + k_{24e}(\Theta_{20}-\overline{\Theta}_4) &= 0 \\
I_{3e}\ddot{\overline{\Theta}}_3 + k_{23e}(\overline{\Theta}_3 - \Theta_{20}) &= 0 \\
I_{4e}\ddot{\overline{\Theta}}_4 + k_{24e}(\overline{\Theta}_4 - \Theta_{20}) &= 0
\end{aligned}
\right\} \qquad (68)
$$

These equations are analogous to equation (48) except for the branching feature. The algebraic equivalent of these equations, analogous to equation (50), can be obtained by substituting harmonic motions

$$\Theta_1 = A_1 e^{i\omega t}, \quad \Theta_{20} = A_{20} \cdot e^{i\omega t}, \text{ etc.} \qquad (69)$$

We want to limit the discussion to a summary of the special features of the Holzer procedure for branched systems, see page 37. The following steps are required:

1. Estimate a frequency ω as before.
2. Start at the branched end of the system (not necessary, but preferred here). Assume an amplitude for the upper branch, say $\overline{A}_3 = 1$. Predict the amplitude A_{20} at the junction.
3. Assume $\overline{A}_4 = 1$ at the lower branch and predict an amplitude $\hat{A}_{20}$ at the junction. In general, $\hat{A}_{20}$ will differ from A_{20} so that we have to correct $\overline{A}_4$ for agreement.
4. Assume $\overline{A}_4 = A_{20}/\hat{A}_{20}$, and treat the lower branch anew. The amplitude A_{20} at the junction must now conform with the upper branch.
5. Transfer the inertia torques, col. ⑥ , from the two branches to the single-line part of the system and add the contribution of the center gear (I_{20}): Ⓐ + Ⓑ + Ⓒ.
6. Complete the Holzer table, and iterate for the correct frequency ω as usual. (Note that it is easier to use the closing condition at the single-line end of the system than working in the opposite direction).

HOLZER TABLE FOR BRANCHED SYSTEM

①	②	③	④	⑤	⑥	⑦	⑧
Station_n	I_{ne}	$I_{ne} \cdot \omega^2$	A_n	$I_{ne}\omega^2 A_n$	$\sum_{i=1}^{n} I_{ne}\omega^2 A_i$	k_n	= ⑥ / ⑦
3	I_{3e}	---	$\bar{A}_3 = 1$	③ · ④	⑤$_n$ + ⑥$_{n-1}$ ⇓	k_{23e}	----
2	I_{21e}	---	A_2 = ---	---- ⟹	Ⓐ	——	——
4	I_{4e}	---	$\bar{A}_4 = 1$	----	-----	k_{24e}	----
2	I_{22e}	---	$\hat{A}_2$ = ---	/	/	——	——
4	I_{4e}	---	$\bar{A}_4 = \frac{A_2}{\hat{A}_2}$	----	----- ⇓	k_{24e}	----
2	I_{22e}	---	A_2 = ---	---- ⟹	Ⓑ	——	——
2	I_{20}	---	A_2	Ⓒ	Ⓐ + Ⓑ + Ⓒ ⇓	k_{12}	----
1	I_1	---	A_1 = ---	---- ⟹	Ⓓ	——	——

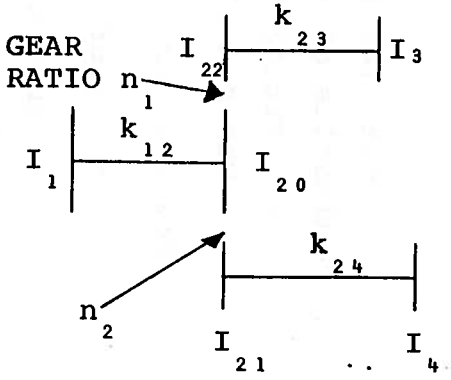

SYSTEM

$k_{23e} = n_1^2 \cdot k_{23}$

$k_{24e} = n_2^2 \cdot k_{24}$

$I_{21e} = n_2^2 \cdot I_{21}$

$I_{22e} = n_1^2 I_{22}$

$I_{3e} = n_1^2 I_3$

$I_{4e} = n_2^2 I_4$

Closing condition:
For correct natural frequency ω, Ⓓ must vanish.

4.5 Steady State Response Analysis

a) Critical Speeds

Torsional critical speeds occur whenever an excitation frequency, due to engine or propeller, equals a natural frequency of the shafting system (resonance). The system has a great number of natural frequencies, strictly speaking an infinite number if we look at it as a continuous system. There also exist infinite sets of excitation harmonics. We must therefore systematically investigate a great number of critical speeds in the range of operating speeds of the engine.

The excitation frequencies are counted by order numbers. The order number is defined as

$$\text{Order number} = \frac{F}{N} = \frac{CPM}{RPM} = \frac{\text{excitation cycles}}{\text{revolution}} = \frac{\text{vibr.}}{\text{rev.}} \tag{70}$$

The lowest frequency of excitation corresponds to the full engine cycle. For a two-stroke engine it is

$$\omega = \frac{2\pi \cdot RPM}{60} \tag{71a}$$

for a four-stroke engine whose cycle takes two revolutions

$$\omega = \frac{2\pi \cdot RPM}{60 \cdot 2} \tag{71b}$$

Besides, for each of these engines we also obtain all integer multiples of these lowest harmonics from a Fourier analysis of the excitation torque.

The set of order numbers is therefore

for the two-stroke engine: 1, 2,3, 4, ...

for the four-stroke engine: 1/2, 1, 1-1/2, 2, 2-1/2, ...

We must compare all of these orders to the set of natural frequencies in checking for critical speeds.

First example: A two-stroke cycle engine runs at a speed of 90 RPM. What are the three lowest harmonics?

For order no. 1

$$\omega = \frac{2\pi \cdot 90}{60} = 9.4 \text{ rad/sec}$$

The second and third order are at 18.8 and 28.2 rad/sec, respectively.

Second example: If a resonance with the lowest harmonic exists at 90 RPM, at which other speeds must we expect other resonances?

Since $\omega_n = 9.4$ rad/sec is a natural frequency of the system, we get a new resonance at 45 RPM where the lowest harmonic is 4.7 rad/sec so that the second harmonic is now in resonance. And so on, for 30, 22.5, ... RPM for the third, fourth, ... harmonic.

The critical speeds are counted by the number of nodes and the order number, for example II/6. for the two-noded 6th order critical.

b) Phase Relationships for Excitation

The combined effect of all sources of excitation in the system (engine and propeller) must be determined properly accounting for the differences in phase.

First looking at a single cylinder of the engine (the propeller is analogous), we represent the torque by means of harmonic analysis

$$T = t_o + \sum_{m=1}^{\infty} t_m \quad e^{i\varepsilon_m} \quad e^{im\omega t} \tag{72}$$

where t_o = steady average torque

t_m = amplitude of m'th excitation torque harmonic

ε_m = phase angle of m'th torque harmonic, usually measured relative to the top dead center position of the piston

ω = lowest frequency of excitation corresponding to engine cycle

Amplitudes t_m and phase angles ε_m are most reliably derived from direct measurement of the gas pressures p in the combustion chamber, Figure 19. The piston force is $P = p \cdot A_o$, A_o = piston area.

According to the geometry of the crank drive, one obtains for the tangential force acting on the crankpin, approximately (Fig. 20)

$$P_T \approx P \cdot \{\sin\alpha(1 + \frac{r}{\ell}\cos\alpha)\} \qquad (73)$$

where α, r, ℓ as in Figure 11.

The torque is correspondingly

$$T = r \cdot P_T = r \cdot A_o \cdot p\{\sin\alpha[1 + \frac{r}{\ell}\cos\alpha]\} \qquad (74)$$

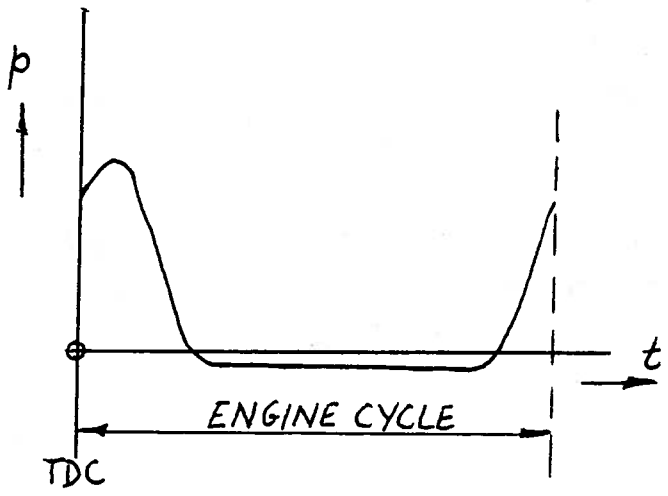

Fig. 19: Gas pressures

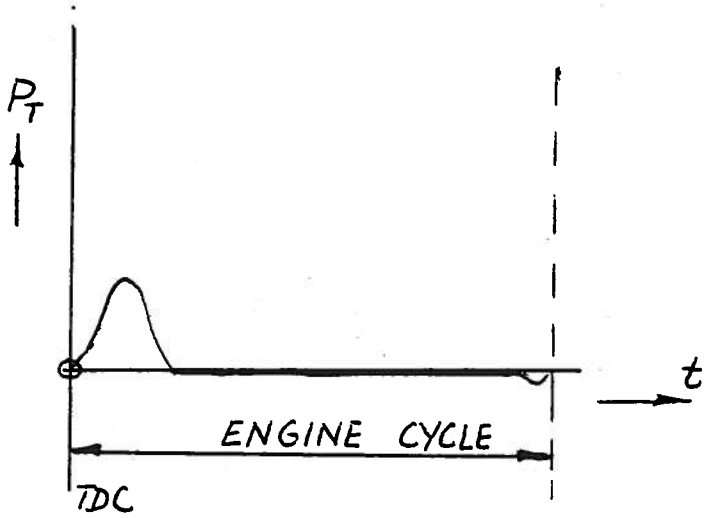

Fig. 20: Tangential force

The foregoing treatment disregards the unbalanced mass forces of the reciprocating drive. It may usually be assumed that the

engine has been sufficiently mass balanced so that this influence becomes negligible. Otherwise it would be no problem to add the mass unbalance forces to the excitation.

If in the earlier stages of design gas pressure diagrams for the engine are not available one can rely on torque harmonics information compiled for typical engines in handbooks such as the BICERA manual referenced on page 25.

The phase angles ε_m are the same for all cylinders for each harmonic. They may therefore be disregarded in the steady-state response analysis if the engine is the only source of excitation in a particular harmonic. But if propeller excitation is also present the phasing of the engine relative to the propeller needs to be accounted for so that the ε_m must be known.

A further significant phase difference among the cylinder is due to the firing sequence.

Suppose for example an eight cylinder four-stroke engine has the firing sequence 1 - 3 - 5 - 7 - 8 - 6 - 4 - 2. The crank arrangement for such an engine is shown in Figure 21. It will ensure that one cylinder fires every quarter of a revolution, or every eighth of an engine cycle.

We may now construct a phase diagram for each order number in which the full circle corresponds to one vibration or excitation cycle. The phase diagram therefore illustrates the timing

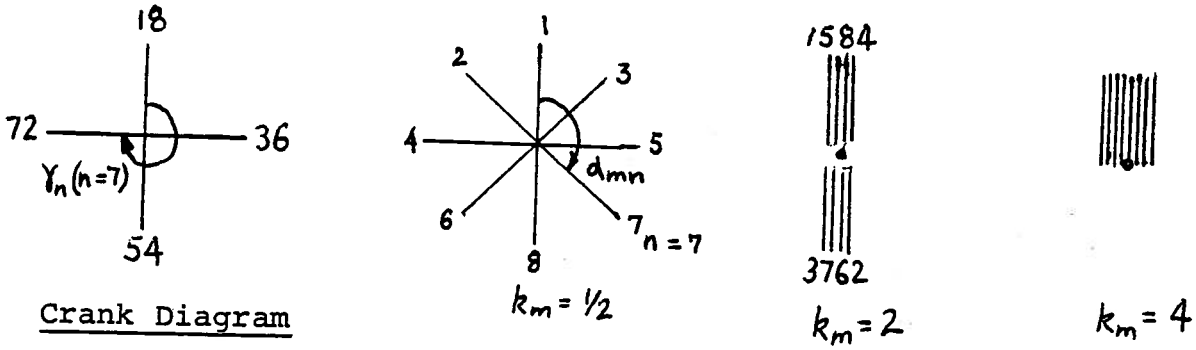

Crank Diagram

Phase Diagrams

Fig. 21: Crank and phase diagrams

of each firing relative to that of cylinder 1. Since in the crank diagram the full circle equals one revolution we have to multiply each angle in it by the order number (= vibrations/ revolution) to convert it into the phase diagram.

For the n'th cylinder, order number k_m

$$\alpha_{mn} = k_m \cdot \gamma_n \tag{75}$$

For example for n = 7, k_m = 1/2, and the above engine, cylinder 7 fires after 3/4 of a revolution (γ_7 = 270 deg). Half a vibration is completed during one revolution, hence the firing occurs after 3/8 of a vibration has elapsed, $\alpha_{1/27}$ = 135 deg.

The angles α_{nj} are required as inputs to the steady-state response analysis.

c) Selection of Firing Sequence by Means of the Phase Vector Sum

The selection of the firing sequence is governed by many factors, for example:

1. Level of excitation in torsional vibrations.
2. Mass balance of the engine.
3. Crankshaft bearing loads.
4. Crankshaft manufacturing method.
5. Induction and exhaust system.

For more details see W. Ker Wilson, "Crankshaft Arrangements and Firing Orders", Marine Engineering and Naval Architect, Oct. 1961, and ASME Journal, Feb. 1962.

Let us assume for simplicity that we are only concerned with the first of the above aspects, and let us discuss a method of evaluating the vibratory characteristics of a certain given firing sequence.

For a given mode shape, Figure 22, and order number k_m the complex torque amplitude of the n'th cylinder is

$$\bar{t}_{mn} = t_m \cdot e^{i\alpha_{mn}} \tag{76}$$

where t_m = Amplitude of m'th torque harmonic, the same for all cylinders (but not for the propeller)

α_{mn} = Phase angle of m'th harmonic at cylinder n, accounting for firing sequence and, if desired, for initial phase ε_m.

The work done by a torque harmonic at station n is proportional to the amplitude A_n at this station. It is therefore permissible to replace the actual torque $\bar{t}_{mn}$ by an equivalent torque at station 1 doing the same work

$$\bar{t}_{mn} \cdot \frac{A_n}{A_1} \quad \text{(at station 1)}. \tag{77}$$

The effect of all cylinders for the m'th harmonic thus equals

$$\bar{T}_m = \sum_{n=1}^{n_{CYL.}} \frac{A_n}{A_1} \bar{t}_{mn} = t_m \cdot \sum_{n=1}^{n_{CYL.}} \frac{A_n}{A_1} e^{i\alpha_{mn}} = t_m \cdot \bar{S}_{mn} \tag{78}$$

The quantity $\bar{S}_{mn}$ is called phase vector sum, and its magnitude is a measure of the resultant excitation. Figure 22 shows how it may be constructed graphically for a given mode shape and order number (k_m = 1/2). For resonant conditions the mode shape is the normal mode known from the transient response analysis.

The phase vector sum is determined for all critical speeds in the operating range. The firing sequence is then selected so as to reduce the worst cases most.

Clearly, the firing sequence is of no influence if all α_{mn}=0, 2π, ... This was the case for order number k_m = 4, Figure 21. The engine speed at which this occurs is called a major critical speed. In this condition the excitation impulses all add up algebraically (not vectorially) which is disadvantageous in particular if in the given modes all amplitudes have the same sign.

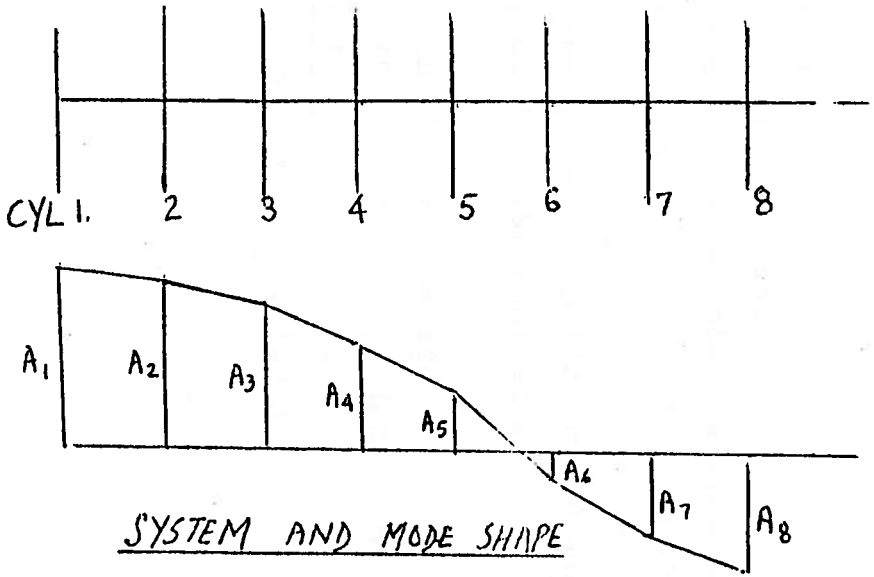

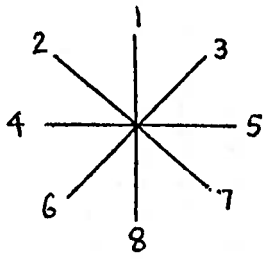

PHASE DIAGRAM, $k_m = 1/2$

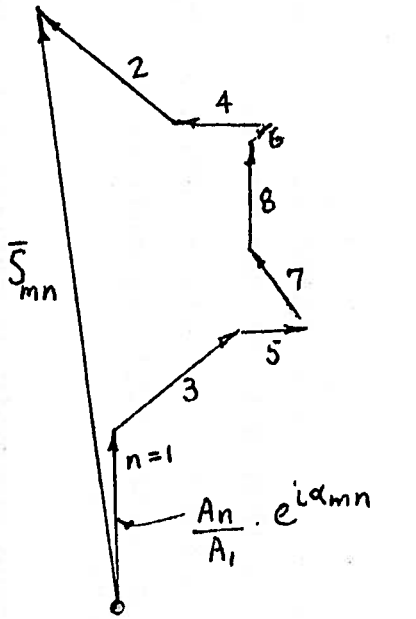

PHASE VECTOR DIAGRAM

Fig. 22: Construction of phase vector sum

Major criticals occur at the order numbers

n_{CYL}, $2n_{CYL}$, $3n_{CYL}$, ... for two-stroke engines,

$0.5n_{CYL}$, n_{CYL}, $1.5n_{CYL}$, ... for four-stroke engines,

d) Steady-State Response Analysis by an Adaptation of the Holzer Method

Given the torsional substitution system of Figure 23. It consists of moments of inertia, I_n, and stiffnesses, k_n, as before, plus excitation and damping. We consider one torque harmonic at a time so that the excitation is given by its complex amplitude $\bar{t}_{mn}$, equation (76).

The damping is given as cylinder-damping (c_n) proportional to the absolute velocity at station n, and as shaft-damping (c_{R_n}) proportional to the velocity difference between two neighboring stations.

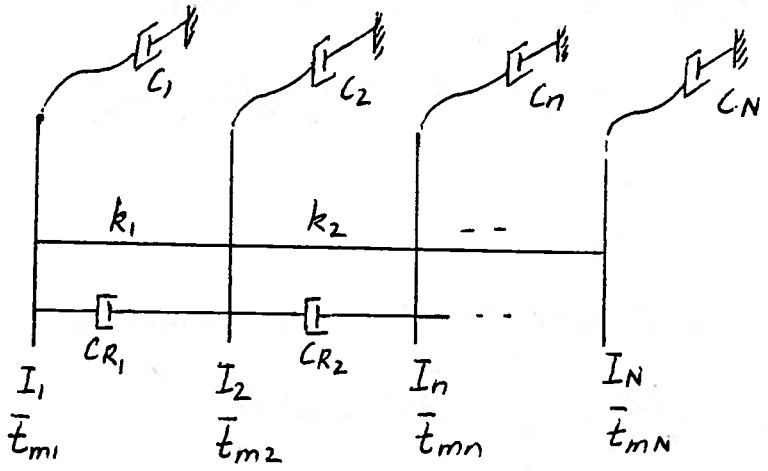

Fig. 23: Substitution system

The situation at the n'th station is shown in Figure 24.

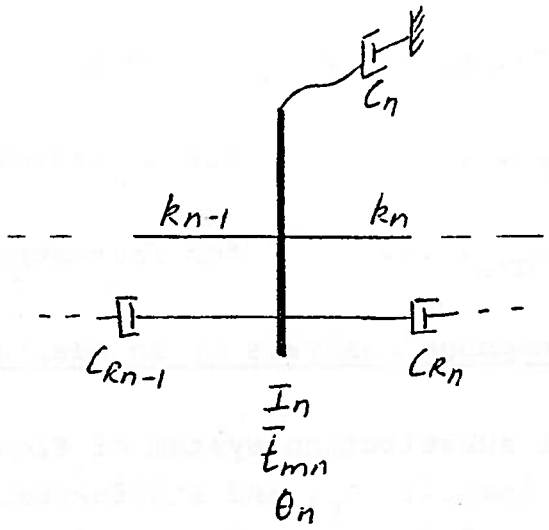

Fig. 24: Mass n

The equation of motion of this mass follows from Newton's Law:

$$I_n\ddot{\theta}_n + c_n\theta_n + c_{R_{n-1}}(\dot{\theta}_n-\dot{\theta}_{n-1}) + c_{R_n}(\dot{\theta}_n-\dot{\theta}_{n+1}) +$$

$$+ k_{n-1}(\theta -\theta_{n-1}) + k_n(\theta_n-\theta_{n+1}) = t_{mn} \qquad (79)$$

where $t_{mn} = \bar{t}_{mn} \cdot e^{i\omega t}$

Separation of variables is accomplished by

$$\theta_n = \bar{A}_n \cdot e^{i\omega t} = A_n \cdot e^{i\psi n} \cdot e^{i\omega t} \qquad (80)$$

Substituting, one obtains a complex algebraic equation

$$-\omega^2 I_n\bar{A}_n + ic_n\omega\bar{A}_n +$$

$$+ ic_{R_{n-1}}\omega\ (\bar{A}_n - \bar{A}_{n-1}) + ic_{R_n}\omega\ (\bar{A}_n - \bar{A}_{n+1}) + \qquad (81)$$

$$+ k_{n-1}\ (\bar{A}_n - \bar{A}_{n-1}) + k_n\ (\bar{A}_n - \bar{A}_{n+1}) = \bar{t}_{mn}$$

Previously, for the free vibration we had the analogous real equation

$$-\omega^2 A_n I_n + k_{n-1}\,(A_n - A_{n-1}) + k_n\,(A_n - A_{n+1}) = 0 \qquad \text{("50")}$$

from which we obtained the recursion

$$A_{n+1} = A_n - \frac{\omega^2 I_n A_n - k_{n-1}(A_n - A_{n-1})}{k_n} =$$

$$A_n - \frac{\sum_{j=1}^{n} I_j \omega^2 A_j}{k_n} \qquad (52)$$

If we sort the terms correspondingly now

$$-\bar{A}_n(\omega^2 I_n - ic_n\omega) + (k_{n-1} + ic_{R_{n-1}}\omega) \cdot (\bar{A}_n - \bar{A}_{n-1}) +$$

$$+ (k_n + ic_{R_n})\,(\bar{A}_n - \bar{A}_{n+1}) - \bar{t}_{mn} = 0 \qquad (82)$$

we get the recursion

$$\bar{A}_{n+1} = \bar{A}_n - \frac{\bar{A}_n \cdot (I_n\omega^2 - ic_n\omega) + \bar{t}_{mn} - (k_{n-1} + ic_{R_{n-1}}\omega)(\bar{A}_n - \bar{A}_{n-1})}{k_n + ic_{R_n}\omega}$$

$$\bar{A}_n - \frac{\sum_{j=1}^{n} (\bar{A}_j (I_j\omega^2 - ic_j\omega) + \bar{t}_{mj})}{k_n + ic_{R_n}\omega} \qquad (83)$$

The following quantities are analogous:

Free vibration	Forced vibration
A_n	$\bar{A}_n$
k_n	$\bar{k}_n = k_n + ic_{R_n}\omega$
$I_j\omega^2$	$I_j\omega^2 - ic_j\omega$
$\sum_{j=1}^{n} I_j\omega^2 A_j$	$\sum_{j=1}^{n} \{\bar{A}_j (I_j\omega^2 - ic_j\omega) + \bar{t}_{mj}\}$

On the basis of this analogy we can devise a modified Holzer table to deal with the steady-state response problem, page 49. The quantities in this table are complex and so are the arithmetical operations. We have shifted the excitation terms to the left-hand side so that the closing condition "right-hand side = o, no free end torque at mass N" still applies. It means that col. $\textcircled{9}_N$ must vanish now.

But the steady-state response problem is different in one important other respect. Instead of the natural frequency, the unknown is now the amplitude function (mode shape) for any given excitation frequency. We want to find the $\overline{A}_n$ - vector in col. $\textcircled{5}$ for which the closing condition is satisfied.

We may proceed in the following steps:

1. Apply the amplitude $\overline{A}_1 = \{1;0\}$ to the system, but no excitation, and determine the torque reaction at the other end, col. $\textcircled{9}_N$: $\overline{F} = f_1 + if_2$.

2. Apply the amplitude $\overline{A}_1 = \{0;1\}$ to the system, but no excitation, and find the torque in col. $\textcircled{9}_N$: $\overline{G} = g_1 + ig_2$ where $g_1 = -f_2$; $g_2 = f_1$.

3. Set $\overline{A}_1 = o$, and apply all excitation torques $\overline{t}_{mn}$, finding the free end torque, col. $\textcircled{9}_N$: $\overline{K} = k_1 + ik_2$.

4. Equate

$$c_1\overline{F} + c_2\overline{G} = -\overline{K} \qquad (84)$$

and solve for the real coefficients c_1, c_2.
(Two real equations for two unknowns).

5. Find $\overline{A}_1 = c_1 + i\,c_2$, and all other amplitudes by running the Holzer table with complete input ($\overline{A}_1$ and all torques). The closing condition must now be satisfied.

HOLZER TABLE FOR STEADY-STATE RESPONSE

①	②	③	④	⑤	⑥	⑦	⑧	⑨	⑩	⑪
Sta n	I_n	$I_n\omega^2$	$I_n\omega^2 - ic_n\omega$	$\bar{A}_n$	$\bar{A}_n(I_n\omega^2 - ic_n\omega)$	$\bar{t}_{mn}$	$[\bar{A}_n(--)+\bar{t}_{mn}]$	$\sum_{j=1}^{n}[--]$	$\bar{k}_n$	$\frac{\Sigma[--]}{\bar{k}_n}$
1	.									
2	.									
3	.									
.	Given	$\omega^2 \cdot ②_n$		$⑤_{n-1} - ⑪_{n-1}$	$④_n \cdot ⑤_n$	Given	$⑥_n + ⑦_n$	$⑨_{n-1} + ⑧_n$	Given	$⑨_n / ⑩_n$
.	.									
.	.									
N										

Closing condition: Col. $⑨_N = 0$

6. The following other quantities can be read from the final Holzer table:

$$\left.\begin{aligned} &\text{Column } (11)_n = \bar{A}_{n+1} - \bar{A}_n = \text{complex twist angle} \\ &\text{Column } (9)_n = \text{complex torque acting on shaft element } k_n \\ &\text{The stress in the element } k_n \text{ is} \\ &\tau = \frac{\text{abs. value of torque}}{\text{section modulus}} = \frac{|\text{col.}(9)_n|}{Z} \end{aligned}\right\} \quad (85)$$

where $Z = \frac{\pi D^3}{16}$ for a circular cross section.

5. SHIP HULL VIBRATIONS

5.1 Survey

The elastic structure of a ship hull is subject to numerous vibratory effects which may be classified at least crudely from the following viewpoints:

a) Transient versus steady-state vibrations.

Most technically significant shipboard vibrations are of the steady-state type. They are caused by periodic excitation generated by the main engine, the auxiliaries, or the propeller.

Transient vibrations may be produced by the motions of the ship in a seaway, wave impact, slamming, an anchor drop maneuver, shocks, impulses and other transient loads. They may play a role in the design if delicate shipboard equipment needs to be protected from impulsive loads or motions.

b) Hull girder versus local vibrations.

There are many ship vibrations in which, more or less, the whole hull girder participates. These vibrations can be treated in analogy to vibrating beams, and the motions at any station

along the ship correspond to motions in the particular degrees of freedom that a beam is capable of.

In distinction from these motions one also observes local hull vibrations, i. e. accentuated motions of smaller parts of the hull structure. The mode shapes of these motions are generally such that they could not be predicted from beam theory, for example the vertical vibration of a deck relative to the neutral axis of the hull girder. Vibrations of masts or superstructures and deck houses are often of this type.

Hull girder vibrations may provide the excitation for local vibrations, and the presence of local vibrations alters the vibratory properties of the main hull girder. The distinction is therefore somewhat artificial, and mainly serves the purpose of justifying simplified, separate treatment of each of the aforementioned categories.

c) Vertical, horizontal and torsional vibrations.

The main hull girder vibrations are classified according to degrees of freedom and mode shapes.

1. Vertical vibrations are transverse, flexural vibrations of the hull in the vertical plane. Free vibrations are possible in mode shapes with 2, 3, 4, ... nodes,
2. Horizontal vibrations are analogous, but in the horizontal plane.
3. Torsional vibrations result in twisting deformations of the hull. Free vibrations result in normal modes with 1, 2, 3, ... nodes.

The torsional and horizontal vibrations are usually coupled.

Vibrations in ships have many similarities to those in other elastic beam-like structures. But, as the following sections will show in more detail, many particular difficulties arise from the peculiarities of the ship's structure and its environment. This may be illustrated by listing the force categories involved in ship vibrations:

Inertia: Ship mass and hydrodynamic mass,

Damping: Structural and hydrodynamic damping,

Spring force: Elasticity of ship structure, differing somewhat from beam,

Excitation: Engine and propeller excitation, wake, and seaway influences.

5.2 Flexural, Shear and Torsional Stiffness

This section and most of those that follow concentrate on the subject of main hull girder vibrations. We will treat these vibrations in analogy to beam vibrations, and we must first describe the properties of a vibrating ship according to the format of beam dynamics.

We will first define the stiffness of actual beams and later discuss the particulars of ships. Regarding the flexural stiffness of a transversely vibrating beam a suitable beam stiffness definition is known from the derivation of Euler's equation of beam vibrations

$$k_1(x) = -\frac{M_B(x)}{y_B''(x)} = E\ I\ (x) \qquad (86)$$

where $M_B(x)$ = bending moment at station x

$y_B(x)$ = bending deflection at x

E = modulus of elasticity

I(x) = section moment of inertia about neutral axis

This equation is valid within the usual approximation of linearized beam theory.

For the shear stiffness of a beam one obtains an analogous "force-deformation" relationship which is derived in detail in a

special handout:

$$k_2(x) = \frac{V(x)}{y_V'(x)} = \leftarrow \text{DEFINITION}$$

$$= \frac{G\,A(x)}{k(x)} \leftarrow \text{FROM BEAM THEORY} \quad \triangleq K(x) \cdot A(x) \cdot G = KAG \tag{87}$$

where:

$V(x)$ = shear force at station x,

$y_V(x)$ = shear deformation at station x

$A(x)$ = cross sectional area

G = shear modulus

$$k(x) = \frac{1}{K(x)} = \frac{A(x)}{I^2(x)} \int_{Z_{MIN}}^{Z_{MAX}} \frac{S^2(z)}{b(z)}\,dz \tag{88}$$

$$S(Z) = \int_{Z}^{Z_{MAX}} b(Z) \cdot Z\,dZ$$ = statical moment of cross section above height Z.

$b(Z)$ = cross section width at height Z

For further details see handout. The factor k, or - as is sometimes preferred K = 1/k -, is a function of the vertical shear stress distribution in the cross section and consequently depends on the shape of the cross section.

For a rectangular cross section we found in a home assignment: k = 1.2. In the rectangle, the shear stresses vary strongly between zero at the ends and a maximum at the neutral axis.

To discuss the opposite extreme, let us consider the case of an I-girder,

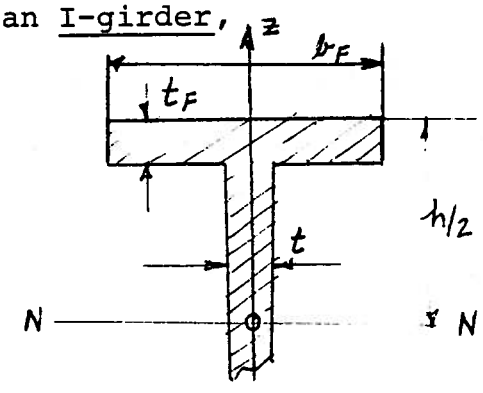

Fig. 25: I-girder

Fig. 25, symmetrical to its neutral axis. In this case the shear stresses in the web of the girder are more nearly uniform. For a crude estimate of the shear stiffness, let us assume that a constant stress is acting in the web corresponding to the actual value at the top of the web.

$$\tau(z) \approx \tau(h/2 - t_F) = \frac{V(x) \cdot S(z)}{I(x) \cdot t} \tag{89}$$

$$S(Z) = A_{FACE} \cdot \frac{h-t_F}{2} + \frac{t}{2}\left(\frac{h^2}{4} - Z^2\right) \approx A_{FACE} \cdot \frac{h}{2} \tag{90}$$

$$I(x) = 2 \cdot A_{FACE}\left(\frac{h - t_F}{2}\right)^2 + 2b_F \frac{t_F^3}{12} + \frac{th^3}{12} \approx 2 \cdot A_{FACE} \cdot \frac{h^2}{4} \tag{91}$$

$$\tau(z) \approx \frac{V(x) \cdot A_{FACE} \cdot h/2}{2 \cdot A_{FACE} \cdot \left(\frac{h}{2}\right)^2 \cdot t} = \frac{V(x)}{2\,\frac{h}{2}\,t} = \frac{V(x)}{A_{WEB}} \tag{92}$$

$$y'_V = \int_{-h/2}^{+h/2} \frac{\tau^2(z)\,t}{G\,V}\,dz = \frac{V^2}{GVA_{WEB}^2} \int_{-h/2}^{+h/2} t\,dz = \frac{V(x)}{G \cdot A_{WEB}} \tag{93}$$

$$k_2 = \frac{V(x)}{y'_V} = G \cdot A_{WEB}, \text{ and } k = \frac{A}{A_{WEB}} \tag{94}$$

A_{WEB} = cross sectional area of web

This derivation underestimates the stresses, and hence slightly overestimates the stiffness , but is sometimes used for estimates.

In summary, relating the shear stiffness consistently to the web area

$$k_2 = \frac{G\,A_{WEB}(x)}{C} \tag{95}$$

one finds for cross sections varying from I-girder to rectangle: C = 1.0 ... 1.2.

The torsional stiffness of simply-connected shiplike cross sections (Fig.26) may be approximated according to Bredt's formula for the torsion of thin-walled hollow cylinders

$$k_3 = \frac{M_T}{\frac{d\phi}{dx}} = \frac{4G\,A_o^2}{\oint \frac{ds}{t(s)}} \qquad (96)$$

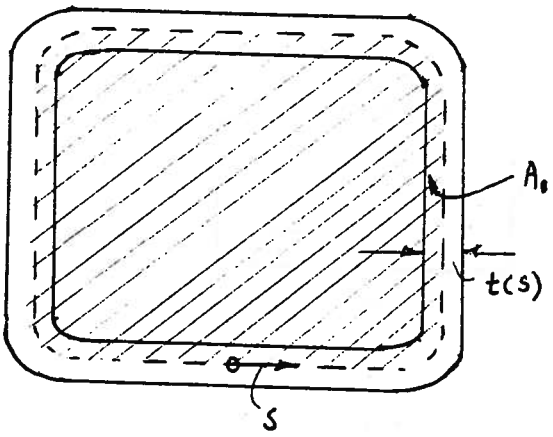

M_T = torque at station x
ϕ = twist angle at station x
s = circumferential coordinate
t(s) = thickness of shell plating
A_o = area inside s-loop

Fig. 26: Shiplike hollow cross section

In applying the above stiffness definitions to ships we must introduce corrections because ship structures differ significantly from simple beams. The effects are illustrated in Figure 27 where the normal and shear stress distributions are compared under three assumptions:

a) If we deal with the hull girder by <u>beam theory</u> a bending moment will produce constant normal stresses σ_x in deck and bottom, and a linear distribution in the web. Deck and bottom are essentially free of shear stresses.

b) The actual stress pattern is predicted much more realistically by <u>plate theory</u>, adapted to the <u>box</u>-like structure of a ship. The center part of Figure 27 shows that the normal stresses in deck and bottom drop from a maximum at the corners to a minimum at the centerplane. At the corner, plate theory predicts higher normal stresses than beam theory. The web is experiencing higher stresses, and consequently carrying a greater share of the load of normal stresses than one would expect by beam theory. The

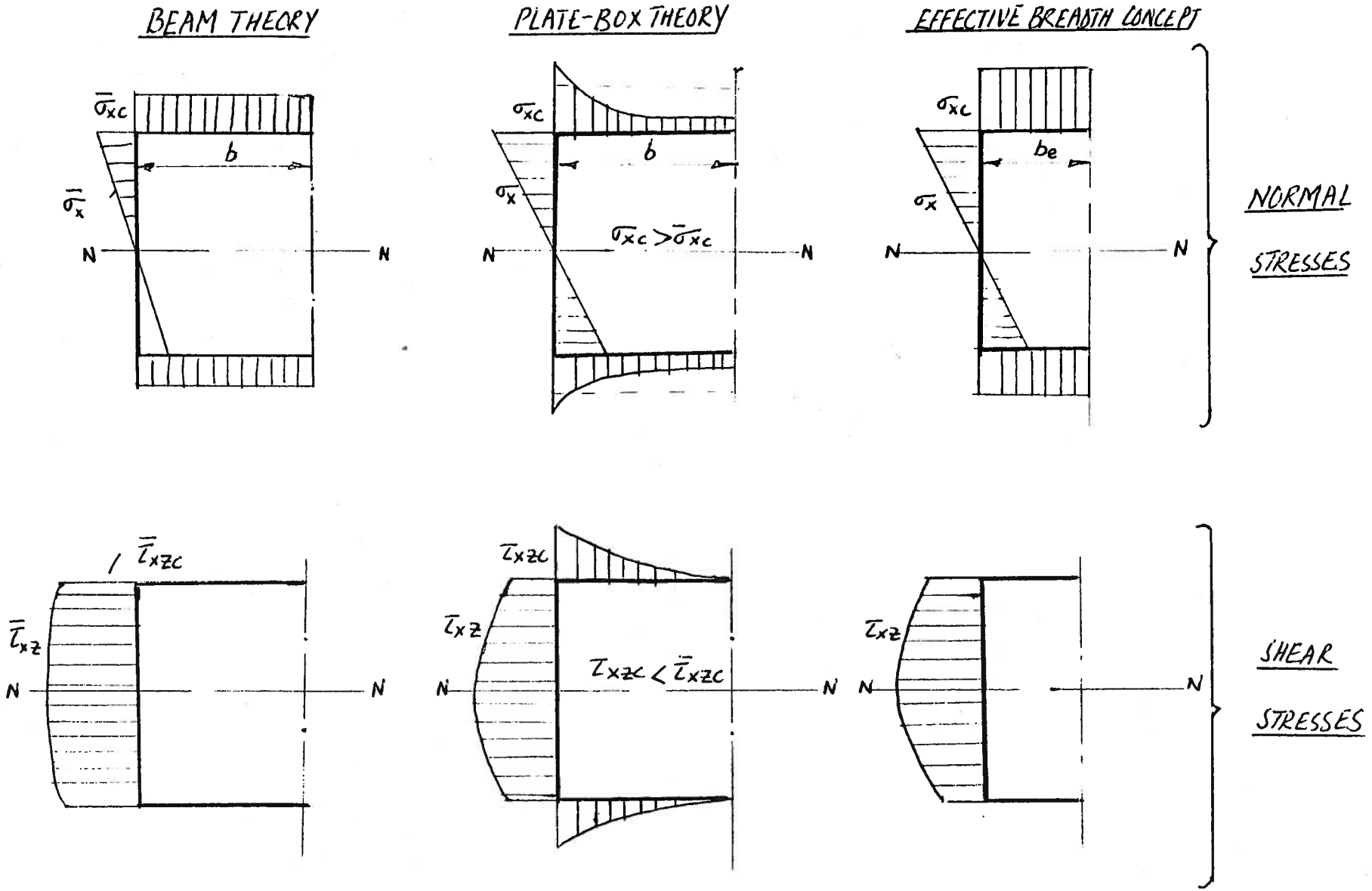

Fig. 27: Stress distribution in half-sections

deck and bottom plating also experiences shear stresses which are due to the bending moment and related to the bending deflection. Consequently, they must not be regarded in determining the shear stiffness, Ref. 8.

c) To simplify the practical determination of stresses the concept of effective breadth is used in ship structural analysis. The face plates of each cross section are replaced with plates of suitably modified breadth, b_e, so that the substitution system, treated by beam theory, will have the correct amount of work done by the web and face plates. The web is hence subjected to σ_{xc} at the corner, and the same stress acts throughout the deck. This defines the effective breadth:

$$b_e = \frac{\int_0^b \sigma_x(b)\,db}{\sigma_{xc}} \tag{97}$$

The numerator integral has to be determined by plate theory. In the literature results are presented for plates under harmonic bending loads (H. Schade, SNAME 1953). Actual bending moment curves, occuring in ship vibrations, may be treated by harmonic analysis

$$M_B(x) = \sum_{i=1}^{\infty} M_i \cdot \cos \frac{i\pi x}{a} \tag{98}$$

a = maximum distance between bending moment zeroes.

The effective breadth for a single bending moment harmonic is

$$b_{ei} = \frac{1 + \frac{a}{bi\pi} \sinh \frac{bi\pi}{a}}{1 + \cosh \frac{bi\pi}{a}} \cdot b \tag{99}$$

To find the resultant effective breadth we have to know the resultant normal force in the face plates for each harmonic

$$X_i = b_{ei} \cdot \sigma_{xci} \tag{100}$$

σ_{xci} = the axial stress in the face plate, due to M_i, computed for the cross section of breadth b_{ei}.

Substituting, we get:

$$b_e = \frac{\sum_i X_i \cos\left(\frac{i\pi x}{2a}\right)}{\sum_i \frac{X_i}{b_{ei}} \cos\left(\frac{i\pi x}{2a}\right)} \tag{101}$$

In many practical cases, the modes of hull vibration are found sufficiently sinusoidal to neglect all but one bending moment harmonic. But it is important that the nodal distances and hence effective breadth and stiffness differ from mode to mode.

In any refined analysis this necessitates a trial and error procedure. One estimates a mode shape, finds bending moment, nodal distance, stiffness, and a new mode shape. This sequence is repeated until satisfactory agreement is reached.

In summary, flexural and shear stiffness depend on the effective breadth, hence on mode shape and dynamic loading as well as on section geometry. The same substitution system may be used for both.

For the shear stiffness of a ship, because of the similarity of the hull girder to the I-girder treated above, the following approximation may prove satisfactory

$$k_2 = G \cdot \sum_{WEBS} A_{WEB} \tag{102}$$

where all longitudinal, vertically continuous members are to be included as webs.

The torsional stiffness of a ship may be computed by equation (96) although this neglects internal walls such as tweendecks, bulkheads, or the doublebottom. The stiffness is thus estimated somewhat too low.

Effects of elastic coupling between torsional and horizontal vibrations are discussed in section 5.5.

5.3 Inertia Forces

An accelerated motion of a body submerged or immersed in a fluid cannot take place without a corresponding accelerated motion of all fluid particles in the fluid continuum. The accelerating force must therefore provide the increments in kinetic energy to the body itself, and to the fluid.

The presence of the fluid has the net effect of an increase in inertia as will be discussed further.

Consider the kinetic energy of the system at some intermediate time

$$2T = M_S \dot{Z}^2 + \rho \int_V \dot{Z}_F^2 \, dV \tag{103}$$

M_S = body or ship mass

$\dot{Z}$ = body or ship velocity

ρ = fluid density

dV = fluid volume element

$\dot{Z}_F$ = velocity of fluid particle

The integration has to be extended over the whole fluid volume V.

In computing the hydrodynamic effects of accelerated motion it is customarily assumed that the fluid is ideal and that a flow potential ϕ exists that satisfies the Laplace equation at any time:

$$\phi(x,y,z,t) = \phi_o \, (x,y,z) \cdot F(t) \tag{104}$$

It can then be shown that the velocities throughout the fluid are related to each other, and hence to the velocity of the body by time-independent factors. For example, if $\phi_o = c \, \hat{\phi}_o$, we obtain

for the velocity normal to the body surface

$$-\frac{\partial\phi}{\partial n} = -c\,\frac{\partial\hat{\phi}o}{\partial n}\cdot F(t) = V_N \cdot F(t) \tag{105}$$

and for the velocity vector somewhere in the fluid

$$-\text{grad}\ \phi = -cF(t)\cdot \text{grad}\ \hat{\phi}_o = \bar{V}\cdot F(t) \tag{106}$$

The constant c may assume any value, but the ratio of any two velocities remains the same. In other words, the velocities in the field are proportional to the velocity of the body.

We can therefore rewrite equation (103)

$$2T = \dot{Z}^2\ \{M_s + \rho \int_V \left(\frac{\dot{Z}_F}{\dot{Z}}\right)^2 dV\} = \dot{Z}^2\{M_s + M_h\} \tag{107}$$

This defines the <u>hydrodynamic mass</u> or <u>added mass</u> as

$$M_h = \rho \int_v \left(\frac{\dot{Z}_F}{\dot{Z}}\right)^2 dV \tag{108}$$

The added mass depends on the shape of the moving body, but is independent of the type of accelerated motion.

In ship vibrations - as in many ship motions problems the added mass is computed on the basis of <u>strip theory</u>. The ship is considered as composed of thin vertical slices or strips, Figure 28, and the flow is assumed to be confined to the plane of each strip without exchange of fluid from strip to strip. The strip method thus converts the three-dimensional flow problem into a sequence of two-dimensional ones.

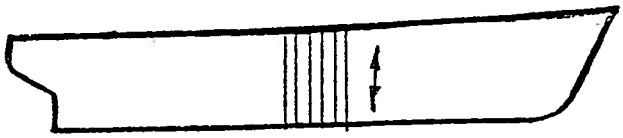

Fig. 28: Strip method

The two-dimensional flow problems have been solved for a great variety of shiplike section shapes. Conformal mapping and many other techniques for boundary value problems of potential flow are suitable to find the potential, the kinetic energy and the added mass of given shapes. The same basic approach is used for the vertical, horizontal, and torsional motions of the strips.

The results are presented in the literature as coefficients of added mass per unit length.

$$\left.\begin{aligned} C_V &= \frac{M_{hV}}{\rho/2\ \pi\ b^2} && \text{for vertical motion} \\ C_H &= \frac{M_{h\,H}}{\rho/2\ \pi\ T^2} && \text{for horizontal motion} \\ C_T &= \frac{J_{hT}}{\rho\ \pi\ T^4} && \text{for torsional motion} \end{aligned}\right\} \quad (109)$$

where

M_{hV}, M_{hH}, J_{hT} = hydrodynamic masses and mass moment of inertia per unit length

ρ = density of fluid (mass/unit volume)

b = half - beam of section

T = draft of section

Results for C_V for a systematic family of shiplike sections, the so-called Lewis - sections, were first obtained in Reference 9. Other important original work was done by Wendel, Reference 11, Landweber and Macagno, for C_H, and Kumai, for C_T. For compilations of the results see:

Lewis, Ref. 3: C_v

Todd, Ref. 4: C_v, C_H, C_T

Leibowitz and Kennard, Ref. 7: C_v, C_H

Wendel, Ref. 11: C_V, C_H, (C_T)

For further details see:

Landweber and M. Macagno, Added Mass of Two-dimensional Forms Oscillating in a Free Surface, Journal of Ship Research, Nov. 1957; also 1959 and 1960, extensions with new titles.

T. Kumai, Added Mass Moment of Inertia Induced by Torsional Vibration of Ships, European Shipbuilding, 1958.

Further references to pertinent work by Prohaska, Grim and Vossers will be found in the above.

The results of the strip method have to be corrected to account for three-dimensional flow effects. F. Lewis, Reference 9, derived the longitudinal reduction factor J (also longitudinal inertial coefficient) for ellipsoids of revolution, defined as the ratio of rigorous (3D) added mass to the strip method approximation, (2D). He treated two- and three-noded vibrations, neglecting the influence of cross-section rotation. The actual distances between vibration nodes can be taken into account.

J. L. Taylor, Transactions INA 1930, included the effects of rotation, but assumed fixed nodal positions. His results for J are lower than those of Lewis, References 3 and 4.

Both correction factors are not exact, but seem acceptable in view of the other major simplification to apply these simple body results directly to the ship, the added mass of each strip being multiplied by J.

Refinements are, however, possible on the basis of Kruppa's results, Reference 14. Kruppa treated ellipsoids of three unequal axes for arbitrary mode shapes with up to five nodes, including rotational effects. He computed the raw data to be combined into the longitudinal inertial coefficient.

Shallow water effects tend to increase the added mass which is of significance for ship operations or vibration tests in shallow water. Corrections can be found in Reference 4.

5.4 Differential Equation of the Vertical Hull Vibration

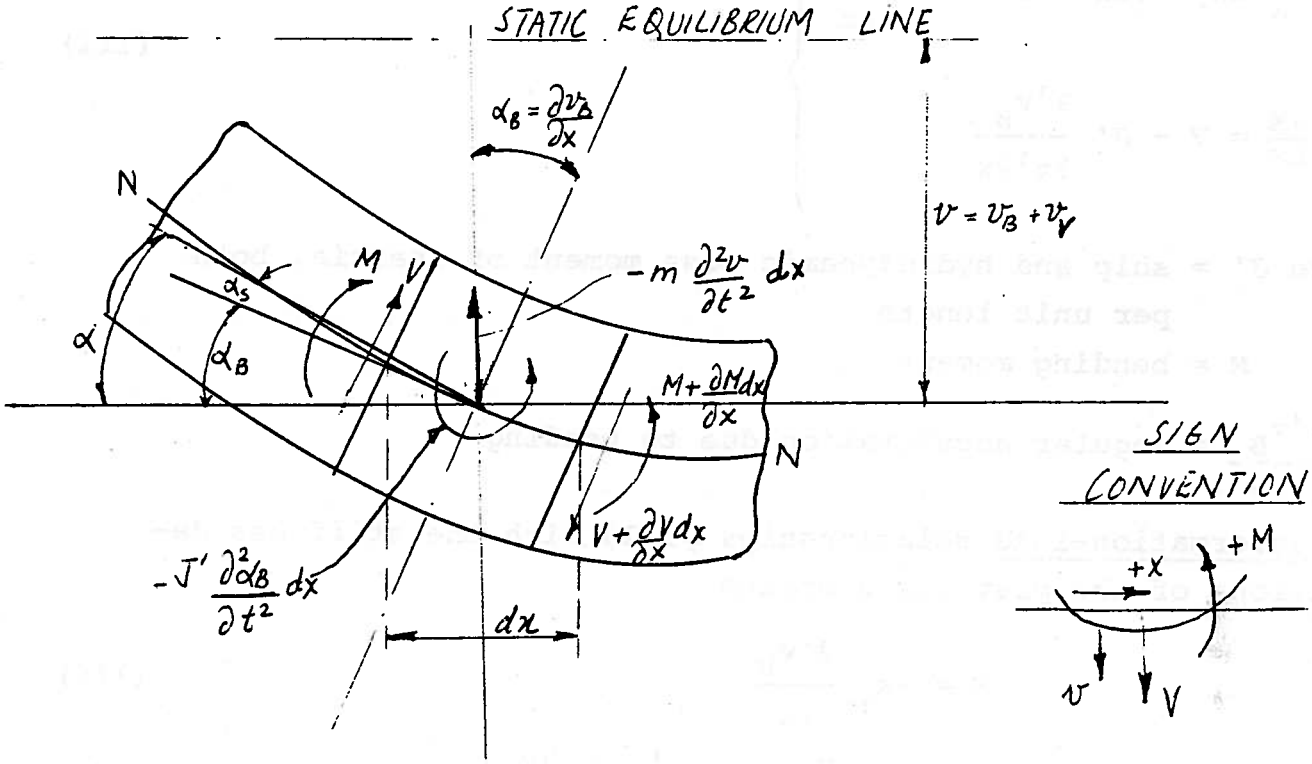

Fig. 29: Free body diagram of shiplike beam element

We will now derive the differential equation for the free vertical vibration of a shiplike beam including the effects of hydrodynamic inertia, rotary inertia and shear deformation. Figure 29 shows the forces acting on the element. The figure also illustrates that the total deformation of the beam, v, is composed of a bending deflection v_B and a shear deformation v_V. The ratio of these contributions is unknown before the analysis.

From the equilibrium of forces:

$$\left.\begin{aligned} \frac{\partial V}{\partial x}\,dx &= m dx\,\frac{\partial^2 v}{\partial t^2} \\ \text{or} \qquad \frac{\partial V}{\partial x} &= m\,\frac{\partial^2 v}{\partial t^2} \end{aligned}\right\} \qquad (110)$$

From the equilibrium of moments:

$$\left.\begin{aligned} \frac{\partial M}{\partial x}\,dx &= V dx - J' dx\,\frac{\partial^3 v_B}{\partial t^2 \partial x} \\ \text{or} \quad \frac{\partial M}{\partial x} &= V - J'\,\frac{\partial^3 v_B}{\partial t^2 \partial x} \end{aligned}\right\} \tag{111}$$

where J' = ship and hydrodynamic mass moment of inertia, both per unit length

M = bending moment

$\frac{\partial^3 v_B}{\partial t^2 \partial x}$ = angular acceleration due to bending

The deformation-load relationships yield with the stiffness definitions of the previous sections

$$M = -k_1\,\frac{\partial^2 v_B}{\partial x^2} \tag{112}$$

$$V = k_2\,\frac{\partial v_V}{\partial x} = k_2\left(\frac{\partial v}{\partial x} - \frac{\partial v_B}{\partial x}\right) \tag{113}$$

We separate variables by expanding deformation and load into an infinite series of eigenfunctions (mode shapes):

$$v = \sum_{j=1}^{\infty} v_j\, e^{i\omega_j t} \tag{114}$$

$$v_B = \sum_{j=1}^{\infty} v_{Bj}\, e^{i\omega_j t} \tag{115}$$

$$v_V = \sum_{j=1}^{\infty} v_{Vj} \cdot e^{i\omega_j t} \tag{116}$$

$$V = \sum_{j=1}^{\infty} V_j \cdot e^{i\omega_j t} \tag{117}$$

$$M = \sum_{j=1}^{\infty} M_j \cdot e^{i\omega_j t} \tag{118}$$

where ω_j = natural frequency of degree j

v_j, v_{Bj}, v_{Vj}, V_j, M_j = amplitudes of motions and forces in j'th mode.

Substituting equations (114-118) and dropping the subscripts j we obtain a set of ordinary differential equations, valid for any natural frequency ω:

From equ. (110): $$\frac{dV}{dx} = -\omega^2 mv \tag{119}$$

From equ. (111): $$\frac{dM}{dx} = V + \omega^2 J' \frac{dv_B}{dx} \tag{120}$$

From equ. (112): $$M = -k_1 \frac{d^2 v_B}{dx^2} \tag{121}$$

From equ. (113): $$V = k_2 \cdot \left(\frac{dv}{dx} - \frac{dv_B}{dx} \right) \tag{122}$$

The purpose of the next transformations is to eliminate v_B from these expressions, and to express M and V in terms of the total deformation v. These relations will be needed in our solution method. Subsequently, the equation of motion will be derived.

For the bending moment, equ. (122) is solved for dv_B/dx, differentiated by dx, and substituted in equ. (121):

$$\frac{dv_B}{dx} = \frac{dv}{dx} - \frac{V}{k_2} \tag{123}$$

$$\frac{d^2v_B}{dx^2} = \frac{d^2v}{dx^2} - V\frac{d}{dx}\left(\frac{1}{k_2}\right) - \frac{dV}{dx}\frac{1}{k_2} \tag{124}$$

$$\boxed{M = -k_1 \frac{d^2v_B}{dx^2} = -k_1\left(\frac{d^2v}{dx^2} - V\frac{d}{dx}\left(\frac{1}{k_2}\right) - \frac{dV}{dx}\frac{1}{k_2}\right)} \tag{125}$$

A similar expression for the shear force is obtained by equating the x-derivative of equation (121) to equation (120).

$$\frac{dM}{dx} = -\left(k_1\frac{d^3v_B}{dx^3} + \frac{dk_1}{dx}\frac{d^2v_B}{dx^2}\right) = V + \omega^2 J'\frac{dv_B}{dx} \tag{126}$$

The third derivative of v_B is obtained by differentiating equation (124)

$$\frac{d^3v_B}{dx^3} = \frac{d^3v}{dx^3} - V\frac{d^2}{dx^2}\left(\frac{1}{k_2}\right) - \frac{dV}{dx}\frac{d}{dx}\left(\frac{1}{k_2}\right) - \frac{d^2V}{dx^2}\frac{1}{k_2} - \frac{dV}{dx}\frac{d}{dx}\left(\frac{1}{k_2}\right) \tag{127}$$

Using equation (119)

$$\frac{d^2V}{dx^2} = -\omega^2 m\frac{dv}{dx} - \omega^2\frac{dm}{dx}v \tag{128}$$

$$\frac{d^3v_B}{dx^3} = \frac{d^3v}{dx^3} - V\frac{d^2}{dx^2}\left(\frac{1}{k_2}\right) + \omega^2 mv\frac{d}{dx}\left(\frac{1}{k_2}\right) + \frac{\omega^2 m}{k_2}\frac{dv}{dx} + \omega^2\frac{dm}{dx}v\left(\frac{1}{k_2}\right) + \omega^2 mv\frac{d}{dx}\left(\frac{1}{k_2}\right) \tag{129}$$

Substituting equation (129) into (126), using (124):

$$-k_1\left\{\frac{d^3v}{dx^3} - V\frac{d^2}{dx^2}\left(\frac{1}{k_2}\right) + \omega^2 mv\frac{d}{dx}\left(\frac{1}{k_2}\right) + \frac{\omega^2 m}{k_2}\frac{dv}{dx} + \omega^2\frac{dm}{dx}v\left(\frac{1}{k_2}\right) + \omega^2 mv\frac{d}{dx}\left(\frac{1}{k_2}\right)\right\} - \frac{dk_1}{dx}\left\{\frac{d^2v}{dx^2} - V\frac{d}{dx}\left(\frac{1}{k_2}\right)\right\} = V + \omega^2 J'\left(\frac{dv}{dx} - \frac{V}{k_2}\right) \tag{130}$$

Collecting terms proportional to V, and solving for V

$$V = \frac{\frac{d}{dx}\left[k_1\left(\frac{d^2v}{dx^2} + \frac{\omega^2 m}{k_2} v\right)\right] + \omega^2 \frac{dm}{dx} v\left(\frac{1}{k_2}\right) + \omega^2 m k_1 v \frac{d}{dx}\left(\frac{1}{k_2}\right) + \omega^2 J' \frac{dv}{dx}}{-1 + \frac{\omega^2 J'}{k_2} + \frac{d}{dx}\left(k_1 \frac{d}{dx}\left(\frac{1}{k_2}\right)\right)} \tag{131}$$

Equations (125) and (131) are the relations between mode shape and load we were looking for.

The equation of motion can be derived by equating equation (119) to the derivative of equation (122), substituting equation (131) for V:

$$\omega^2 m v + \frac{d}{dx}\left[\frac{\frac{d}{dx}\left\{k_1\left(\frac{d^2v}{dx^2} + \frac{\omega^2 m}{k_2} v\right)\right\} + \omega^2 \frac{dm}{dx} v \frac{1}{k_2} + \omega^2 m k_1 v \frac{d}{dx}\left(\frac{1}{k_2}\right) + \omega^2 J' \frac{dv}{dx}}{-1 + \frac{\omega^2 J'}{k_2} + \frac{d}{dx}\left(k_1 \frac{d}{dx}\left(\frac{1}{k_2}\right)\right)}\right] = 0 \tag{132}$$

This is a fourth order linear homogeneous differential equation with variable coefficients for the mode shape v(x). The four integration constants which one would get upon integration have to be determined from the boundary conditions

$$V(0) = V(\ell) = M(0) = M(\ell) = 0 \tag{133}$$

The beam has free-free ends, i.e. no shear forces or moments at the ends.

If a mode shape is known or estimated it is possible, at least by trial and error, to solve for the natural frequency ω.

Equation (132) is the generalization of Euler's beam equation which may be obtained from it by the limiting process

$$\left.\begin{aligned} J' &\to 0 \\ k_2 &\to \infty \\ k_1 &\to EI(x) \end{aligned}\right\} \tag{134}$$

Hence

$$\omega^2 mv + \frac{d}{dx}\ \frac{d}{dx}\ \left[-k_1\ \frac{d^2v}{dx^2}\right] \tag{135}$$

which with

$$\omega^2 v = -\frac{d^2v}{dt^2} \tag{136}$$

is equivalent to the partial differential equation

$$\frac{\partial^2}{\partial x^2}\left[EI(x)\ \frac{\partial^2 v}{\partial x^2}\right] + m\ \frac{\partial^2 v}{\partial t^2} = 0 \tag{137}$$

i.e. Euler's equation.

5.5 Differential Equation of the Torsional-Horizontal Hull Vibration

Figure 30 shows a situation sketch for an element of length dx of a shiplike beam vibrating in the torsional-horizontal coupled mode. The forces shown are acting in two different planes, located at x and at x + dx.

The section center of gravity is denoted as C_1 at station x and C_2 at station x + dx. They are separated by distance $d\xi$ because of the curvature of the neutral axis ξ (x). The keel point K is used as the origin.

The shear center of the section is denoted as S, at station x, and as S_2 at station x + dx. The shear center line η (x) may also be curved so that S_1 and S_2 are in general separated by $d\eta$. The shear center is defined as the point through which the shear stress resultant may be thought acting. For an open section it may be located outside the section. (See e.g. Timoshenko, Strength of Materials).

Any combination of shear force and torsional moment acting upon an element at station x may be decomposed as a shear force V acting through the centroid C_1 and a free torsional moment M_T. The elastic reaction of the element at station x + dx has a resultant V + dV acting through the shear center C_2.

The inertia force acts through the center of gravity ($C_1 \approx C_2$), and the rotational inertia results in a free couple.

The shear center does not in general coincide with the center of gravity of the section. Any horizontal shear force V will therefore almost invariably be associated with a torsional couple. This connection causes the coupling between the horizontal and the torsional modes, as we shall see again from the differential equation. The magnitude of the coupling effects depends on the distance between those two centers, $\rho(x) = \eta(x) + \xi(x)$.

It follows from the equilibrium of the elment that

$$dM_T = J'' \frac{\partial^2 \phi}{\partial t^2} dx + \rho dV + V d\eta \qquad (138)$$

where J" = torsional moment of inertia, including hydrodynamic effects

ϕ = torsional displacement.

If in analogy to the treatment in equations (114) through (118) we separate variables and look at one particular normal mode

$$\phi(x,t) = \phi(x) \cdot e^{i\omega t} \tag{139}$$

equation (138) becomes

$$\frac{dM_T}{dx} = -\omega^2 J''\phi + \rho \frac{dV}{dx} + V \frac{d}{dx} \tag{140}$$

The other two equilibrium conditions, equations (110), (111), or (119), (120) carry over from the case of pure flexural vibrations:

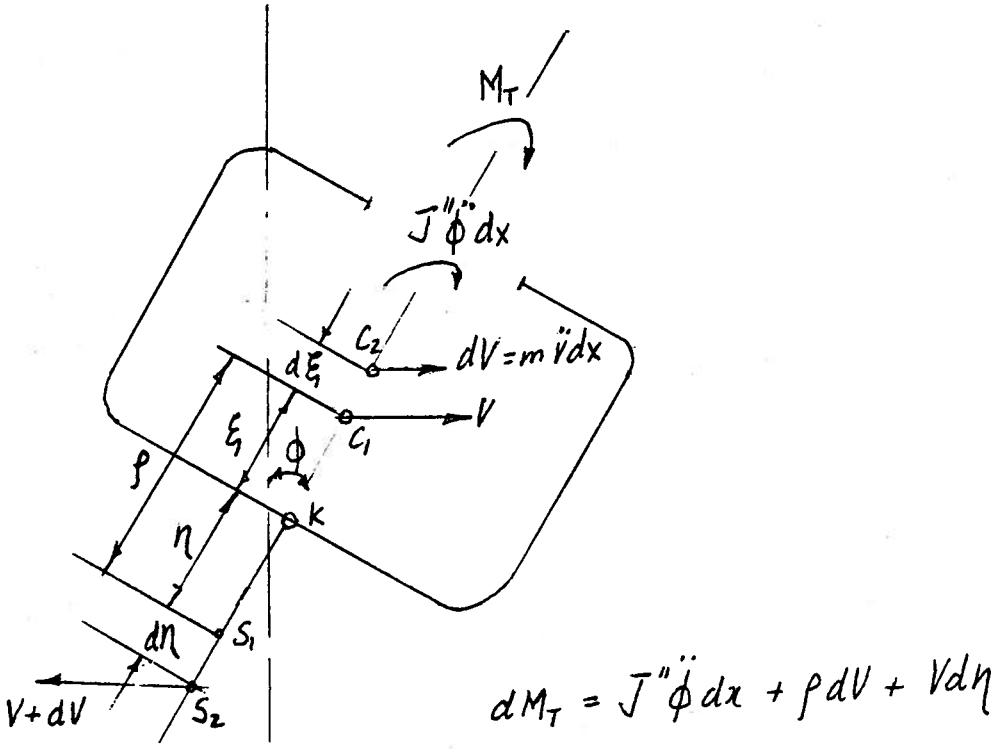

Force Diagram of Element

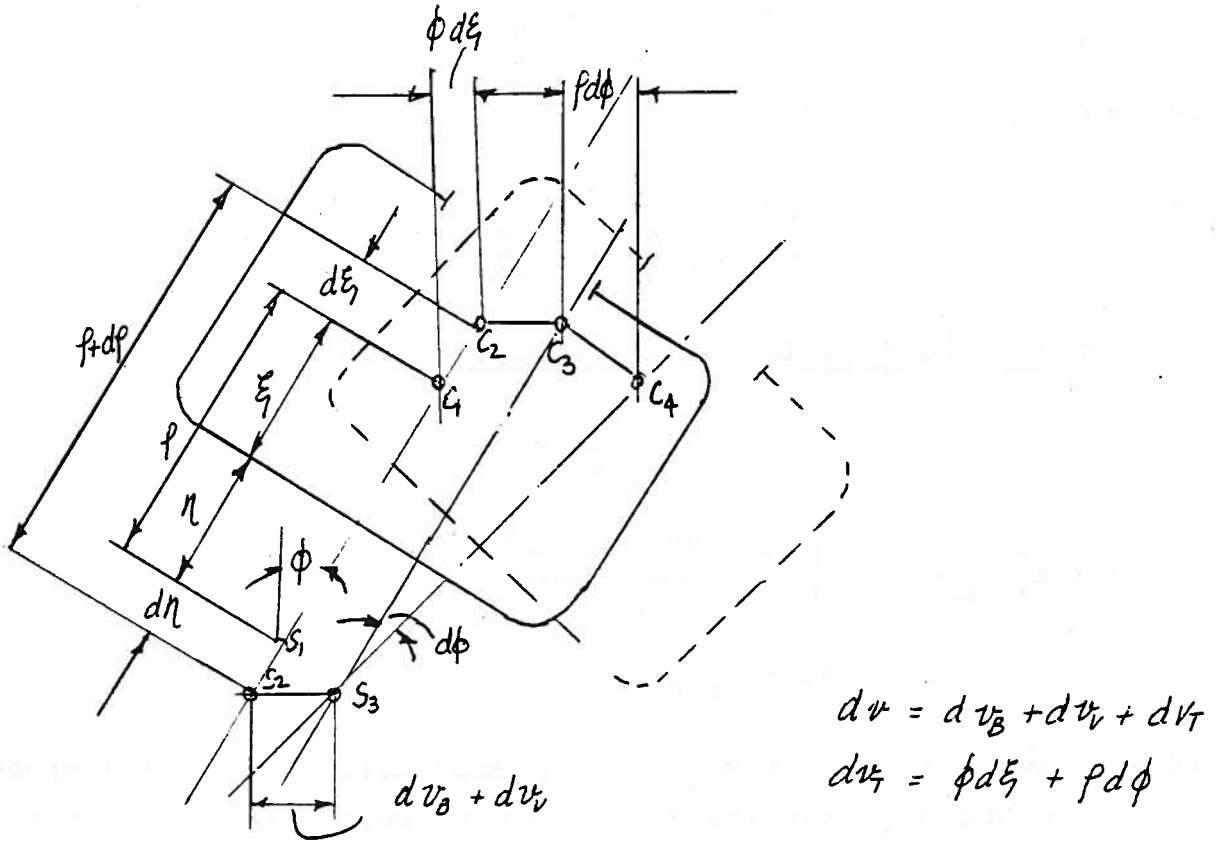

Deformations of Element

Fig. 30: Force and deformation diagrams for horizontal-torsional vibration

$$\frac{dV}{dx} = -\omega^2 mv \tag{119}$$

$$\frac{dM}{dx} = V + \omega^2 J' \frac{dv_B}{dx} \tag{120}$$

It must be noted that the total displacement v is now composed of three parts: Bending, shear, and torsion (Fig. 30)., and in

the absence of end constraints the shear center may be assumed to be the center of twist about which the rotation takes place:

$$v = v_B + v_V + v_T \tag{141}$$

where $d\,v_T = \phi \cdot d\xi + \rho d\phi$ (142)

or

$$\frac{dv_T}{dx} = \phi \frac{d\xi}{dx} + \rho \frac{d\phi}{dx} \tag{143}$$

The load-deformation relationships are as before

$$M = -k_1 \frac{d^2 v_B}{dx^2} \tag{121}$$

$$V = k_2 \frac{dv_V}{dx} = k_2 \left(\frac{dv}{dx} - \frac{dv_B}{dx} - \frac{dv_T}{dx} \right) \tag{122a}$$

$$M_T = k_3 \frac{d\phi}{dx} \tag{96a}$$

We now have a system of six simultaneous differential equations for the couples flexural-shear-torsional beam vibrations, i.e. three dynamic equilibrium conditions (140) to (120*), and three load-deformation relationships (121), (122a), (96a). These equations, in connection with the definitions (141) and (143), are sufficient to solve the free vibration problem. The free-end boundary conditions are now formulated as

$$M = V = M_T = o \text{ at } x = o \text{ and } x = L \tag{143-1/2}$$

In analogy to the developments in equations (123) through (132), it is again possible to eliminate all deformation variables but v and ϕ, and to obtain direct expressions for M, V, M_T in terms of these variables. The results are (Ref. 8):

$$M = -k_1\left[\frac{d^2v}{dx^2} - v\,\frac{d\left(\frac{1}{k_2}\right)}{dx} + \frac{\omega^2 m}{k_2}\,v - \frac{d}{dx}\left(\phi\frac{d\xi}{dx} + \rho\,\frac{d\phi}{dx}\right)\right] \tag{144}$$

$$V = \frac{1}{\frac{d}{dx}\left(k_1\frac{d}{dx}\left(\frac{1}{k_2}\right)\right) + \omega^2\,\frac{J'}{k_2} - 1}\left\{\frac{d}{dx}\left[k_1\left(\frac{d^2v}{dx^2} + \frac{\omega^2 m}{k_2}\,v\right)\right] + \omega^2 m k_1\frac{d}{dx}\left(\frac{1}{k_2}\right)v + \right.$$

$$\left. + \omega^2 J'\,\frac{dv}{dx} - \frac{d}{dx}\left[k_1\frac{d}{dx}\left(\phi\,\frac{d\xi}{dx} + \rho\,\frac{d\phi}{dx}\right)\right] - \omega^2 J'\left(\phi\,\frac{d\xi}{dx} + \rho\,\frac{d\phi}{dx}\right)\right\} \tag{145}$$

$$M_T = k_3\,\frac{d\phi}{dx} \tag{146}$$

Correspondingly, one obtains for the equations of motion

$$0 = \omega^2 m v + \frac{d}{dx}\left\{\frac{1}{\frac{d}{dx}\left(k_1\,\frac{d}{dx}\left(\frac{1}{k_2}\right)\right) + \frac{\omega^2 J'}{k_2} - 1}\left\{\frac{d}{dx}\left[k_1\left(\frac{d^2v}{dx^2} + \omega^2\,\frac{mv}{k_2}\right)\right] + \right.\right.$$

$$\left.\left. + \omega^2 m k_1\,\frac{d}{dx}\left(\frac{1}{k_2}\right)v + \omega^2 J'\,\frac{dv}{dx} - \frac{d}{dx}\left[k_1\frac{d}{dx}\left(\phi\frac{d\xi}{dx} + \rho\,\frac{d\phi}{dx}\right)\right] - \omega^2 J'\left(\phi\frac{d\xi}{dx} + \right.\right.\right.$$

$$\left.\left.\left. + \rho\,\frac{d\phi}{dx}\right)\right\}\right\} \tag{147a}$$

and

$$0 = \frac{d}{dx}\left\{\frac{1}{d\eta/dx}\left[\frac{d}{dx}\left(k_3\,\frac{d\phi}{dx}\right) + \omega^2 J''\phi + \omega^2 m\rho v\right]\right\} + \omega^2 m v \tag{147b}$$

These equations become uncoupled if the shear centers are located in the neutral axis, i.e. $\rho = 0$, and if the slope of the neutral axis remains negligible, $d\eta/dx \to 0$.

It is not intended to present a solution method for the above set of equations. But section 5.6 deals with the analogous case of coupled flexure and shear, and it will be evident that a procedure analogous to the discrete disk initial value technique

presented there can be used. Such a technique is described by Csupor in Ref. 8, Leibowitz and Kennard, Ref. 7, describe a very similar procedure.

5.6 Solution Techniques, Natural Frequencies and Mode Shapes

a) The Discrete Disk Method

Many of the conventional solution techniques that can be applied successfully to transient response problems in flexural beam vibrations lead into difficulties when it comes to beams subject to bending and shear. This will be illustrated by a few examples in subsequent sections.

One method that avoids these difficulties rather elegantly is the discrete disk method, which for the present purpose was formulated by Csupor, Ref. 8. The description presented here will follow Csupor's outline rather closely. (See also Adams and Welch, TMB Report 582, July 1947).

The method starts with the approximation of substituting a system of discrete masses (disks) for the actual, more or less continuous ship mass distribution, Figure 31. The disks are obtained by lumping the distributed mass at the centroid of any given segment (integration process). The disks carry translational as well as bending rotational inertia. They are connected by elements that represent the segment bending and shear stiffness properties, but have no mass. The segment stiffness constants can be obtained by applying unit loads to the segment ends and determining the deformations on the basis of the local stiffness coefficients. But frequently one can simplify the procedure by arranging for segments of constant or almost constant stiffness.

Regarding the necessary number of segments, Csupor recommends to use at least five times $n_{min} = r + 2$, where r = degree of vibration, n_{min} = minimum number of disks to produce the corresponding mode shape. For example, for the first-degree, two-noded

vibration $5 \cdot n_{min} = 15$ disks are to be recommended for a sufficiently realistic approximation. It should be noted in passing that the discrete disk method as just introduced is the physical equivalent of the mathematical technique of finite differences. This technique, which has been applied to the ship vibrations problem extensively, leads to exactly the same set of equations. Compare References 6 and 7.

Let us now first consider the equilibrium situation at some segment between station i and station k = i + 1, Figure 31. In analogy to equations (119) and (120), shear force and bending moment change from the left-hand side of disk i to the left-hand side of disk k as follows:

$$V_k = V_i + m_i v_i \omega^2 \tag{148}$$

$$M_k = M_i + J' \frac{dv_B}{dx} \omega^2 + V_k \cdot h_k = M_{ck} + V_k \cdot h_k \tag{149}$$

Fig. 31: Discrete disk system definitions (From Csupor, Ref. 8):

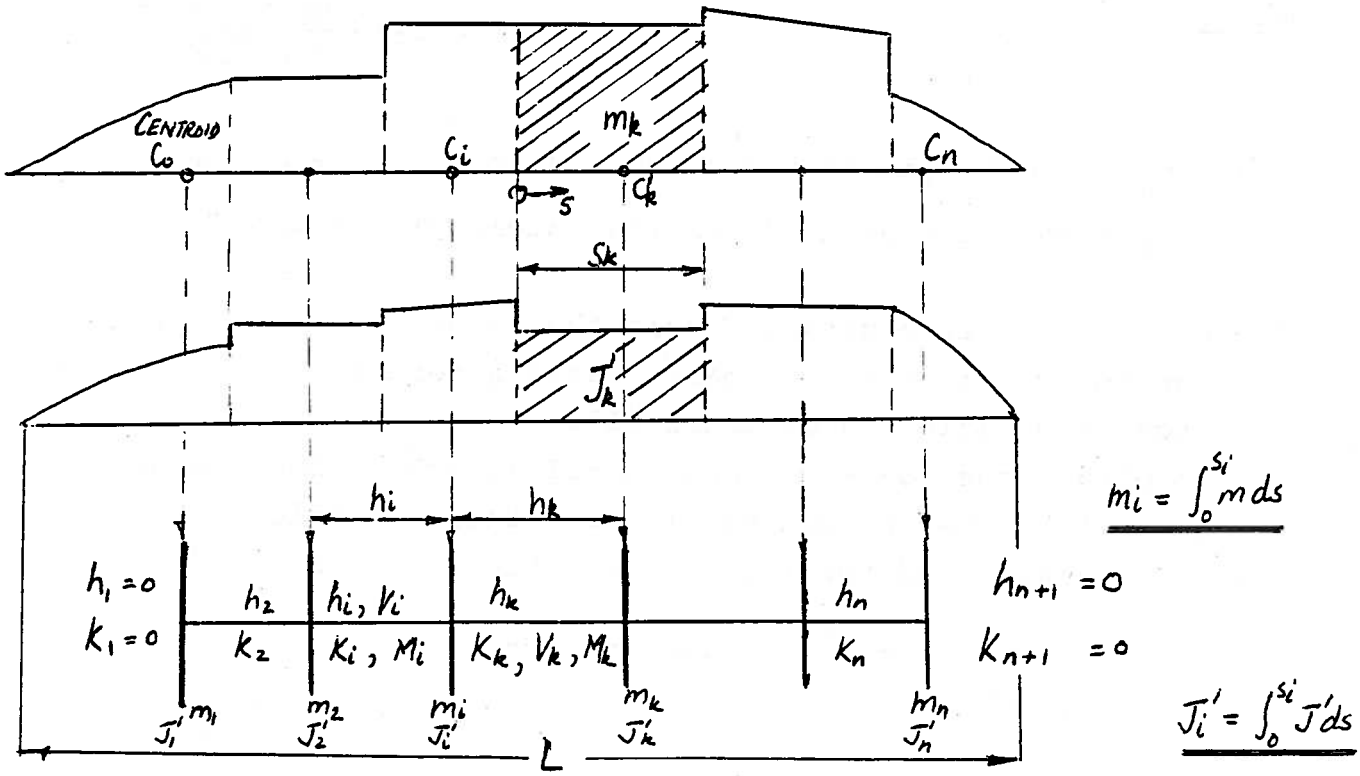

Discrete Disk Substitution System

Figure 31: (cont.)

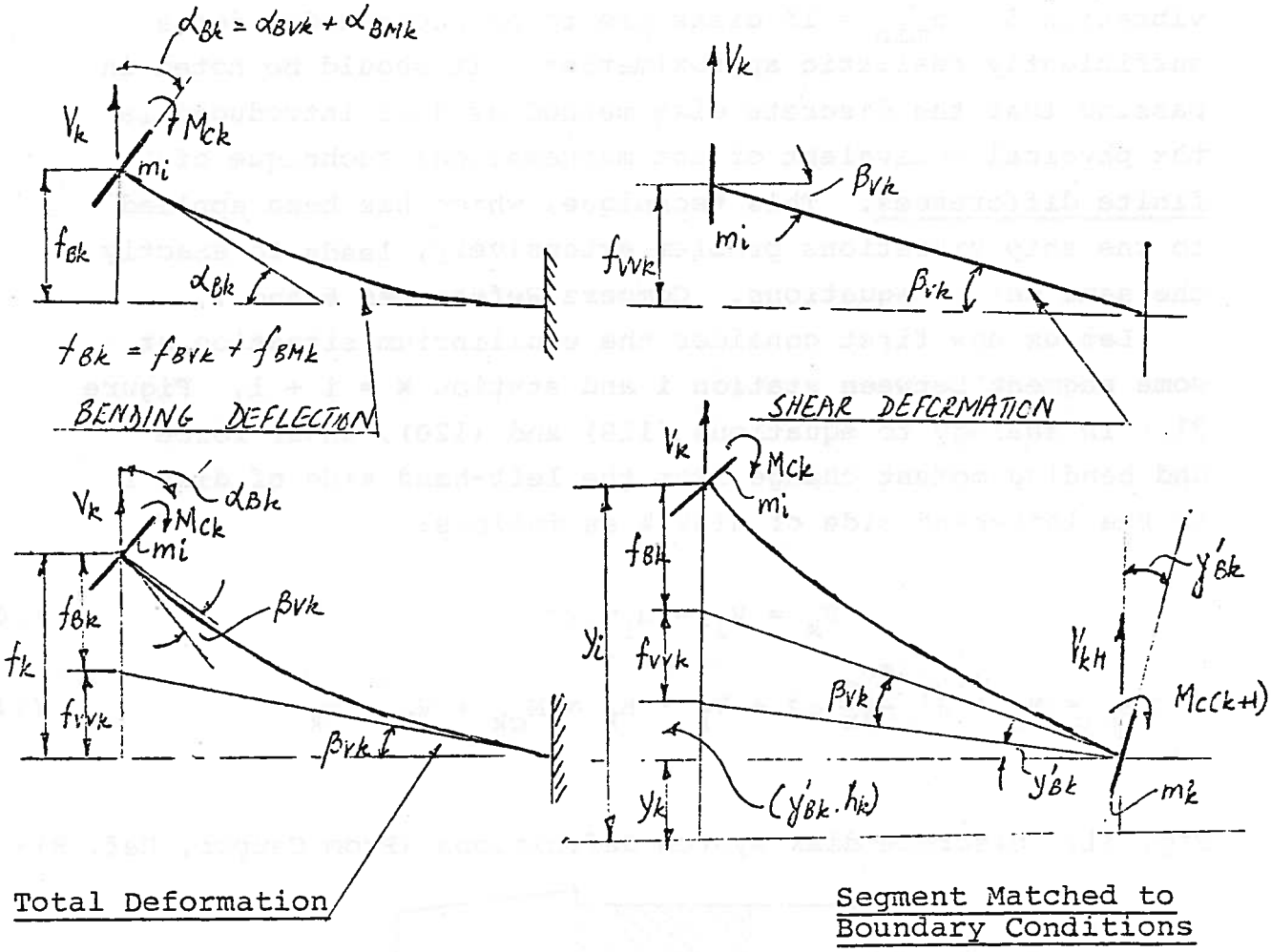

where h_k = the length of the segment under consideration

M_{ck} = constant part of bending moment within interval

The shear force is constant within the interval ($= V_k$), but the bending moment has a linearly varying term ($= V_k \cdot x$, x = distance from beginning of interval).

To obtain the load-deformation relationships for the segment, we assume that the uniform segment stiffness coefficients are known as a result of the lumping operation. For segment k:

k_{1k} = bending stiffness

k_{2k} = shear stiffness

We can now define bending and shear stiffness constants for the end deformations of the whole segment with bending or shear loads applied, respectively. The first subscript will denote the type of deformation (bending or shear), the second one the type of load. The following equations are results of elementary beam theory. All deformation quantities are for station k relative to station i.

Bending deflection due to end load V_k:

$$K_{BVk} = \frac{f_{BVk}}{V_k} = \frac{h_k^3}{3\ k_{1k}} \tag{150}$$

Rotation due to end load V_k:

$$\tilde{K}_{BVk} = \frac{\alpha_{BVk}}{V_k} = \frac{h_k^2}{2\ k_{1k}} \tag{151}$$

Bending deflection due to end moment M_{ck}:

$$K_{BMk} = \frac{f_{BMk}}{M_{ck}} = \frac{h_k^2}{2\ k_{1k}} \tag{152}$$

Rotation due to end moment M_{ck}:

$$\tilde{K}_{BMk} = \frac{\alpha_{BMk}}{M_{ck}} = \frac{h_k}{k_{1k}} \tag{153}$$

Shear deformation due to end load V_k:

$$K_{VVk} = \frac{f_{VVk}}{V_k} = \frac{h_k}{k_{2k}} \tag{154}$$

The total deformations of the segment may now be expressed in terms of these stiffness coefficients by means of superposition.

For the segment translation:

$$f_k = f_{BVk} + f_{VVk} + f_{BMk} = V_k \, (K_{BVk} + K_{VVk}) + M_{ck} \cdot K_{BMk} \qquad (155)$$

For the segment rotation:

$$\alpha_k = \alpha_{BVk} + \alpha_{BMk} = V_k \cdot \tilde{K}_{BVk} + M_{ck} \cdot \tilde{K}_{BMm} \qquad (156)$$

The absolute deformations at station k are obtained by combining the above segment deformation and the deformations at station i, Figure 31:

$$v_k = v_i - f_k - h_k \cdot \frac{dv_{Bk}}{dx} \qquad (157)$$

where

$$\frac{dv_{Bk}}{dx} = \frac{dv_{Bi}}{dx} - \alpha_k \qquad (158)$$

The equations (157) and (158) in connection with (148), (149), (155) and (156) permit finding the deformations and forces at the far end of the system for any given frequency ω and given set of initial values of the deformations at the near end.

It is therefore possible to construct an initial value solution technique for the transient response problem, thereby avoiding the complexities of a direct solution of the eigenvalue problem. This is in general analogy to the Holzer technique for shaft vibrations presented in section 4.2.

The steps of the procedure are as follows:

1. Estimate a natural frequency ω.
2. At station 1, set $V_1 = 0$, $M_1 = 0$ (free-free end).

3. At station 1, assume $v_1 = 1$. The mode shape is thus normalized, the natural frequencies will not be affected.

4. At station 1, the bending deflection slope dv_{B1}/dx must be estimated so that it will be compatible with the amplitude estimate $v_1 = 1$. But the ratio of bending and shear deformations is unknown at the beginning so that it is of advantage to express the bending slope estimate as*

$$\frac{dv_{B1}}{dx} = C_1 \cdot \xi \tag{159}$$

where C_1 = estimated value of slope

ξ = unknown correction factor

The factor ξ is carried through the computations as unknown. All computational results for the deformation and loads will therefore have a constant part and one proportional to ξ. They may be treated as vectors of the form

$$G = \{G_1 ; G_2 \xi\} \triangleq G_1 + G_2 \xi \tag{160}$$

and vectorial arithmetic may be used in the computation.

It is advisable to estimate the slope C_1 as accurately as possible to ensure numerical stability and rounding accuracy of the computation. Csupor, Ref. 8, recommends:

$$C_1 = C_{1n} \cdot \frac{v_1}{L} \tag{161}$$

where L = ship length, and C_{1n} from the table:

Degree of vibration	I	II	III	IV	V
C_{1n}	3.3	4.3	6.4	7.6	8.9

*This step is a little simpler than in Csupor's original procedure.

5. From the above input the internal loads and deformations can be computed station by station, using equations (148) and (158).

6. This leads to two expressions for shear force and bending moment at the last station N of the system:

$$V_{N+1} = \{C_2;\ C_3\xi\} \tag{162}$$

$$M_{N+1} = \{C_4;\ C_5\xi\} \tag{163}$$

These expressions have to vanish together for any correct natural frequency estimate (free-free end condition).

$$C_2 + C_3\xi = 0 \qquad \text{(Shear force zero)} \tag{164}$$

$$C_4 + C_5\xi = 0 \qquad \text{(Bending moment zero)} \tag{165}$$

This is possible only if the two equations are linearly dependent, or

$$\begin{vmatrix} C_2 & C_3 \\ C_4 & C_5 \end{vmatrix} = 0 \tag{166}$$

Otherwise, we may determine ξ to satisfy the shear force equation, but there will remain a rest moment

$$M_R = C_4 + C_5\ \xi_{V=0} \tag{167}$$

or vice versa for the rest shear force

$$V_R = C_2 + C_3\ \xi_{M=0} \tag{168}$$

7. Plotting the rest quantities M_R, V_R against the frequency estimates results in diagrams similar to Figure 32. These diagrams in connection with a mode count help to converge to any desired natural frequency by iteration and interpolation.

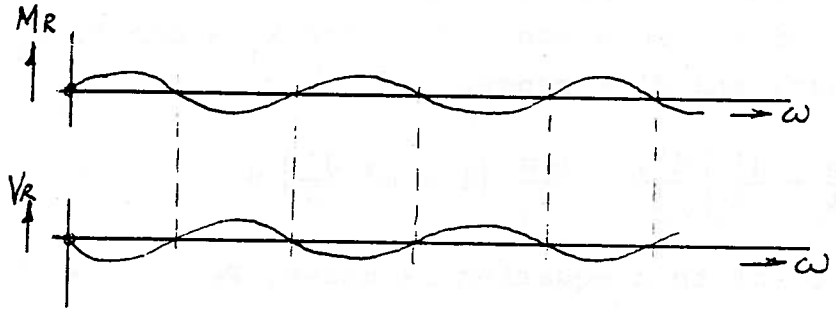

Fig. 32: Rest terms against frequency

For matrix variants of the discrete disk method see Ref. 8.

b) The Stepped Beam Method

In this approximate method the ship is replaced with a stepped beam so that we get a piecewise continuous rather than a discrete system. The situation is similar to the top of Figure 31 except the segments are assumed to have constant inertia and stiffness values.

This method was first introduced into ship vibration analysis by Csupor, Ref. 8. We want to give a summary of the main assumptions and features of the method. We refer to the original for more details.

In principle, the continuous substitution system is a better approximation for the actual ship than a lumped system having the same number of segments. One would consequently expect a more accurate solution. But this is at the expense of a more complicated treatment of the dynamics of each segment. The discrete disk method can reach similar accuracy levels by introducing enough disks, but in that event it is possibly inferior in

in computing time although a conclusive comparison remains to be made.

The stepped beam method treats each beam segment by means of the Timoshenko equation for the prismatical beam, which includes rotary inertia and shear effects. This equation is a special case of our equation (132), for k_1 = const, k_2 = const, m = const, and J' = const.

$$\frac{d^4v}{dx^4} + \omega^2 \left(\frac{m}{k_2} + \frac{J'}{k_1}\right) \frac{d^2v}{dx^2} - \frac{\omega^2 m}{k_1} \left(1 - \omega^2 \frac{J'}{k_2}\right) v = 0 \tag{169}$$

The solution of this equation is known, Refs. 1, 6, 8:

$$v(x) = A \cdot \sinh(\alpha x) + B \cosh(\alpha x) + C \sin(\beta x) + D \cos(\beta x) \tag{170}$$

where

$$\alpha = \sqrt{\frac{-p + \sqrt{p^2 + 4q}}{2}} \tag{171}$$

$$\beta = \sqrt{\frac{p + \sqrt{p^2 + 4q}}{2}} \tag{172}$$

$$p = \omega^2 \cdot \left(\frac{m}{k_2} + \frac{J'}{k_1}\right) \tag{173}$$

$$q = \omega^2 \frac{m}{k_1} \left(1 - \omega^2 \frac{J'}{k_2}\right) \tag{174}$$

In applying this solution to a beam segment, we determine the coefficients A, B, C, D, from the boundary conditions at its left-hand end, equation (170) is then used to predict the conditions at the right-hand end of the segment.

It is convenient to use the quantities v_{iL}, v'_{iL}, v''_{iL} and v'''_{iL} to characterize the condition at the left-hand end (L). The corresponding quantities at the other end (R) may then be determined from the following matrix operation:

$$\bar{v}_{iR} = A_i \cdot \bar{v}_{iL} \tag{175}$$

where

v_{iL}, v_{iR} = column matrices of the four v_i-derivatives at (L) and (R)

A_i = transformation matrix, determined from the conditions outlined above.

In making the transition to the next segment, k, we must keep in mind that the derivatives of v_i, that is v_i', v_i'', v_i''' are not continuous at the segment transition, but v_i, v_{Bi}, M, and V are. The step is made by satisfying:

$$v_B' = v' - \frac{V}{k_2} \tag{176}$$

$$M = -k_1 v'' - k_1 \omega^2 \frac{m}{k_2} v \tag{177}$$

$$V = \frac{-k_1}{1 - \omega^2 \frac{J'}{k_2}} v''' - \frac{k_1}{1 - \omega^2 \frac{J'}{k_2}} pv' \tag{178}$$

p as in equation (173).

These equations are the prismatic beam equivalents of equations (123), (125), and (131) with p from equation (173).

The operation may again be written in matrix form:

$$\bar{v}_{kL} = B_i \cdot \bar{v}_{iR} = B_i \cdot A_i \cdot \bar{v}_{iL} \tag{179}$$

where

$\bar{v}_{kL}$ = column matrix of v_i-derivatives at (L)-end of segment $k = i + 1$.

B_i = transition matrix from (iR) to (kL).

The basic step of equation (179) is used in an initial value procedure exactly analogous to that for the discrete disk system.

At the near end of the system, segment 1, we assume the condition

$$\bar{v}_{1L} = \begin{pmatrix} 1 \\ C_1 \\ a_1 \\ a_2 \end{pmatrix} \xi \qquad (180)$$

where a_1, a_2 are set according to equations (177) and (178) with the free-free end condition.

At the far end, by multiple use of (179), we predict a corresponding matrix $\bar{v}_{nR}$, which will satisfy the free-free end closing condition only if the frequency estimate was correct.

The details concerning ξ, and the frequency interpolation receive analogous treatment as explained under 5-6 A.

c) The Method of Successive Approximations.

In the technical literature the method to be presented next is usually known as Stodola method after the man who applied it to turbine rotor dynamics in a certain graphical form (Stodola, "Dampf-und Gasturbinen", 1929). It was later adapted to ship vibration problems by F. Horn. The basic approach is, however, related to previously known mathematical techniques in the treatment of differential equations. It seems that the first application to beam vibration problems goes back to J. Morrow, "Vibrations of Beams of Irregular Section," Phil. Mag., 1905. A good description of Morrow's method was given by Todd, Reference 4. The Stodola variant is discussed in References 6 and 8. We want to introduce the method for a shiplike beam with shear deformation, but without rotary inertia. We can use equations (119) through (122) as follows:

From (119): $$V = -\omega^2 \int_o^x mv\,dx + C_o \qquad (181)$$

From (120): For $J' \to o$:

$$M = -\omega^2 \int_0^x \int_0^x \int_0^x mvdxdx + C_o x + C_1 \qquad (182)$$

From (121):

$$\frac{dv_B}{dx} = \omega^2 \int_0^x \frac{1}{EI(x)} \int_0^x \int_0^x mvdxdxdx + \bar{C}_o x^2 + \bar{C}_1 x + \bar{C}_2 \qquad (183)$$

From (122):

$$\boxed{\frac{v(x)}{\omega^2} = \int_0^x \int_0^x \frac{1}{EI(x)} \int_0^x \int_0^x mvdxdxdxdx - \int_0^x \frac{1}{k_2} \int_0^x mvdxdx + \bar{\bar{C}}_o x^3 + \bar{\bar{C}}_1 x^2 + \bar{\bar{C}}_2 x + \bar{\bar{C}}_3} \qquad (184)$$

The same result could have been derived from equation (132) letting $J' \to o$. It should be noted that for $J' \neq o$ no straightforward expression similar to (184) can be obtained and the method meets with difficulties.

EXAMPLE:

The case of a ship hull girder in pure bending: $k_2 \to \infty$.

Given information about the ship: $I(x)$, $m(x) = M_{SHIP}(x) + M''(x)$

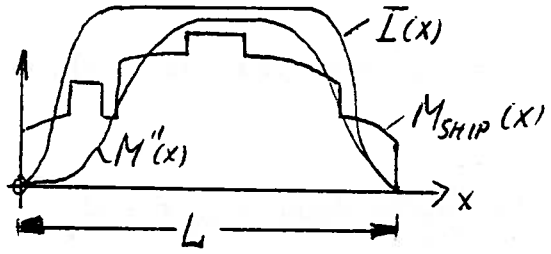

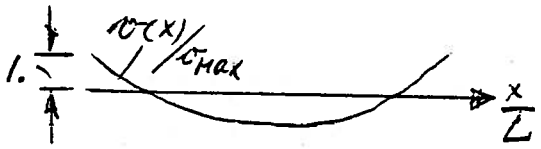

ASSUMED MODE SHAPE

M'' = hydrodynamic mass

Make sure that the ship is balanced statically:

$$\int_0^L M_{SHIP}(x) \cdot g dx = \Delta$$

$$\int_0^L M_{SHIP}(x) \cdot g \cdot x dx = X_{LCB} \cdot \Delta$$

First guess of mode shape from prismatic beam:

$\frac{x}{L}$	0 1	0.05 0.95	0.1 0.9	0.15 0.85	0.2 0.8	0.25 0.75	0.3 0.7	0.35 0.65	0.4 0.6	0.45 0.55	0.5
$\frac{v(x)}{v_{MAX}}$	+ 1.000	+ 0.768	+ 0.537	+ 0.313	+ 0.097	− 0.099	− 0.272	− 0.414	− 0.521	− 0.586	− 0.608

SOLUTION PROCEDURE:

Step 1.: Choice of amplitude scale.

The results will be independent of the amplitudes assumed since only amplitude ratios and natural frequencies are of interest.

It is convenient to choose a value of v_{MAX} so that the maximum acceleration, $a_{MAX} = \omega^2 v_{MAX} = g$.

Step 2.: Shear force.

A mode shape is estimated according to the table for $v(x)/v_{MAX}$. Let the first estimate be denoted as $v^*(x)/v_{MAX}$. Then from equation (119 and (181):

$$V(x) = -\omega^2 \int_0^x m(x) v_{MAX} \cdot \frac{v^*(x)}{v_{MAX}} \, dx + C_o = -\int_0^x W(x) \, \frac{v^*(x)}{v_{MAX}} \, dx + C_o$$

where $W(x) = m(x) \cdot g$ = weight per unit length, including added mass.

Step 3.: Bending moment.

The dynamic bending moment is derived by integration of V(x), using equations

$$M(x) = \int_0^x V(x) dx = \ldots = -\int_0^x \int_0^x W(x) \cdot \frac{v^*(x)}{v_{MAX}} \, dxdx + C_o x + C_1$$

Step 4.: End conditions.

The vibrating beam must have free-free ends, i.e. zero shear force and bending moment at x=0 and x=L. The condition at x=0 is met if we let $C_o = C_1 = 0$. But the condition at the far end is not automatically satisfied for the first estimated mode shape $v^*(x)/v_{MAX}$. To obtain a correct mode shape complying with

the end conditions the first estimate must be translated and rotated. This may be done by trial and error as in a longitudinal strength calculation, or directly, using

$$v(x) = v^*(x) + ax + b,$$

finding a and b from the end conditions:

$$\int_0^L W(x)\,\frac{v(x)}{v_{MAX}}\,dx = 0 = \int_0^L W(x)\,\frac{v^*(x)}{v_{MAX}}\,dx + a\int_0^L W(x)\,x\,dx + b\int_0^L W(x)\,dx$$

$$\int_0^L\int_0^x W(x)\cdot\frac{v(x)}{v_{MAX}}\,dxdx = 0 = \int_0^L\int_0^x W(x)\,\frac{v^*(x)}{v_{MAX}}\,dxdx + a\int_0^L\int_0^x W(x)\,x\,dxdx + b\int_0^L\int_0^x W(x)\,dxdx$$

This represents two simultaneous equations for a and b with the six integrals as coefficients.

Steps 2 and 3 must now be repeated for the corrected mode shape.

Step 5.: Slope.

The bending moments are proportional to $\frac{d^2v_B}{dx^2}$, and integration leads to the slope curve,

$$\frac{dv_B(x)}{dx} = \frac{1}{E}\int_0^x \frac{1}{I(x)}\int_0^x\int_0^x W(x)\,\frac{v(x)}{v_{MAX}}\,dxdxdx + \overline{C}_2$$

$$= \frac{1}{E}\int_0^x \frac{M(x)}{I(x)}\,dx + \overline{C}_2$$

Step 6.: Deflection.

From equations (122) or (184), for $k_2 \to \infty$

$$\underline{\underline{v(x)}} = \int_{oo}^{xx}\int \frac{M(x)}{EI(x)}\, dxdx + \bar{\bar{C}}_2 x + \bar{\bar{C}}_3 = \int_{o}^{x} \frac{dv_B(x)}{dx} dx + \bar{\bar{C}}_2 x + \bar{\bar{C}}_3 \quad (*)$$

The integral can be plotted, and $\bar{\bar{C}}_2$ is determined so that the curve is tilted into a horizontal position. The coefficient $\bar{\bar{C}}_3$ allows us to shift the reference axis in order to obtain a suitable two-noded shape. In order to compare the resulting mode shape from (*) to that originally assumed, $v(x)/v_{MAX}$, we subdivide the curve found so that the ratios

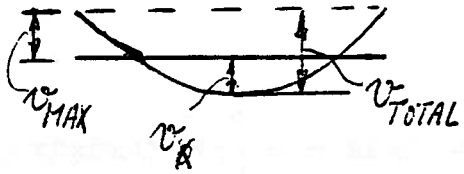

v_{MAX}/v_{TOTAL} and v/v_{TOTAL} are the same as originally assumed.

On this relative basis one may compare the "pure shape" of input and output. If the agreement is not "satisfactory" the result is used as new input to Step 2, and another approximation is calculated.

Step7.: Natural frequency.

If the output mode shape sufficiently resembles the input the natural frequency is obtained from the definition of a_{MAX} in Step 1.:

$$\omega^2 = \frac{g}{v_{MAX}}$$

The value of v_{MAX} is scaled off the resulting curve for $v(x)$ after reference line adjustment as explained in Step 6.

If only the natural frequency is of interest a crude approximation of the mode shape will be sufficient.

Adaptations of the method to higher degrees are errorprone and not to be recommended, Reference 8.

d) The Energy Theorem and Rayleigh's Principle

The kinetic energy of a vibrating beam with both types of inertia is

$$T = \int_0^L \left\{ \frac{m}{2} \left(\frac{\partial v}{\partial t}\right)^2 + \frac{J'}{2} \left(\frac{\partial^2 v_B}{\partial t \partial x}\right)^2 \right\} dx \qquad (188)$$

and the potential energy with both types of stiffness

$$V = \frac{1}{2} \int_0^L \left\{ k_1 \left(\frac{\partial^2 v_B}{\partial x^2}\right)^2 + k_2 \left(\frac{\partial v_V}{\partial x}\right)^2 \right\} dx \qquad (189)$$

Substituting a motion in any particular normal mode shape

$$v\ (x,t) = v(x) \cdot e^{i\omega t} \qquad (190)$$

$$T = \frac{1}{2}(-\omega^2)\int_0^L (mv^2 + J' v_B'^2)\, dx\, e^{2i\omega t} \tag{191}$$

$$V = \frac{1}{2}\int_0^L (k_1 v_B''^2 + k_2 v_V'^2)\, dx\, e^{2i\omega t} \tag{192}$$

From the energy theorem $\frac{d}{dt}(T + V) = 0$:

$$\omega_n^2 = \frac{\int_0^L (k_1 v_B''^2 + k_2 v_V'^2)\, dx}{\int_0^L (mv^2 + J' v_B'^2)\, dx} \tag{193}$$

This equation is exact for any correct mode shape. But it may also be used as an approximation if we substitute reasonable estimates instead. An admissible function for this purpose is defined as one satisfying the geometrical boundary conditions of the problem and being differentiable twice. It needs neither satisfy the dynamical boundary conditions (shear force and bending moment), nor, of course, the differential equation.

Rayleigh's principle states then that the quotient (193) has a minimum for the correct eigenfunction. Each estimate of v_B, v_V results in an upper bound for ω_n^2, and one must skillfully select admissible functions that result in low approximations.

Unfortunately this method is of no immediate usefulness in ship vibrations because we do not have even a crude estimate of the separate bending and shear deformations. Equation (193) may help, however, to discuss the effect of small changes in system parameters if the original mode shapes are known.

e) Empirical Formulas

There have been many attempts to estimate the natural frequencies of the hull at an early stage of the design by means of quick, approximate formulas. Since the characteristics of the design are known only crudely at this time, one is interested in formulas based on a few significant parameters whereas the more subtle influences are accounted for by means of more or less empirical coefficients.

Regarding the transverse beam modes, we want to keep in mind that according to the energy method the natural frequency expression is of the following general form, equation (193):

$$\omega_n^2 = \frac{\int_0^L k_1 \, v_B''^2 \, dx + \int_0^L k_2 \, v_V'^2 \, dx}{\int_0^L mv^2 \, dx + \int_0^L J' v_B'^2 \, dx} \qquad (193)$$

Any simplification of this formula will inevitably result in some scatter in the correlation of measured data so that we must not expect a single empirical coefficient. All the formulas to be presented in the following must be used with care and should be limited to ships of similar mass and stiffness distributions.

1) Fundamental frequency of vertical vibration

An old, but still relatively successful formula is due to Schlick (INA 1894):

$$N = \phi \sqrt{\frac{I_x}{\Delta L^3}} \qquad (194)$$

where

N = fundamental frequency in cycles per minute

I_x = moment of inertia of midship section about neutral axis in^{2}ft^2, counting only the continuous longitudinal members

Δ = displacement in long tons

L = length of ship in ft

ϕ = an empirical coefficient

Schlick gave the following values for ϕ:

$\phi = 1.568 \cdot 10^5$ for very fine ships (destroyers)

$\phi = 1.435 \cdot 10^5$ for fine ships (passenger liners)

$\phi = 1.279 \cdot 10^5$ for cargo ships, full lines

Todd, Ref. 4, found a little different values and recommended:

$\phi = 1.3 \cdot 10^5$ for large tankers in full load

$\phi = 1.12 \cdot 10^5$ for cargo ships at about 60 percent of their full load displacement

We note that Schlick's formula contains the bending stiffness and translational inertia influences of equation (193), but does not directly account for the influences of shear and rotary inertia.

A formula given by Todd and later modified by Todd and Marwood is of similar nature, but has the advantage that only the principal characteristics of the ship are involved, but not I_x (see Reference 4). Todd's equation:

$$N = \beta \sqrt{\frac{B \cdot D^3}{\Delta L^3}} \tag{195}$$

where

N = frequency in cycles per minute

B = molded beam in feet

D = molded depth at side in feet

Δ = displacement in long tons

L = length between perpendiculars in feet

β = empirical coefficient, with:

β = 61,000 for large tankers, fully loaded

β = 45,000 for cargo ship, 60 percent loaded

Burrill's formula (NECI 1934-35) tries to account for shear effects in order to reduce the variation in the coefficient:

$$N = \phi \sqrt{\frac{I_x}{\Delta L^3 \left(1 + \frac{B}{2T}\right)(1 + r)}} \tag{196}$$

where

N = frequency in cycles per minute

$$r = \frac{3.5\ D^2(3a^3 + 9a^2 + 6a + 1.2)}{L^2\ (3a + 1)} \qquad (197)$$

= J. L. Taylor's shear correction factor

I_x = moment of inertia of midship section in (feet)^4

Δ = displacement in long tons

L = length between perpendiculars in feet

B = molded beam in feet

T = draft in feet

D = depth in feet

a = B/D

ϕ = empirical coefficient, where Burrill found ϕ = 200,000 ± 5%

For some other, generally more elaborate formulas, see References 4, 5 and 6.

2) Fundamental frequency of horizontal vibration

If we assume the distributions of ship stiffness and inertia to be similar in the vertical and horizontal modes the natural frequencies would be related as

$$\frac{N_H}{N_V} \approx \sqrt{\frac{I_{xH} \cdot \Delta'_V}{I_{xV} \cdot \Delta'_H}} \qquad (198)$$

where

I_{xV}, I_{xH} = vertical and horizontal midship moments of inertia

Δ'_V, Δ'_H = displacements in vertical and horizontal modes including added mass effects

For the two-noded vibrations this ratio was observed to be fairly uniformly between about 1.3 and 1.5, References 4 and 6.

3) Higher flexural modes

For a uniform beam with free end conditions the lowest three natural frequencies would have ratios as 1:2.76:5.4 for any of the flexural modes.

For ships the steps are smaller. Reference 6, on the basis of the average of seven ships, recommends the simple rule (for vertical and horizontal modes):

$$1:2:3:4: \ldots.$$

Todd, Reference 4, quoting numerous observations, gets to the same conclusion regarding the average, but shows a fair amount of variation with ship type. While tankers conform with the above average rule, ore carriers exhibit greater, and passenger and cargo ships smaller variations than average.

4) Torsional frequencies

The fundamental torsional frequency can be estimated by Horn's formula:

$$N = 60 \cdot k \sqrt{\frac{g \cdot k_3}{\Delta \cdot (B^2 + D^2) \cdot L}} \qquad (199)$$

where, in any consistent units:

B = molded beam
D = depth
L = length
g = acceleration of gravity (length/second^2)
Δ = displacement
k_3 = torsional stiffness, defined as in equation (96)
k = empirical coefficient

Horn found k = 1.58, 3.00, and 4.07 for the first three torsional modes (Werft, Reederei und Hafen 1925). In the case of a Mariner ship the ratios of these values were found to be

similar, but in one other case even the fundamental mode showed a big discrepancy in k, References 4 and 6. Experimental evidence is still too scant for any definitive conclusions.

Kumai suggested the slightly more elaborate formula: References 4 and 5:

$$N = \frac{60}{2\pi} \sqrt{C_P} \cdot \lambda \sqrt{\frac{g\, k_3}{\Delta(1 + \eta) r_o^2\, L}} \qquad (200)$$

where, in any consistent units:

N = natural frequency in cycles per minute
C_P = prismatic coefficient
g = acceleration of gravity (length/second^2)
k_3 = torsional stiffness as in equation (96)
Δ = displacement
r_o = radius of gyration $\approx 0.306 \sqrt{B^2 + D^2}$
η = coefficient of torsional mass moment of inertia
L,B,D = length, beam, depth of ship
λ = coefficient obtained by Kumai by analysis of tapered beam. For values, see Reference 5.

5.7 Propeller Excitation

The impressive amount of work done in the field of propeller excitation may be appreciated by looking at References 18-34, which are perhaps representative, but far from complete. Propeller bearing and hull surface forces have both received considerable attention from analysts and experimenters.

a) Bearing forces

1) General discussion

Bearing forces (propeller forces) are experienced by the propeller operating in a nonuniform wake field in the vicinity of the hull and its appendages. The propeller transmits these

forces into the hull by way of the shaft bearings.

The total effect of hydrodynamic excitation at the propeller may be resolved into six components: three forces and three moments, Figure 33. The longitudinal force, F_X, and the moment, Q_X, represent thrust and torque variations that excite the shafting system and whose reactions are taken up by the thrust bearing and the engine. The other four components, F_y, F_z, Q_y, Q_z, excite the ship hull through the stern bearing, and some neighboring bearings if the stern frame is not perfectly rigid.

The analysis of the bearing forces starts from a given wake velocity field. This velocity field may be obtained either from direct model test (wake survey), or from data for similar ships. In this context, it is of great value that a large amount of wake survey data, derived from numerous single-screw and twin-screw models tested at NSRDC (ex DTMB), has been published by Hadler and Cheng, Reference 30. These data are furnished for various typical stern configurations. The results are presented in the form of harmonic components of the longitudinal and tangential wake velocities, V_L and V_T, respectively. For example, for the case of a single screw (starboard-port symmetry),

$$V_L(r, \Theta) = \sum_{k=0}^{\infty} a_k(r) \cdot \cos k\Theta \tag{201}$$

$$V_T(r, \Theta) = \sum_{k=0}^{\infty} b_k(r) \cdot \sin k\Theta \tag{202}$$

where Θ = angular coordinate in propeller plane, Figure 34.

To illustrate the basic force mechanism by which the wake fluctuations produce force oscillations, let us consider the simple case of the flow about a foil in a slowly varying inflow (quasi-steady case), Figure 35.

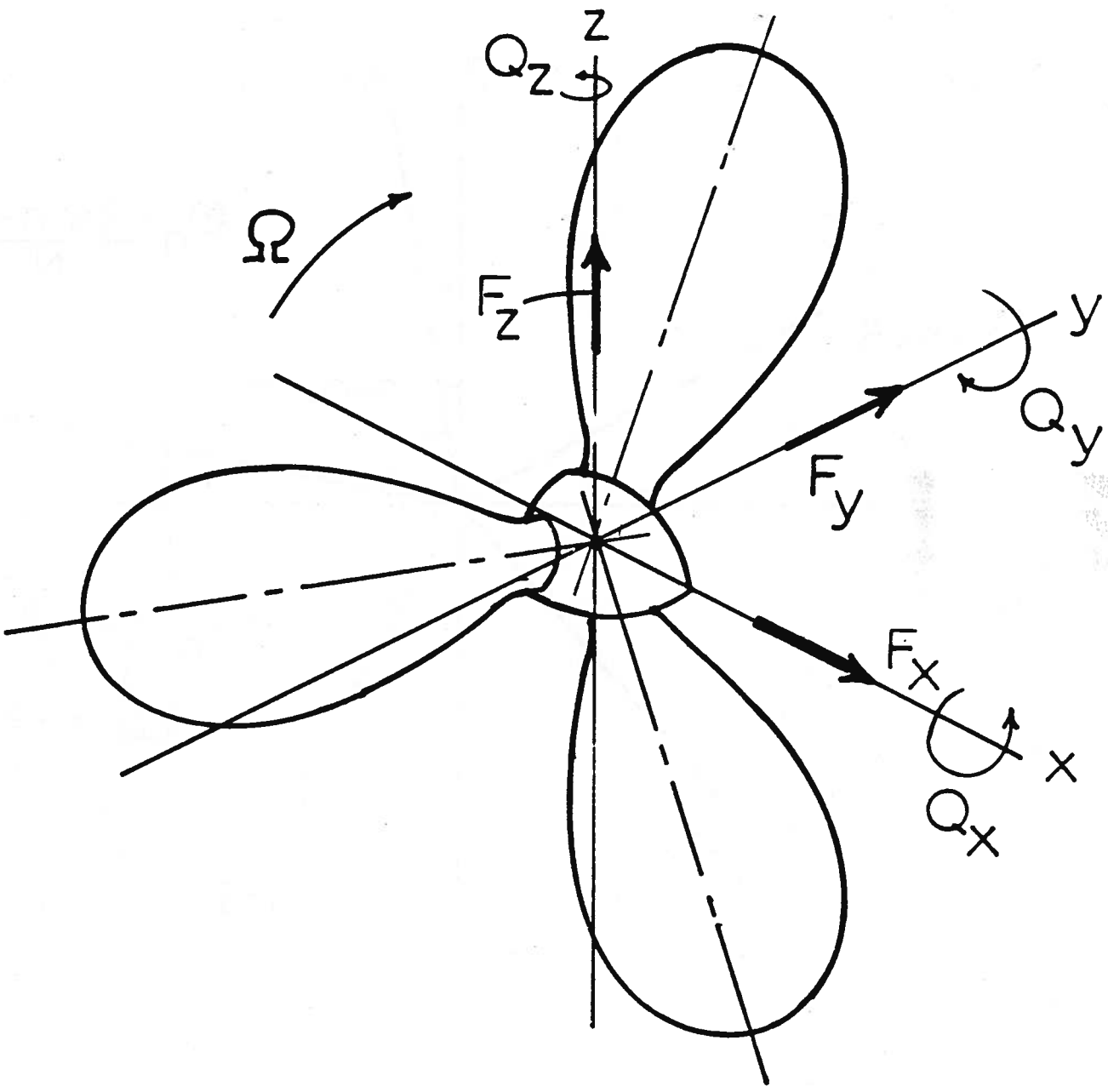

Fig. 33 : Orientation of propeller forces and displacements

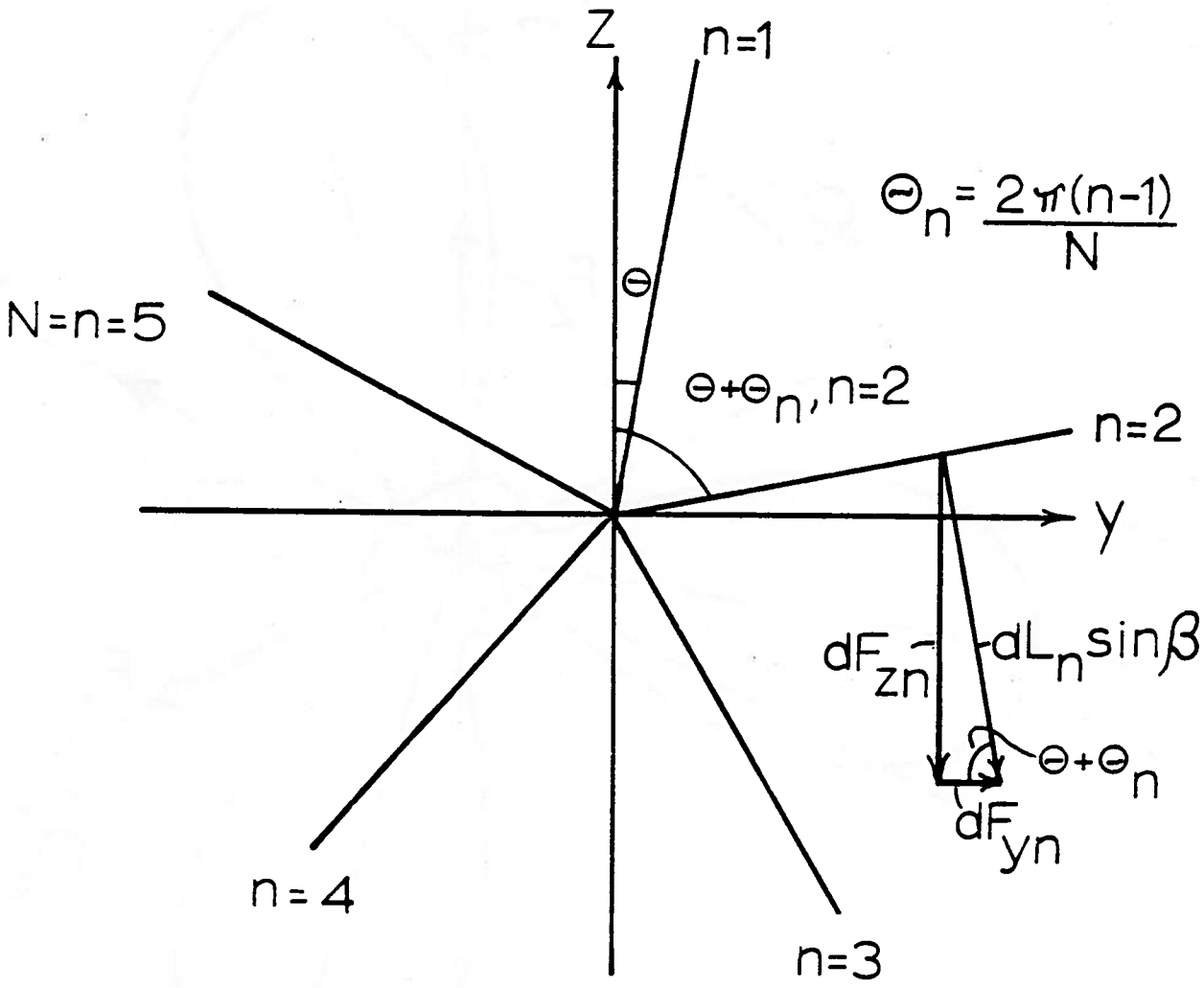

Fig.34 : Angles and force decomposition

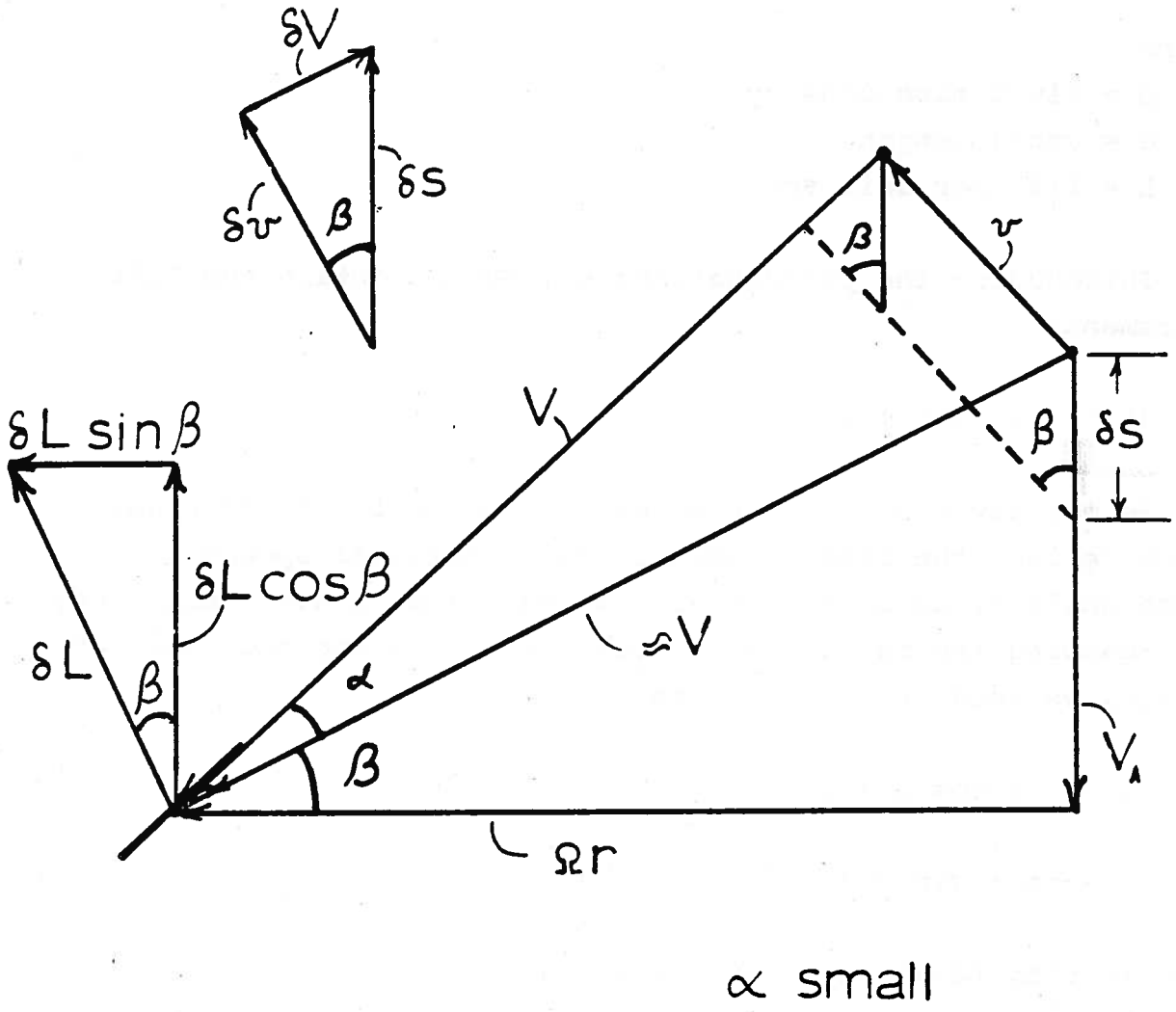

Fig. 35 : Velocity diagram

The lift of the foil for a small angle of attack, $\alpha \approx v/V$, is from thin airfoil theory:

$$L \sim \rho/2\ V^2\ c \cdot 2\pi\alpha = \pi\rho cvV \tag{203}$$

where

ρ = fluid mass density

c = chord length

L = lift per unit span

Introducing the perturbations δv, δV, we obtain the lift increment:

$$\delta L \approx \pi\rho c\ (V\delta v + v\delta V) \tag{204}$$

We may now regard the element as a propeller blade element, which defines the role of advance and rotational speeds and pitch angle β, as in Figure 35. If we assume a wake variation, δs, reducing the net advance speed and increasing the angle of attack, we read from the figure:

$$\delta v = \delta s \cos\beta \cdot e^{i\omega t} \tag{205}$$

$$\delta V = -\delta s \cdot \sin\beta \cdot e^{i\omega t} \tag{206}$$

Substituting (205) and (206) into (204):

$$\delta L \approx \pi\rho c\delta s\ (V\cos\beta - v\sin\beta)\ e^{i\omega t} \tag{207}$$

and with $V\cos\beta = \Omega r$, Ω = angular velocity of propeller, r = blade section radius, and $(v\tan\beta)/V \ll 1$:

$$\delta L \approx \pi\rho c\ \Omega r\,\delta s\ e^{i\omega t} \tag{208}$$

The integral of this expression over the radius would represent a crude two-dimensional, quasi-steady approximation of the variable lift acting on one blade.

Several refinements are, of course, necessary. The most advanced theory on this subject was recently presented by Tsakonas, Breslin, and Miller, Reference 29. This theory is an unsteady lifting surface propeller theory properly allowing for the helicoidal vortex wake, blade interference, finite aspect ratio and arbitrary velocity distribution in the wake. The theory is valid for small angles of attack, thin blades without cavitation, and negligible drag effects. Further simplifications were necessary in the numerical evaluation of the theory. But the correlation of the theory with tests taken behind wake screens was surprisingly good despite all approximations.

The result of the hydrodynamic theory is an expression for the lift of a blade element at radius r of the n'th blade, being at the instantaneous angular position $\Theta + \Theta_n$, Figure 34.

$$dL_n = \mathrm{Re}\left\{\sum_{k=0}^{\infty} C_k \cdot e^{ik(\Theta+\Theta_n)}\right\} dr, \quad k\Theta = \omega t = k\Omega t \tag{209}$$

where

Θ = angle of reference blade, n = 1

$\Theta_n = \frac{2\pi(n-1)}{N}$, N = number of blades,

and C_k = complex amplitude of k'th harmonic.

Note that, contrary to the simple case of equation(208),the force has a phase lag relative to the corresponding wake harmonic because of unsteady effects.

The longitudinal, transverse and vertical component of the lift element are (Figures 34 and 35):

$$\left.\begin{aligned} dF_{xn} &= dL_n \cos\beta \\ dF_{yn} &= dL_n \sin\beta \cos(\theta+\theta_n) \\ dF_{zn} &= dL_n \sin\beta \cos(\theta+\theta_n) \end{aligned}\right\} \qquad (210)$$

where β = hydrodynamic pitch angle.

The effect of all blades is obtained by summation. It will be shown in section 2 that in this summation only the forces of blade frequency, $N\Omega$, or its integer multiples, are retained. The results for the blade-frequency forces are:

$$\left.\begin{aligned} dF_x &= \mathrm{Re}\left\{N \cdot e^{iN\Omega t} C_N\right\} \cos\beta \, dr \\ dF_y &= \mathrm{Re}\left\{\frac{N}{2} e^{iN\Omega t} (C_{N-1} + C_{N+1})\right\} \sin\beta \, dr \\ dF_z &= \mathrm{Re}\left\{\frac{N}{2i} e^{iN\Omega t} (C_{N-1} - C_{N+1})\right\} \sin\beta \, dr \end{aligned}\right\} \qquad (211)$$

Corresponding expressions are obtained for the moments, Reference 29. The total propeller force is obtained by radial integration of the above expressions. It is interesting to note that these formulas reveal the reasons for the beneficial effect of propeller blade skew-back on bearing force excitation, which has been observed frequently. If the complex amplitudes C_N, etc. are sufficiently out of phase radially remarkable cancellation effects may take place.

It is also worth noting that the outer radii seem to be contributing more to the thrust fluctuation (cos β) than the inner ones, and conversely for the other two forces.

However, the main conclusion from equation (211) is the fact that only forces of blade frequency and its multiples are acting on the propeller ($\lambda N\Omega$). The blade frequency term (λ=1) is practically by far the most important part.

Further, one observes that:

1. The thrust variation dF_x (and the torque variation dQ_x) of an N-bladed propeller is proportional to the blade-force harmonic of order N, C_N, and is caused by the corresponding wake harmonic.

2. The lateral and vertical forces, dF_y, dF_z, (and the corresponding moments dQ_y, dQ_z) are proportional to combinations of the blade-force harmonics of order (N-1) and (N+1) and these wake harmonics cause the excitation.

Therefore, to get a complete picture of blade-frequency propeller excitation, we must look at the radial distribution of the blade-force harmonics C_{N-1}, C_N, C_{N+1}, both by amplitude and phase.

This information in conjunction with wake data (e.g. Hadler and Cheng, SNAME 1965) will guide the designer in selecting the number of blades from the vibrational viewpoint.

It must be added, however, that regarding surface force excitation the propeller does not act as a filter. All harmonics present in the wake result in pressure variations of blade frequency and its multiples) that are transmitted to the hull surface.

2) Proof

We want to prove now that only the forces of blade frequency, $N\Omega$, and its integer multiples, $\lambda N\Omega$, are acting on the propeller whereas all other blade forces cancel each other when summing up over all blades. Starting from (210) for the longitudinal, transverse and vertical components of the lift element we obtain by summation for an N-bladed propeller

$$dF_x = \mathrm{Re}\left\{\sum_{k=0}^{\infty}\ \sum_{n=1}^{N} C_k \cdot e^{ik(\Theta+\Theta_n)}\right\}\cos\beta\ dr \qquad (212)$$

$$\left.\begin{aligned} dF_y &= \mathrm{Re} \sum_{k=0}^{\infty} \sum_{n=1}^{N} C_k \cdot e^{ik(\theta+\theta_n)} \cdot \cos\ (\theta+\theta_n)\ \sin\beta\ dr \\ dF &= \mathrm{Re} \sum_{k=0}^{\infty} \sum_{n=1}^{N} C_k \cdot e^{ik(\theta+\theta_n)} \cdot \sin\ (\theta+\theta_n)\ \ \sin\beta\ dr \end{aligned}\right\} \quad (212)$$

We can now derive two addition theorems

$$\begin{aligned} \mathrm{Re}\left\{e^{ik(\theta+\theta_n)} \cdot \cos(\theta+\theta_n)\right\} &= \cos[k(\theta+\theta_n)] \cdot \cos(\theta+\theta_n) = \\ &= \tfrac{1}{2}\left\{\cos[(k+1)(\theta+\theta_n)]+\cos[(k-1)(\theta+\theta_n)]\right\} = \\ &= \tfrac{1}{2}\ \mathrm{Re}\left\{e^{i(k+1)(\theta+\theta_n)} + e^{i(k-1)(\theta+\theta_n)}\right\} \end{aligned} \quad (213)$$

$$\begin{aligned} \mathrm{Re}\left\{e^{ik(\theta+\theta_n)} \cdot \sin(\theta+\theta_n)\right\} &= \cos[k(\theta+\theta_n)] \cdot \sin(\theta+\theta_n) = \\ &= \tfrac{1}{2}\left\{\sin[(k+1)(\theta+\theta_n)]-\sin[(k-1)(\theta+\theta_n)]\right\} = \\ &= \tfrac{1}{2}\ \mathrm{Im}\left\{e^{i(k+1)(\theta+\theta_n)} - e^{i(k-1)(\theta+\theta_n)}\right\} = \\ &= \mathrm{Re}\left\{\tfrac{1}{2i}\ (e^{i(k+1)(\theta+\theta_n)} - e^{i(k-1)(\theta+\theta_n)}\right\} \end{aligned} \quad (214)$$

Substituting (213, (214) in (212)

$$\begin{aligned} dF_x &= \mathrm{Re}\left\{\sum_{k=0}^{\infty} \sum_{n=1}^{N} C_k\ e^{ik(\theta+\theta_n)}\right\} \cos\beta\ dr \\ dF_y &= \mathrm{Re}\left\{\tfrac{1}{2} \sum_{k=0}^{\infty} \sum_{n=1}^{N} C_k \left(e^{i(k+1)(\theta+\theta_n)} + e^{i(k-1)(\theta+\theta_n)}\right)\right\} \sin\beta\ dr \\ dF_z &= \mathrm{Re}\left\{\tfrac{1}{2i} \sum_{k=0}^{\infty} \sum_{n=1}^{N} C_k\ e^{i(k+1)(\theta+\theta_n)} - e^{i(k-1)(\theta+\theta_n)}\right\} \sin\beta\ dr \end{aligned} \quad (215)$$

These expressions contain summations of the form

$$S = \sum_{k=0}^{\infty} \sum_{n=1}^{N} e^{iq\Theta} \cdot e^{iq\Theta_n} = \sum_{k=0}^{\infty} e^{iq\Theta} \sum_{n=1}^{N} e^{iq\Theta_n} \tag{216}$$

where $q = (k-1)$, k, or $(k+1)$

and $\Theta_n = \frac{2\pi(n-1)}{N}$

It can be shown that

$$\sum_{n=1}^{N} e^{iq\Theta_n} = \sum_{n=1}^{N} e^{i\frac{2\pi q(n-1)}{N}} = \begin{cases} N \text{ for } q = \lambda N, \ \lambda = \text{integer} \\ 0 \text{ for } q \neq \lambda N \end{cases} \tag{217}$$

Resubstituting k for $q = \lambda N$, with $\Theta = \Omega t$

$$\left.\begin{aligned} dF_x &= \text{Re}\left\{\sum_{\lambda=1}^{\infty} N \cdot C_{\lambda N} e^{i\lambda N\Omega t}\right\} \cos\beta \, dr \\ dF_y &= \text{Re}\left\{\frac{N}{2} \sum_{\lambda=1}^{\infty} e^{i\lambda N\Omega t} (C_{\lambda N-1} + C_{\lambda N+1})\right\} \sin\beta \, dr \\ dF_z &= \text{Re}\left\{\frac{N}{2i} \sum_{\lambda=1}^{\infty} e^{i\lambda N\Omega t} (C_{\lambda N-1} - C_{\lambda N+1})\right\} \sin\beta \, dr \end{aligned}\right\} \tag{218}$$

b) Surface forces

Surface forces have been found to be more important than bearing forces in twin-screw vessels, but also with some single-screw stern arrangements, Reference 18. Much new knowledge has been acquired about these effects in recent years, References 3, 12, 13, 21-23, and 27.

The basic effect is easily described. As the blades of the propeller pass by the stern frame and other adjacent parts of the hull structure, they cause a cyclic pressure perturbation at the hull of blade frequency (and of the multiples of blade frequency). The pressure disturbances are caused by both the thickness and loading of the blades (displacement flow and circulatory flow).

The effects are magnified by the nonuniformity of the wake and the presence of the hull (image effect).

The prediction of propeller-induced field pressures is possible at various levels of refinement. In reference 21, Breslin and Tsakonas presented a theory, accounting for thickness and loading (lifting line model), for the free-field pressures of a uniform-wake propeller. The pressures could be expressed in simple asymptotic formulas, and good correlation with tests was obtained. In Reference 13, Tsakonas, Breslin, and Jen discuss the effects of a nonuniform wake.

The presence of a wall is more difficult to account for, except in the case of a flat plate parallel to the propeller axis at which the pressures would be intensified by a factor of 2 (image effect). In Reference 27, Breslin and Eng showed a procedure of calculating the intensification effect for a ship-shaped boundary by means of the three-dimensional potential flow program of Hess and Smith. They also used a refined lifting surface theory by Kerwin, Reference 31, to predict the propeller-induced pressures. The whole procedure was too time-consuming for design purposes, and further efforts to cut the computer time would be of significance.

Until these difficulties are resolved, the designer can use, as a simple shortcut, pressures predicted by Tsakonas, Breslin, and Miller, Reference 29, or the asymptotic formulas of Breslin and Tsakonas, Reference 21. In this connection he would have to apply semiempirical intensification factors tailored to suit the shape of a ship.

Let us assume then that from any of these procedures we shall have available expressions for the vertical and transverse components of the hull surface forces of excitation by amplitude and phase. After beamwise integration of the corresponding pressure components, we obtain forces per unit length.

$$\left.\begin{aligned} p_V(x,t) &= \bar{p}_V(x) \cdot e^{i\omega t} \\ p_T(x,t) &= \bar{p}_T(x) \cdot e^{i\omega t} \end{aligned}\right\} \qquad (219)$$

where

$p_V(x,t)$, $\bar{p}_V(x)$ = vertical force per unit length, and its complex amplitude

$p_T(x,t)$, $\bar{p}_T(x)$ = transverse force per unit length, and its complex amplitude

5.8 Steady-State Response

Several methods have been applied to the steady-state response analysis of ship hulls, Reference 6, notably modal analysis, the impedance method, analog computer techniques, and the finite difference method. The method of modal analysis, well-known in beam vibration theory, meets with some fundamental objections when damping is involved, but has proven practically acceptable, Reference 6. Finite difference techniques (discrete disk substitution system for ship) have been successful and are fairly universally applicable.

In the following a new solution technique shall be proposed which is based on a stepped beam approximation of the ship. It is an adaptation of Csupor's transient response technique of Reference 8. The fact that mass, damping and excitation remain continuously distributed variables in each beam segment gives the method some superiority over the discrete disk system, but at

the expense of more computational effort in the treatment of each beam segment. In most other respects the two methods are exactly analogous. The equation of motion for the forced vertical vibration is derived from Figure 36:

Equilibrium of forces:

$$m \frac{\partial^2 \bar{v}}{\partial t^2} dx = \frac{\partial \bar{V}}{\partial x} dx - c \frac{\partial \bar{v}}{\partial t} dx + \bar{p}\ (x,t)\ dx$$

or

$$\frac{\partial \bar{V}}{\partial x} = m \frac{\partial^2 \bar{v}}{\partial t^2} + c \frac{\partial \bar{v}}{\partial t} - \bar{p}\ (x,t) \tag{220}$$

where m = mass per unit length, including hydrodynamic mass

c = damping force coefficient per unit length

= $S m \omega$, $S \approx 0.03$, Ref. 6

$\bar{p}$ = complex excitation force per unit length

$\bar{v}$ = complex total displacement

$\bar{V}$ = complex shear force

Equilibrium of moments:

$$\frac{\partial \bar{M}}{\partial x} = \bar{V} - J' \frac{\partial^3 \bar{v}_B}{\partial t^2 \partial x} \tag{221}$$

where $\bar{M}$ = complex bending moment

$\bar{v}_B$ = complex bending displacement

J' = rotary inertia of beam element

The load-deformation relationships are in correspondence to the stiffness definitions (86) and (87)

$$\bar{M} = -k \frac{\partial^2 \bar{v}_B}{\partial x^2} \tag{222}$$

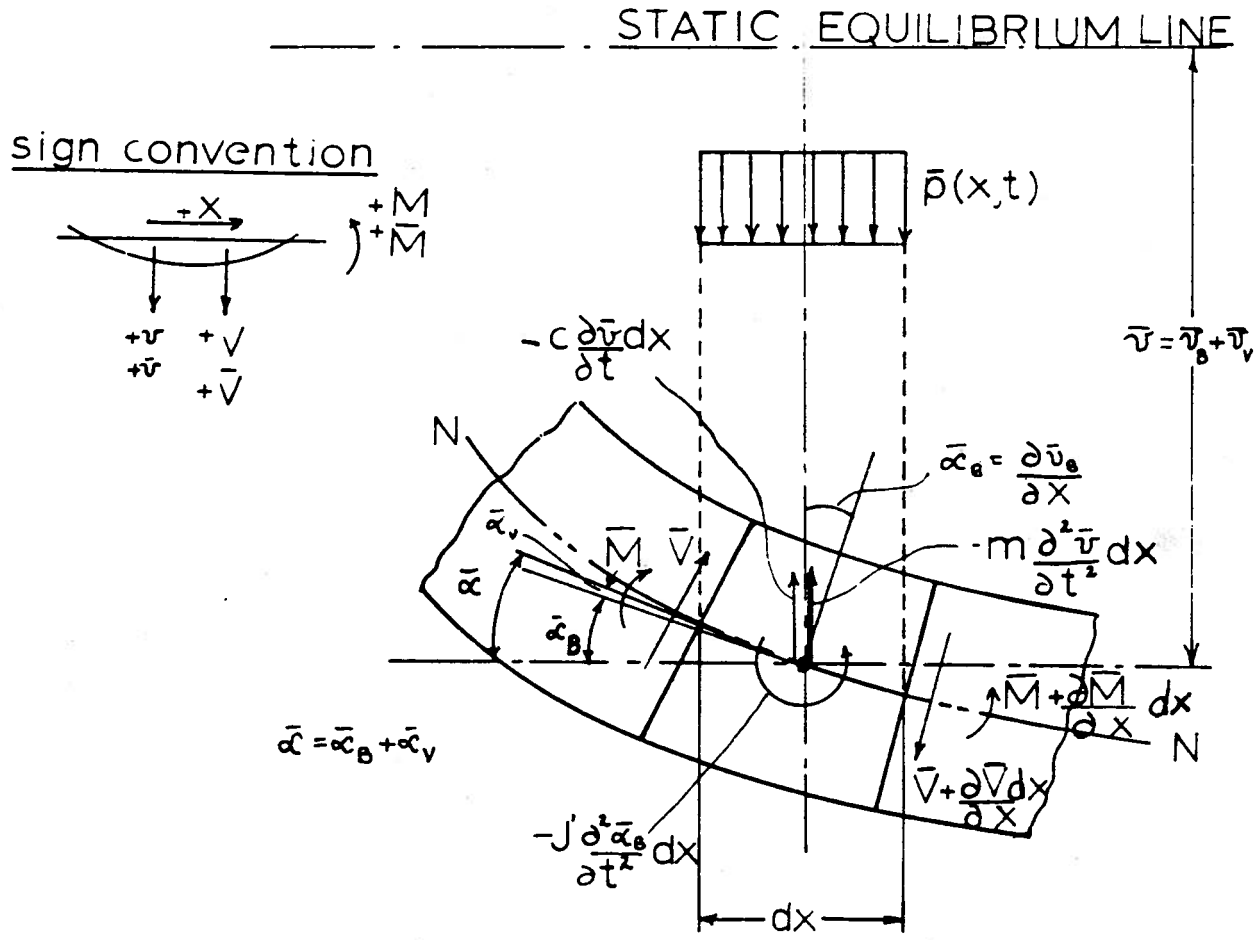

barred quantities are complex

Fig.36:Free body diagram of shiplike beam element

$$\bar{V} = k_2 \frac{\partial \bar{v}_V}{\partial x} = k_2 \left(\frac{\partial \bar{v}}{\partial x} - \frac{\partial \bar{v}_B}{\partial x} \right) \tag{223}$$

$\bar{v}_V$ = complex shear displacement

Separation of variables is accomplished by

$$\left.\begin{aligned} \bar{v}(x,t) &= \bar{v}(x) \cdot e^{i\omega t} \\ \bar{v}_B(x,t) &= \bar{v}_B(x) \cdot e^{i\omega t} \\ \bar{V}(x,t) &= \bar{V}(x) \cdot e^{i\omega t} \\ \bar{M}(x,t) &= \bar{M}(x) \cdot e^{i\omega t} \\ \bar{p}(x,t) &= \bar{p}(x) \cdot e^{i\omega t} \end{aligned}\right\} \tag{224}$$

Substituting and dropping the time-dependent terms:

$$\begin{aligned} &\text{From (220):} \quad \frac{d\bar{V}}{dx} = -\omega^2 m\bar{v} + ic\omega\bar{v} - \bar{p} \\ &\text{From (221):} \quad \frac{d\bar{M}}{dx} = \bar{V} + \omega^2 J' \frac{d\bar{v}_B}{dx} \\ &\text{From (222):} \quad \bar{M} = -k_1 \frac{d^2\bar{v}_B}{dx^2} \\ &\text{From (223):} \quad \bar{V} = k_2 \left(\frac{d\bar{v}}{dx} - \frac{d\bar{v}_B}{dx} \right) \end{aligned} \tag{225}$$

This set of four complex differential equations is used to deal with the dynamics of each beam segment. The stepped beam method keeps the quantities m, c, $\bar{p}$ constant within each segment. In a preliminary step of the procedure the equation of motion is determined for each segment with its given parameters. It is

then possible to prescribe boundary conditions at the left-hand end of a segment and determine the conditions at its right-hand end.

Suppose we give the quantities $\bar{v}_{iL}$, $\bar{v}'_{iL}$, $\bar{v}''_{iL}$, $\bar{v}'''_{iL}$ at the left hand end (L) of segment i. The corresponding quantities at the other end (R) are then

$$\bar{\bar{v}}_{iR} = A_i \, \bar{\bar{v}}_{iL} \tag{226}$$

where

$\bar{\bar{v}}_{iL}$, $\bar{\bar{v}}_{iR}$ = matrices of the $\bar{v}_i$ -derivatives at (L) and (R)

A_i = transformation matrix for beam segment

In making the transition to the next beam element, k, we use that $\bar{v}$, $\bar{v}_B$, $\bar{M}$, and $\bar{V}$ are continuous, but $\bar{v}'$, $\bar{v}''$, $\bar{v}'''$, are not because of shear deformation effects. In making the transition we use equations (225) and the conditions

$$\bar{v}_{iR} = \bar{v}_{kL}, \; \bar{v}_{BiR} = \bar{v}_{BkL}, \; \bar{M}_{iR} = \bar{M}_{kL}, \; \bar{V}_{iR} = \bar{V}_{kL}$$

In matrix form the operation may be summarized as

$$\bar{\bar{v}}_{kL} = B_i \, \bar{\bar{v}}_{iR} = B_i A_i \, \bar{\bar{v}}_{iL} \tag{227}$$

$\bar{\bar{v}}_{kL}$ = matrix of $\bar{v}_k$ - derivatives at (L) - end of segment k = i + 1.

These equations are used internally in the actual solution procedure. The technique proceeds in the following steps:

1. Assume the amplitude $\bar{v}_{iL}$ = {1; o} at the left end of the beam, but $\bar{v}'_{iL}$ = o, and no excitation in the system. Set $\bar{v}''_{iL}$ and

$\bar{v}'''_{iL}$ corresponding to the free end conditions. Find the complex rest moment and shear force at the far end. For example $\bar{V}_R = f_1 + if_2$.

2. Apply the amplitude $v_{iL} = \{o; 1\}$. The rest shear force would now equal

$$\bar{V}_R = -f_2 + if_1$$

3. Analogously, apply the slopes $\bar{v}'_{iL} = \{1; o\}$ and $\bar{v}'_{iL} = \{o; 1\}$ in successive steps with no excitation. Determine rest quantities.

4. Apply $\bar{v}_{iL} = \bar{v}'_{iL} = o$ at the near end, but all the excitation, and find rest quantities.

5. By superposition, find a linear combination of the first four inputs that cancels the effect of the excitation at the far end so that the free-end conditions are satisfied there. This will lead to a system of equations for four unknowns.

6. With properly determined coefficients, repeat calculation with all inputs and excitation applied to determine actual response. The end conditions will be satisfied automatically.

7. Evaluate response, decomposing amplitude and phase of the complex quantities.

This method has not yet been applied, but should have similar properties as the discrete disk or finite difference method.

Interesting results from steady-state response computations are reported in: W. B.Hinterthan, W. R. Fontaine, "Prediction of Hull Vibration," First Conference on Ship Vibration, Hoboken, 1965.

6. PREVENTION AND CURE OF SHIP VIBRATION

In preventing ship vibration problems while the design is still on paper and in curing trouble by alterations in the finished stage, we rely on essentially the same catalog of measures, although obviously there are differences in the feasible scope. In the following no special distinction will be made between these two stages, and it will be self-evident to what extent certain measures are applicable in each case.

The literature is full of special case histories, which are recommended for reading, and good surveys are given in References 4, 5 and 6.

Reference may also be made to my paper "On the Steady-State Ship Hull Response," presented to SOBENA in August 1968, where a rational design and selection process is discussed under the assumption that comprehensive information on the vibratory behavior of the hull is available. In contrast, the following will deal with current practice where decisions are often hampered by lack of full, reliable evidence.

Before discussing measures for vibration reduction we must define standards of acceptable vibration. The question has a subjective element because beside the possibility of structural failure by dynamic loads and fatigue, vibrations are also objectionable because of their effect on the human and his working and living environment.

The tolerable level of vibration amplitude depends much on the frequency, whereas the sensitivity to accelerations is fairly uniform throughout the frequency range. Most suggested sensitivity scales are therefore pertinent to accelerations. (Conversion: $a = (2\pi f)^2 \cdot y$, $v = 2\pi f y$, y = displacement amplitude, v = velocity amplitude, f = frequency, cps). To give a few examples (for more details see originals, and Dieudonné, TINA 1959):

Lewis, U.S. Navy, Ref. 3:

$v \leqslant 0.75$ cm/sec for tolerable vibration.

Kumai, Ref. 5; thresholds of unpleasantness:

$a \leq 0.015$ cm/sec^2 for horizontal vibrations,

$a \leq 0.03$ cm/sec^2 for vertical vibrations.

We now want to turn to a discussion of vibration reducing measures. The basic strategies may be listed as follows:

1. Reduce excitation
2. Avoid resonances
   a) by selection of operating speed
   b) by choice of mass distribution
   c) by choice of stiffness distribution
3. Increase damping (not actually feasible)
4. Introduce new degrees of freedom.

Excitation reduction.

Periodic shipboard excitation may be due to the main engine, the propeller, and the auxiliaries.

Shaft frequency excitation is in general due to unbalance. Engine unbalance is a particular problem of reciprocating engines (diesels) whose cylinders have unbalanced mass forces (horizontal and vertical). A multi-cylinder engine with a rigid base can be mass-balanced so that the resultant excitation force and moments are minimized. Complete mass-balance of force and moments requires a minimum of six cylinders for four-stroke engines, and twelve cylinders for two-stroke engines. For more details about favorable cylinder numbers, see marine engineering literature.

Propeller unbalance may be due to differences among the blades in their mass or pitch distribution. For some recommendations on propeller manufacturing tolerances, see Reference 3.

Unbalance of the shafting system may be caused by misalignment and static deflections of the hull. It may result in flexural criticals of the shaft (whipping).

The hydrodynamic reasons for propeller blade frequency

excitation (and blade frequency multiples) have been explained in the sections on bearing and surface forces. These forces depend on the wake field and many characteristics of propeller design and stern configuration.

The clearances of the propeller are a most significant parameter. Figures 36 and 37 (from Tachmindji, McGoldrick, "Note on Propeller-Excited Hull Vibration," JSR 1959) show the trends for the propeller-induced pressure variations. The maximum pressure fluctuation occurs in a plane a little ahead of the propeller. This suggests generous forward axial clearance, but also a fair amount of distance from the rudder. The benefits from sufficient tip clearance are similar, but returns diminish rapidly beyond t/d = 0.15. This constitutes only a single case, and for more detailed information one may refer to the asymptotic formulas by Breslin and Tsakonas, SNAME 1959.

Rake in the propeller is a means of providing more forward axial clearance at the expense of rudder clearance.

In practice, the tip clearance was sometimes increased by cropping the blades if the corresponding increase in RPM could be afforded.

The beneficial effect of skew-back on the bearing forces has been mentioned in section 5.7. Similar advantages may be expected for the surface forces.

The occurence of cavitation has adverse effects on bearing and surface forces.

Obstructions in the propeller inflow regime (condenser scoops, etc.) ought to be avoided to enhance low propeller excitation.

Avoidance of resonances.

The chances of avoiding resonant conditions throughout the range of operating speeds and loading conditions are practically nil. Figure 38 (from McGoldrick and Russo, SNAME 1955) shows the resonant hull frequency bands for S.S. Gopher Mariner, and

$$K_p = \frac{p}{\rho n^2 d^2}$$

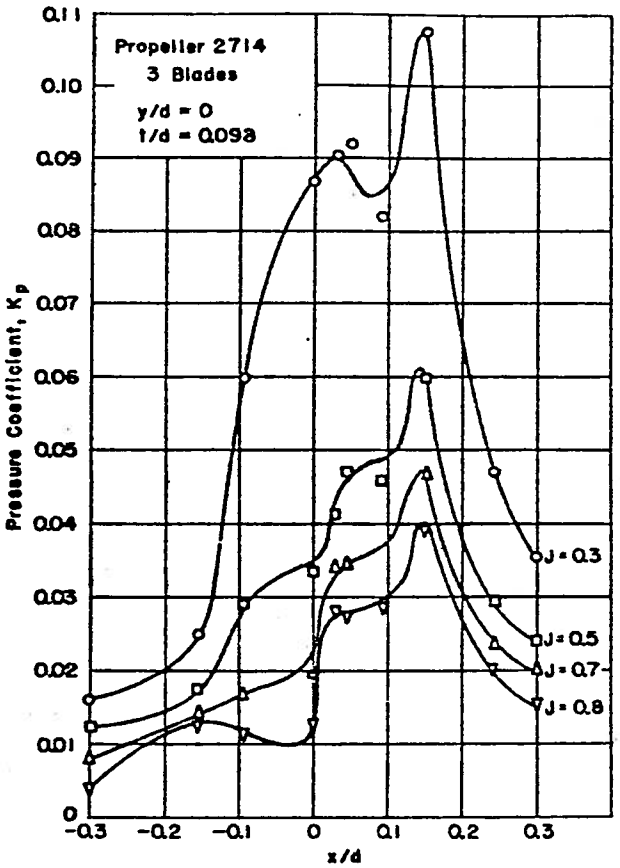

Figure 36 – Variation of Pressure Amplitude with Axial Distance from Propeller

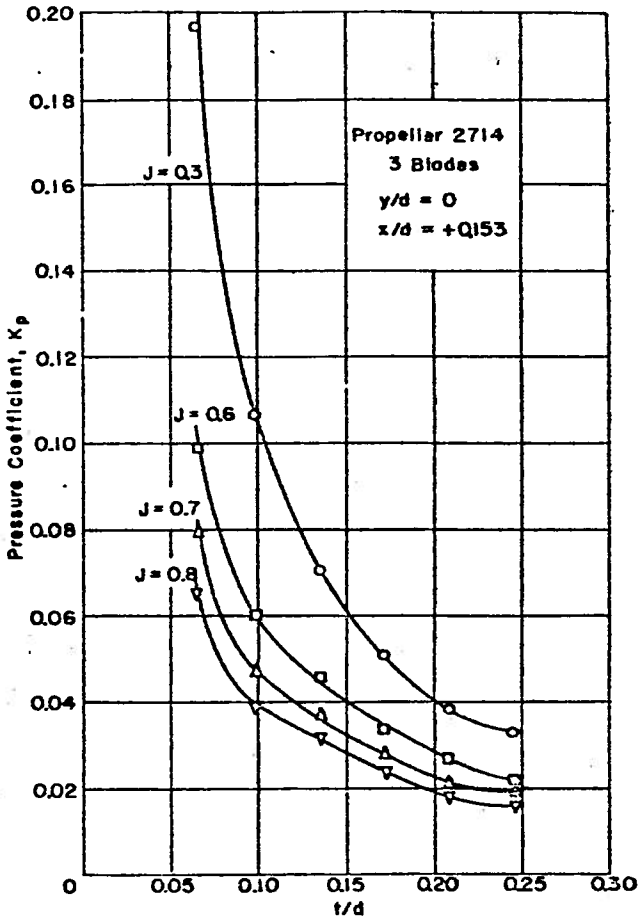

Figure 37– Variation of Pressure Amplitude with Radial Tip Clearance t (in a Plane Ahead of the Propeller Plane)

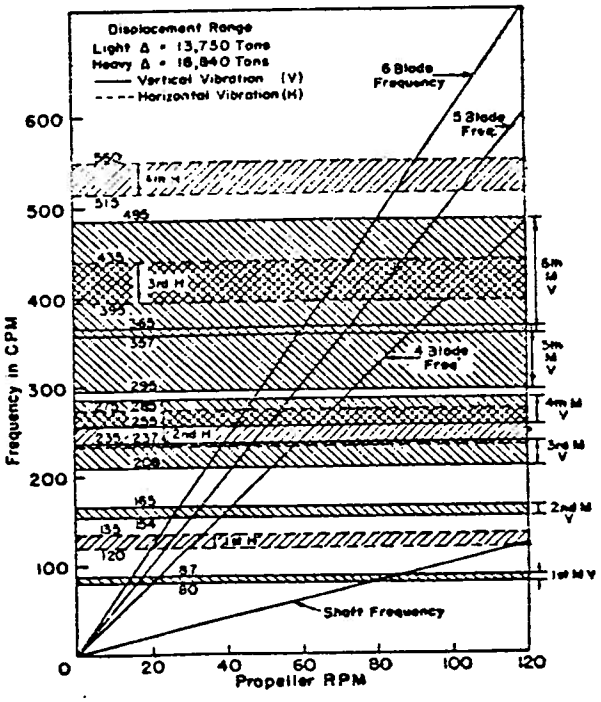

Figure 38 – Frequency of Hull Vibrations versus Propeller RPM Based on Experimental Data, GOPHER MARINER, with Torsional Effects Neglected

(From Figure 1 of Reference 6).

The above figures were reproduced from Reference 34.

the shaft and blade frequencies as a function of the propeller speed. The shaft frequency is between the two-noded horizontal and the two noded vertical resonance in the range of 85 to 115 RPM. But the blade-frequency for 4 to 6 blades can not avoid being in reconance with some of the higher modes at speeds fairly close to the full power condition.

Fortunately, many of these resonances turn out to be of tolerable severity so that in the present example a four-bladed propeller could even by afforded.

The freedom in the choice of mass and stiffness distributions for the hull girder is also very limited. The effect of some systematic variations in ship proportions, arrangement (engine room location), loading, and structural stiffness, on the dynamic response of the hull is discussed in a reference by R. G. Kline and R. W. Clough, SNAME 1967. See also Reference 4.

It should be noted that concentrating weights near nodal points tends to increase the natural frequency of the corresponding mode. Conversely, locating the machinery space and other light spaces near nodal points will tend to reduce the natural frequency.

In the same context it must be kept in mind also that engine unbalance exciting forces will do no work in points of zero displacement (nodes) whereas the unbalance moments do no work where the slope is zero (antinode).

The natural frequencies in ballast have been found to be somewhat higher than in the full load condition as one might expect. Todd, Reference 4, states that the differences in the two-noded vertical frequencies were in excess of those computed from Schlick's formula.

Resilient mountings.

Mounting shipboard equipment on soft springs may be done for two reasons: To protect the equipment from the effects of excessive motions of its base (transient or steady-state); or if

the component is a source of excitation itself, to reduce the effect of this excitation upon its vicinity and the hull girder in general.

In both cases the natural frequency of the mounting must be low compared to the frequencies it is supposed to filter out. The function of the installation may be understood from the dynamics of a simple mass-spring system. In the first case, we use the fact that a base-excited system shows vanishing motions of the mass at high excitation frequencies. In the other case, we take advantage of the property of a mass-excited system that the force acting on the base point approaches zero for high frequencies.

Care must be taken to avoid the ill effects of bottoming of the mass due to impulsive loads.

Local vibrations, sprung-mass effects.

Local vibrations are a frequent occurrence aboard ships. Vibrating panels of decks, bulkheads, the shell plating, masts, parts of the superstructure, struts, skegs, rudders and other appendages are typical examples.

Most of these vibrations occur at relatively high frequencies, near and above the highest hull modes (6V, 4H) that are of significance. These frequencies are the resonant frequencies of the local structural elements.

Because of the resonant nature of these vibrations a small, otherwise unnoticeable amount of excitation, transmitted through the hull girder to the base of the local element, is sufficient to cause significant vibrations.

The analysis of local vibrations can best be accomplished by treating the vibrating elements as sprung masses. In the general case, one would work with a substitution system consisting of a lumped, effective mass and a system of spring supports, capable of moving in six degrees of freedom. This model serves to predict the local resonant frequencies. See References 6 and 7 for some

rules for the lumping operation, and for the dynamic analysis of the system.

The presence of local modes may influence the dynamic properties of the main hull. McGoldrick, Reference 6, states that this is of significance if the local mass is above 0.5 percent of the displacement and if the local natural frequency is within the range of significant hull frequencies (< 800 cpm). The effect may be understood as an extended analogy of the absorber effect described in section 3. One observes that:

a) The hull natural frequencies below the local resonant frequency are lowered, those above are raised.

b) The additional degree of freedom results in one additional resonant hull mode. The two hull modes neighboring to the local resonance may be very similar modes, only differing in the phase between mass and hull. One of these modes may be counted as the additional mode.

The cure of local vibrations is often relatively simple. Moderate stiffening is usually sufficient to remove the resonance. Stiffening is most effective in the antinodes of the mode shape. In panel vibrations it may be possible to reduce the free span by redistributing stiffeners without installing more weight. For more recommendations, see References 4 and 6.

Local Stern Vibrations.

In some instances significant vibrations have occurred in ship sterns that could not be fully explained by beam theory, the motions in deck and bottom structure being inconsistent with simple flexural hull modes. Reference 5 gives an interesting case study.

As an explanation for the effects, several interesting hypotheses are advanced in Reference 5 (in the order of significance):